Calhoun
Institutional Archive of the Naval Postgraduate School

Calhoun: The NPS Institutional Archive

DSpace Repository

Theses and Dissertations | 1. Thesis and Dissertation Collection, all items

2012-03

Evaluation of Sea Ice Kinematics and their Impact on Ice Thickness Distribution in the Arctic

Murnane; Mark

Monterey, California. Naval Postgraduate School

https://hdl.handle.net/10945/6838

Downloaded from NPS Archive: Calhoun

http://www.nps.edu/library

Calhoun is the Naval Postgraduate School's public access digital repository for research materials and institutional publications created by the NPS community. Calhoun is named for Professor of Mathematics Guy K. Calhoun, NPS's first appointed -- and published -- scholarly author.

Dudley Knox Library / Naval Postgraduate School
411 Dyer Road / 1 University Circle
Monterey, California USA 93943

NAVAL POSTGRADUATE SCHOOL

MONTEREY, CALIFORNIA

THESIS

EVALUATION OF SEA ICE KINEMATICS AND THEIR IMPACT ON ICE THICKNESS DISTRIBUTION IN THE ARCTIC

by

Mark Murnane

March 2012

Thesis Advisor:	Wieslaw Maslowski
Thesis Co-Advisor:	Ron Kwok

Approved for public release; distribution is unlimited

THIS PAGE INTENTIONALLY LEFT BLANK

REPORT DOCUMENTATION PAGE			Form Approved OMB No. 0704-0188

Public reporting burden for this collection of information is estimated to average 1 hour per response, including the time for reviewing instruction, searching existing data sources, gathering and maintaining the data needed, and completing and reviewing the collection of information. Send comments regarding this burden estimate or any other aspect of this collection of information, including suggestions for reducing this burden, to Washington headquarters Services, Directorate for Information Operations and Reports, 1215 Jefferson Davis Highway, Suite 1204, Arlington, VA 22202-4302, and to the Office of Management and Budget, Paperwork Reduction Project (0704-0188) Washington DC 20503.

1. AGENCY USE ONLY *(Leave blank)*	**2. REPORT DATE** March 2012	**3. REPORT TYPE AND DATES COVERED** Master's Thesis

4. TITLE AND SUBTITLE Evaluation of Sea Ice Kinematics and their Impact on Ice Thickness Distribution in the Arctic

5. FUNDING NUMBERS

6. AUTHOR(S) Murnane, Mark

7. PERFORMING ORGANIZATION NAME(S) AND ADDRESS(ES)
Naval Postgraduate School
Monterey, CA 93943-5000

8. PERFORMING ORGANIZATION REPORT NUMBER

9. SPONSORING /MONITORING AGENCY NAME(S) AND ADDRESS(ES)
N/A

10. SPONSORING/MONITORING AGENCY REPORT NUMBER

11. SUPPLEMENTARY NOTES The views expressed in this thesis are those of the author and do not reflect the official policy or position of the Department of Defense or the U.S. Government. IRB Protocol number _____N/A_____.

12a. DISTRIBUTION / AVAILABILITY STATEMENT
Approved for public release; distribution is unlimited

12b. DISTRIBUTION CODE
A

13. ABSTRACT (maximum 200 words)

Sea ice area and thickness have been on the decline in the Arctic over the past several decades. Understanding the role of ice motion, deformation, and export is important to determining if the Arctic will continue toward seasonal ice coverage or if natural variability is capable of reversing this trend. We have analyzed sea ice model output and satellite data to advance the understanding of potentially critical physical processes and feedbacks in the region. In particular, comparisons of RGPS data and sea ice results from ice-ocean and fully coupled regional climate models have been made to evaluate model skill in representing ice kinematics. Both sea ice model configurations maintain a $1/12^{o}$ (~9km) horizontal spacing and multiple thickness categories in each grid cell. Advanced model representation of sea ice deformations, combined with high spatial resolution, allow direct comparison with satellite data for resolving small-scale linear kinematic features, which contribute to changes in sea ice thickness distribution. These results offer an improved insight into what forces determine the survivability of sea ice in the Arctic.

14. SUBJECT TERMS
Arctic Ocean, Sea Ice Variability, Coupled Ice-Ocean Model, Sea Ice Dynamics, Sea Ice Thickness Distribution

15. NUMBER OF PAGES
121

16. PRICE CODE

17. SECURITY CLASSIFICATION OF REPORT	**18. SECURITY CLASSIFICATION OF THIS PAGE**	**19. SECURITY CLASSIFICATION OF ABSTRACT**	**20. LIMITATION OF ABSTRACT**
Unclassified	Unclassified	Unclassified	UU

NSN 7540-01-280-5500

Standard Form 298 (Rev. 2-89)
Prescribed by ANSI Std. 239-18

THIS PAGE INTENTIONALLY LEFT BLANK

Approved for public release; distribution is unlimited

EVALUATION OF SEA ICE KINEMATICS AND THEIR IMPACT ON ICE THICKNESS DISTRIBUTION IN THE ARCTIC

Mark Murnane
Lieutenant Commander, United States Navy
B.S., University of Notre Dame, 1999

Submitted in partial fulfillment of the
requirements for the degree of

MASTER OF SCIENCE IN METEOROLOGY AND PHYSICAL OCEANOGRAPHY

from the

NAVAL POSTGRADUATE SCHOOL
March 2012

Author: Mark Murnane

Approved by: Wieslaw Maslowski
Thesis Advisor

Ron Kwok
Thesis Co-Advisor

Jeffrey Paduan
Chair, Department of Oceanography

THIS PAGE INTENTIONALLY LEFT BLANK

ABSTRACT

Sea ice area and thickness have been on the decline in the Arctic over the past several decades. Understanding the role of ice motion, deformation, and export is important to determining if the Arctic will continue toward seasonal ice coverage or if natural variability is capable of reversing this trend. We have analyzed sea ice model output and satellite data to advance the understanding of potentially critical physical processes and feedbacks in the region. In particular, comparisons of RGPS data and sea ice results from ice-ocean and fully coupled regional climate models have been made to evaluate model skill in representing ice kinematics. Both sea ice model configurations maintain a $1/12^{o}$ (~9km) horizontal spacing and multiple thickness categories in each grid cell. Advanced model representation of sea ice deformations, combined with high spatial resolution, allow direct comparison with satellite data for resolving small-scale linear kinematic features, which contribute to changes in sea ice thickness distribution. These results offer an improved insight into what forces determine the survivability of sea ice in the Arctic.

THIS PAGE INTENTIONALLY LEFT BLANK

TABLE OF CONTENTS

I. INTRODUCTION....1
A. BACKGROUND AND MOTIVATION FOR SEA ICE RESEARCH....1
1. Atmospheric Influences....3
2. Sea Ice Thickness....7
3. Sea Ice Age....10
B. INTENT OF STUDY....11
C. OVERVIEW....13

II. NAVY RELEVANCE....15
A. STRATEGIC GUIDANCE....17
B. ARCTIC NATIONS....19
C. U.S. NAVY ARCTIC CAPABILITIES....21
D. OBSERVATIONAL AND TRAINING OPPORTUNITIES....24

III. DESCRIPTION OF NUMERICAL MODELS AND OBSERVATIONAL DATA....27
A. MODEL DESCRIPTIONS....27
1. Polar Ice Prediction System (PIPS)....27
2. Parallel Ocean Program (POP)—Community Ice CodE (CICE)....29
3. Regional Arctic Climate System Model (RACM)....30
B. RADARSAT GEOPHYSICAL PROCESSOR SYSTEM (RGPS) DATA SET....32
1. RGPS Data Validation....35
2. RGPS Sea Ice Deformation Calculations....37

IV. RESULTS....41
A. SEASONAL DRIFT AND DEFORMATION....41
1. PIPS and CICE Comparison to RGPS Data....41
2. RACM Comparison to RGPS Data....49
B. SMALL-SCALE DEFORMATIONS....54
1. Shear Deformation Analysis....54
2. Alternative Model Shear Estimations....59
C. REGIONAL DEFORMATION COMPARISON....69

V. DISCUSSION AND SYNTHESIS OF RESULTS....75
A. LARGE-SCALE DISPLACEMENT AND DEFORMATIONS....75
B. SMALL-SCALE DEFORMATIONS....77
C. REGIONAL DEFORMATION COMPARISON....79

VI. CONCLUSIONS AND FUTURE RECOMMENDATIONS....81
A. CONCLUSIONS....81
B. FUTURE RECOMMENDATIONS....84
1. Model Data Limitations....84
2. Satellite Observations....85

3. Additional Model Parameterizations 86
LIST OF REFERENCES 89
INITIAL DISTRIBUTION LIST 99

LIST OF FIGURES

Figure 1. Arctic sea ice extent through September 2011 (From National Snow and Ice Data Center [NSIDC] 2011) 3

Figure 2. Sketch of a (a) positive phase and a (b) negative phase of the Arctic Oscillation induced atmospheric patterns (From Wallace 2011)..... 5

Figure 3. Regression maps of the first two leading modes to the (a and b) winter and (c and d) summer mean Northern Hemisphere SLP field using the NCEP Reanalysis dataset from 1948 to 2008. Contour intervals are 0.5 hPa (see color bars). The black arrows in (a) and (c) indicate the cyclonic (anticyclonic) wind anomaly during the +AO (-AO). In (b) and (d), the black arrows indicate wind anomalies between the western and eastern Arctic during +DA and –DA phases that accelerate or decelerate the TDS (in red-dashed arrows), respectively (From Wang et al. 2009). 6

Figure 4. (a) Winter Arctic Ocean sea ice thickness from ICESat (2004-2008). (b) Interannual changes in ice thickness from the submarine (RA) and ICESat campaigns (After Kwok and Rothrock 2009; Kwok and Sulsky 2010). 9

Figure 5. Median age of March sea ice in 1985 (left) and 2011 (right). Overall, the proportion of young ice (light blue) has increased. By March 2011, ice more than four years old (dark blue) accounts for less than 10 percent of the Arctic ice cover (From Maslanik et al. 2007) 11

Figure 6. Map of the Arctic Region showing the Arctic Ocean, adjacent seas and political boundaries. Red line shows average 10°C isotherm for July (From U.S. Central Intelligence Agency, 2012). 16

Figure 7. Potential Summer Shipping Lanes (From Arctic Marine Shipping Assessment (AMSA), 2009) 19

Figure 8. Existing DoD Bases and Facilities in Alaska and the Arctic (From DoD, 2011) 23

Figure 9. NPS model domain and bathymetry. 28

Figure 10. RACM pan-Arctic model domain. WRF and VIC model domains include the entire colored region. POP and CICE domains are bound by the inner blue rectangle. Arctic System domain is bound by the red line (From Maslowski et al. 2012, in press)..... 31

Figure 11. Nominal repeat coverage of the Arctic Ocean over a 24-day cycle (From Kwok and Cunningham 2000) 34

Figure 12. Differences in regional advection and deformation between model and RGPS estimates, November 1996 to April 1997. Model-derived regional boundaries are in black, RGPS boundaries are in color. Vectors (model in black, RGPS in color) near the center of each region show the average displacement of the boundary samples computed from model and RGPS data. 43

Figure 13. Differences in regional advection and deformation between model and RGPS estimates, November 1997 to April 1998. Model-derived regional boundaries are in black, RGPS boundaries are in color. Vectors (model in

black, RGPS in color) near the center of each region show the average displacement of the boundary samples computed from model and RGPS data. 44
Figure 14. Differences in regional advection and deformation between model and RGPS estimates, October 1998 to April 1999. Model-derived regional boundaries are in black, RGPS boundaries are in color. Vectors (model in black, RGPS in color) near the center of each region show the average displacement of the boundary samples computed from model and RGPS data. 45
Figure 15. Differences in regional advection and deformation between model and RGPS estimates, November 1999 to April 2000. Model-derived regional boundaries are in black, RGPS boundaries are in color. Vectors (model in black, RGPS in color) near the center of each region show the average displacement of the boundary samples computed from model and RGPS data. 46
Figure 16. Differences in regional advection and deformation between model and RGPS estimates. RGPS results (top row) from 2000–2001 season are compared to two seasons ((1990–1991 and 1991–1992) of each model run; RACMa (second row), RACMb (third row), RACMg (fourth row), and RACMh (fifth row). Model-derived regional boundaries are in black, RGPS boundaries are in color. Vectors (model in black, RGPS in color) near the center of each region show the average displacement of the boundary samples computed from model and RGPS data. 51
Figure 17. Examples showing correspondence between patterns of 6-day shear deformation from model fields and RGPS estimates. Linear kinematic features (indicated by arrows) in the model seem to line up with patterns from RGPS results (Adapted from Kwok et al. 2008). 55
Figure 18. December 1997 shear example with 6-day average model field shown (top row) with comparison of daily shear snapshots from the same 6-day period (bottom two rows). Additional features present in daily snapshots compared to 6-day average. 57
Figure 19. February 1997 shear example with 6-day average model field shown (top row) with comparison of daily shear snapshots from the same 6-day period (bottom two rows). Additional features present in daily snapshots compared to 6-day average. 58
Figure 20. December 1996 example of alternative shear calculations from POP-CICE S3 model output. Top rows show shear deformations from multi-day averaged velocity fields, averaged through division of the number of time steps in the 6-day window. Bottom rows show a summation of the shear deformations from multi-day averaged velocity pairs at different time steps. 61
Figure 21. December 1997 example of alternative shear calculations from POP-CICE S3 model output. Top rows show shear deformations from multi-day averaged velocity fields, averaged through division of the number of time steps in the 6-day window. Bottom rows show a summation of the shear

deformations from multi-day averaged velocity pairs at different time steps....62
Figure 22. December 1998 example of alternative shear calculations from POP-CICE S3 model output. Top rows show shear deformations from multi-day averaged velocity fields, averaged through division of the number of time steps in the 6-day window. Bottom rows show a summation of the shear deformations from multi-day averaged velocity pairs at different time steps....63
Figure 23. December 1999 example of alternative shear calculations from POP-CICE S3 model output. Top rows show shear deformations from multi-day averaged velocity fields, averaged through division of the number of time steps in the 6-day window. Bottom rows show a summation of the shear deformations from multi-day averaged velocity pairs at different time steps....64
Figure 24. February 1996 example of alternative shear calculations from POP-CICE S3 model output. Top rows show shear deformations from multi-day averaged velocity fields, averaged through division of the number of time steps in the 6-day window. Bottom rows show a summation of the shear deformations from multi-day averaged velocity pairs at different time steps....65
Figure 25. February 1997 example of alternative shear calculations from POP-CICE S3 model output. Top rows show shear deformations from multi-day averaged velocity fields, averaged through division of the number of time steps in the 6-day window. Bottom rows show a summation of the shear deformations from multi-day averaged velocity pairs at different time steps....66
Figure 26. February 1998 example of alternative shear calculations from POP-CICE S3 model output. Top rows show shear deformations from multi-day averaged velocity fields, averaged through division of the number of time steps in the 6-day window. Bottom rows show a summation of the shear deformations from multi-day averaged velocity pairs at different time steps....67
Figure 27. February 1999 example of alternative shear calculations from POP-CICE S3 model output. Top rows show shear deformations from multi-day averaged velocity fields, averaged through division of the number of time steps in the 6-day window. Bottom rows show a summation of the shear deformations from multi-day averaged velocity pairs at different time steps....68
Figure 28. Time series (1997–1998) of the mean 6-day regional shear derived from model and RGPS ice drift for regions S1 through S5 (defined previously) between November 1997 and April 1998. 70
Figure 29. Time series (1998–1999) of the mean 6-day regional shear derived from model and RGPS ice drift for regions S1 through S5 (defined previously) between November 1998 and April 1999. 71

Figure 30. Time series (1999–2000) of the mean 6-day regional shear derived from model and RGPS ice drift for regions S1 through S5 (defined previously) between November 1999 and April 2000. 72

LIST OF TABLES

Table 1. Average seasonal RGPS displacements (Drgps) of the boundary points of the five regions, model displacements (Dmodel) as a fraction of Drgps, directional differences ($\Delta\theta$) between model and RGPS displacement vectors (negative to the right of RGPS vector), seasonal percentage area change of the five regions, and model area change difference from RGPS estimates.....48

Table 2. Average seasonal RGPS displacements (Drgps) of the boundary points of the five regions, model displacements (Dmodel) as a fraction of Drgps, directional differences ($\Delta\theta$) between model and RGPS displacement vectors (negative to the right of RGPS vector), seasonal percentage area change of the five regions, and model area change difference from RGPSestimates.....53

Table 3. Statistical comparison of seasonal shear values from Figures 28 through 30. Mean, Standard Deviation (Std Dev), Maximum (Max), Minimum (Min), and Correlation (CORREL) values of shear are displayed by region (all values $*10^{-2}$). 73

THIS PAGE INTENTIONALLY LEFT BLANK

LIST OF ACRONYMS AND ABBREVIATIONS

AD	Arctic Dipole
AMD	Air and Missile Defense
AMSA	Arctic Marine Shipping Assessment
AO	Arctic Oscillation
AR4	Fourth Assessment Report
ASF	Alaska SAR Facility
AVHRR	Advanced Very High Resolution Radiometer
CAA	Canadian Arctic Archipelago
CBA	Capabilities Based Assessment
CICE	Community Ice CodE
CSA	Canadian Space Agency
DA	Arctic Dipole Anomaly
DoD	Department of Defense
ECMWF	European Centre for Medium–Range Weather Forecasting
EVP	Elastic–Viscous–Plastic
FY	First Year
GHG	Greenhouse Gas
HA/DR	Humanitarian Assistance/Disaster Relief
HSPD	Homeland Security Presidential Directive
IABP	International Arctic Buoy Program
IBCAO	International Bathymetry Chart of the Arctic Ocean
ICESat	Ice, Cloud, and land Elevation Satellite
ICEX	Ice Exercise
IPCC	Intergovernmental Panel on Climate Change
ISR	Intelligence, Surveillance, and Reconnaissance
ITP	Ice–Tethered Profiler
JPL	Jet Propulsion Laboratory
LANL	Los Alamos National Laboratory
LIM	Lagrangian Ice Motion
LKF	Linear Kinematic Feature

MDA	Maritime Domain Awareness
MIZ	Marginal Ice Zone
MEaSUREs	Making Earth Science data records for Use in Research Environments
MSL	Mean Sea Level
MY	Multi–Year
NAME	Naval Postgraduate School Arctic Modeling Effort
NAO	North Atlantic Oscillation
NAM	Northern Annular Mode
NASA	National Aeronautics and Space Administration
NCAR	National Center for Atmospheric Research
NCEP	National Center for Environmental Prediction
NORAD	North American Aerospace Defense Command
NPS	Naval Postgraduate School
NSIDC	National Snow and Ice Data Center
NSPD	National Security Presidential Directive
NSR	Northern Sea Route
ONR	Office of Naval Research
PIPS	Polar Ice Prediction System
POP	Parallel Ocean Program
QDR	Quadrennial Defense Review
RACM	Regional Arctic Climate System Model
RGPS	RADARSAT Geophysical Processor System
SAR	Synthetic Aperture Radar
SAT	Surface Air Temperature
SCICEX	Scientific Ice Expedition
SLP	Sea Level Pressure
SMMR	Scanning Multichannel Microwave Radiometer
SSM/I	Special Sensor Microwave/Imager
TDS	Transpolar Drift Stream
TFCC	Task Force Climate Change
ULS	Upward Looking Sonar
UNCLOS	United Nations Convention on the Law of the Sea

UN	United Nations
UNEP	United Nations Environment Programme
USGS	U.S. Geological Survey
USCG	U.S. Coast Guard
VIC	Variable Infiltration Capacity
WMO	World Meteorological Organization
WRF	Weather Research and Forecasting

THIS PAGE INTENTIONALLY LEFT BLANK

ACKNOWLEDGMENTS

The quality of this work would not have been possible without the guidance and support of my advisor, Wieslaw Maslowski. His depth of knowledge on the subject of Arctic sea ice was an inspiration for this work as he provided the direction necessary to navigate this complex and important topic. Thank you for keeping me on track and guiding my efforts towards a better understanding of this dynamic environment.

I would like to offer special thanks for the collaborative efforts of Ron Kwok and Shirley Pang at the Jet Propulsion Laboratory. The generosity of time and assistance given to the incorporation and adaptation of their previous work was instrumental in defining and validating this work. It has been a pleasure to work with you both, and I truly appreciate your collective efforts to provide the background upon which this study was based.

A debt of gratitude is owed to Jaclyn Clement Kinney, as significant portions of this work would not have been possible without her insight and unflagging support in both the technical aspects of programing and analyzing data, as well as her assistance in the writing portion. Thank you for your ability to translate complex issues into basic, fundamental concepts.

Thank you to Andrew Roberts, whose efforts in this thesis process and in-depth comprehension of sea ice dynamics and modeling truly helped tie this thesis together. Thanks to Robert Osinski for the development of the CICE model and to Steve Okkonen who greatly helped with the programing effort.

I would also like to thank my family and friends, especially my mother, for supporting me in this effort and for providing the foundation upon which all of my successes depend.

Lastly, I would like to thank my wife, who not only inspires me to be a better person, but also drives me and supports my every effort in both the professional and personal realm. Thank you dearly for your abiding love and encouragement.

This work is dedicated to the memory of my father, whose love of all things frozen inspired and guided my life from a rink in the back yard, to the mountains in winter, and now to exploring the Arctic.

I. INTRODUCTION

A. BACKGROUND AND MOTIVATION FOR SEA ICE RESEARCH

The Earth's climate system is a constantly changing environment, which can be considered in balance only through the interdependence of its dynamic constituents. While the atmosphere tends to capture our attention on a daily basis through changing weather patterns, it is the ocean's variability and its interaction with the atmosphere that provide the main controls on large-scale climate patterns (Bindoff et al. 2007). Understanding air-sea interactions has been integral to our comprehension of how the climate reacts to the global changes that have been observed in recent history. One of the emerging areas for climate research is to study the Arctic, where a layer of sea ice has perennially altered the air-ocean interface. The sea ice acts as a barrier between the ocean and atmosphere, and the kinematics of this ice greatly impacts the heat exchange, momentum flux, and mass balance of sea ice in the Arctic (Rampal et al. 2009; Moritz et al. 2002). Changes to sea ice coverage due to kinematic forcing have large implications for these balances and climate at hemispheric and global scales more generally (Kwok and Sulsky 2010; Alexeev 2010).

Over the last several decades, observations of the Arctic point towards a greatly diminished ice cap due to a variety of environmental factors. While global temperatures have been on the rise over the last century, the Arctic atmosphere has warmed by almost two times the global average in the last 100 years (IPCC 2007a). This trend has been largely attributed to changes in the last 20 to 40 years, where surface air temperature increased significantly greater than previous rates (Overland et al. 2004; Chylek et al. 2009). This enhanced temperature increase in the Arctic has been well documented and has been attributed to a positive feedback loop unique to ice covered regions (Perovich et al. 2007; Serreze et al. 2009). As the climate warms, the length and intensity of the melt season is increased which leads to less sea ice surviving to the next fall. This increases the absorption of solar energy by the open ocean, which increases its sensible heat content (Serreze et al. 2009). This additional oceanic heat delays the formation of new ice in the fall and winter, promoting enhanced upward heat fluxes into the atmosphere,

which is maintained in the lower troposphere by strong low-level stability (Serreze et al. 2009). This polar amplification is caused in part by the dark ocean surface left behind from the melting process, which has a much lower albedo (~0.07), a measure of surface reflectivity as a fraction of the incident solar radiation, than bare sea ice or snow-covered ice (0.65 to 0.85) (Perovich et al. 2002). Larger open water surface and heat content of the upper ocean can not only further melt sea ice, but also alter oceanic and atmospheric circulation patterns, and add more water vapor into the lower atmosphere by releasing heat stored in the mixed layer before freezing in the fall. This amplifies the impact on air temperature increase as water vapor causes a regional greenhouse effect to the lower atmosphere (Langen and Alexeev 2007). The positive feedback loop has helped to perpetuate the increased warming conditions recently observed in the Arctic, and is one of the reasons scientists fear that this region might be approaching a new regime of seasonal sea ice coverage.

The primary observational evidence of this negative trend in sea ice has been in the analysis of sea ice extent from satellite passive microwave imagery since the late 1970s (Johannessen et al. 2004; Comiso et al. 2008; Kwok et al. 2008; Kwok and Sulsky 2010). Sea ice extent is defined as the area of ocean with at least 15 percent sea ice coverage (within a satellite footprint). This definition allows for the inclusion of melt ponds on the ice pack to alleviate the inability of satellite imagery to differentiate between water from these features (with sea ice below) and that of open ocean. Based on this definition, sea ice in the Arctic region has extended from 14 to 16 million square kilometers in late winter (March) and from six to eight million square kilometers by the end of each summer (September) during 1979-2000 (National Snow and Ice Data Center (NSIDC) 2011). In the last decade however, sea ice extent in September has been trending between 4 to 6 million square kilometers of coverage (Figure 1). This decline in ice extent was one of the first indicators of accelerating climate warming in the Arctic, which can be linked to the positive feedback loop related to the ice-albedo effect.

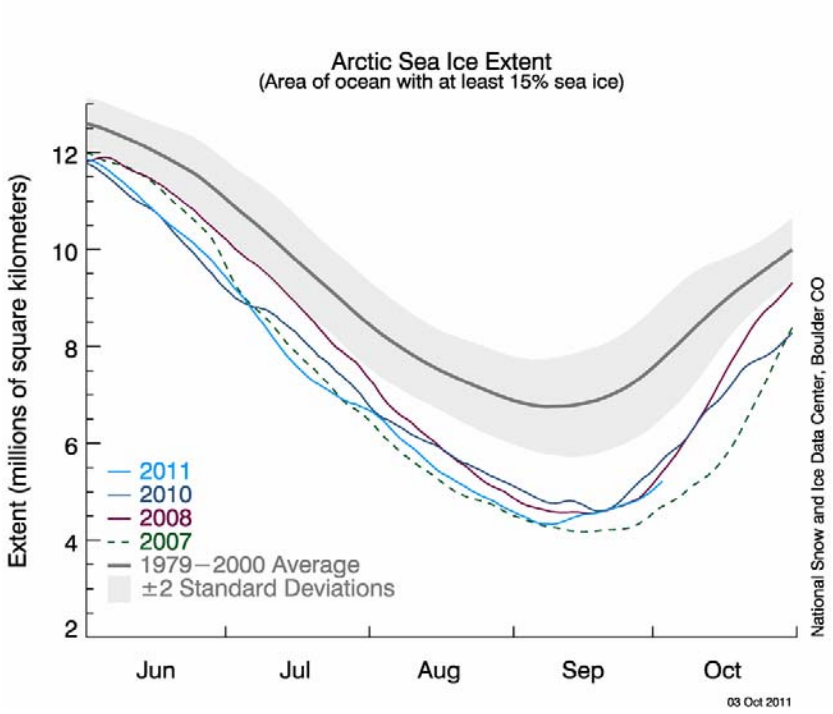

Figure 1. Arctic sea ice extent through September 2011 (From National Snow and Ice Data Center [NSIDC] 2011)

1. Atmospheric Influences

Sea ice loss is not limited to reduction in just areal extent, however, as export of old and thick ice out of the Arctic basin and thermodynamic forcing from the ocean and atmosphere has led to a decrease in overall ice thickness as well. The thickness of sea ice influences characteristics of the ice cover as a thermodynamic barrier as well as greatly impacting the dynamic nature of ice motion. Dynamic processes in sea ice are determined by ice thickness, strength, and the coupling of forces from the air above and ocean below. Ice motion has been linked to large-scale atmospheric circulation patterns associated with the Arctic Oscillation (AO) or the North Atlantic Oscillation (NAO), also referred to as the Northern Annular Mode (NAM) (Thompson and Wallace 1998; Serreze et al. 2007). The AO develops as atmospheric pressure patterns around Iceland and Azores dominate the regional flow field for extended periods of time. A positive phase of the AO occurs when a negative sea level pressure (SLP) anomaly remains over the pole with a positive SLP anomaly dominating the mid-latitudes, and a negative phase

occurs when this pattern is weakened or reversed. The NAO is seen as a pattern on the Atlantic side that works to amplify or diminish the effects of the AO through the covariability between the strength of the Icelandic Low and the Azores High (Serreze et al. 2007). During a positive NAO, a strong low pressure system is present in the North Atlantic near Iceland, and a strong high pressure system is seen in the subtropics near the Azores, which combined increase the intensity of the Westerlies across the midlatitudes deflecting the storm track further north into the Arctic (Maslanik et al. 1996; McPhee et al. 1998). Changes in storm tracks can either increase (+NAO) or decrease (-NAO) the energy and atmospheric mass imported to the Arctic, which determines the overall strength of the AO (Serreze et al. 2007).

While the AO/NAO/NAM have an impact on weather patterns and storm propagation in the mid-latitudes, in the Arctic they also impact the flow of sea ice as pressure differences can change prevailing wind patterns. During a negative phase of the AO, a positive pressure sets up an anticyclonic (clockwise), zonal flow in the Beaufort Gyre, which is believed to cause the ice to converge and raft in this region due to Coriolis forcing. This process would allow sea ice to increase in thickness and remain longer in the Arctic basin, which would lead to an increase in the presence of older, thicker ice. During a positive phase of the AO, this atmospheric pattern is weakened or reversed which would tend to allow ice to flow more freely along the principle pathway out of the Arctic through Fram Strait, between Greenland and Svalbard (Figure 2). From the late 1980s through the mid-1990s, the AO entered a strongly positive phase, which was seen as the primary atmospheric forcing that lead to an increased ice export through Fram Strait and the decrease in sea ice thickness as it was thought to induce both the warming and export necessary to account for the observed trends (Thompson and Wallace 1998; Rigor and Wallace 2004). Since 2002, however, the AO has shifted back to a largely neutral to negative phase, while sea ice extent record lows have continued to be observed throughout the last decade (Maslanik et al. 2007). This has led climate scientists to search for a new explanation for the rapid ice loss in the Arctic, or to question whether or

not sea ice presence in the Arctic has reached a new regime of the overall forcing that determines ice motion and seasonal survivability of ice within the region (Lindsay and Zhang 2005).

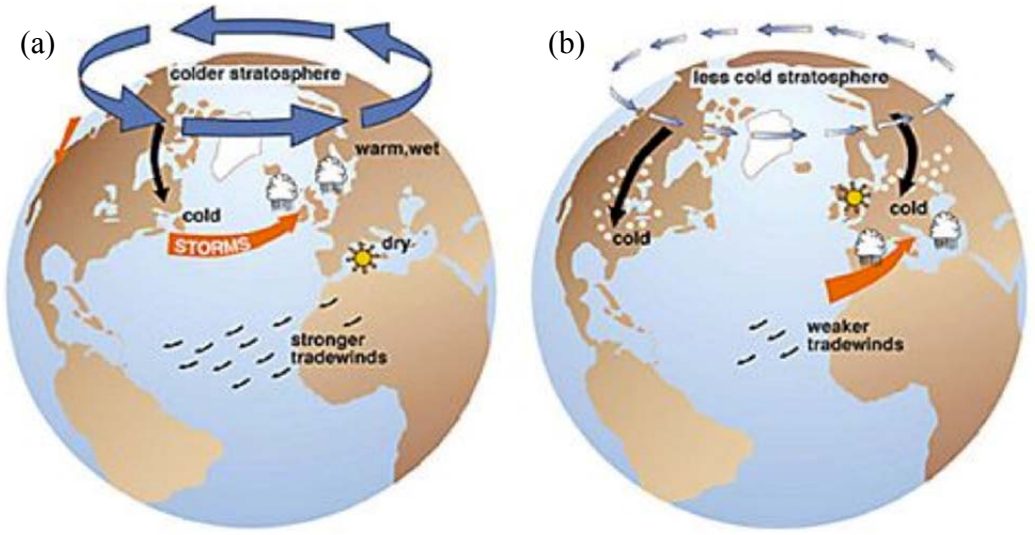

Figure 2. Sketch of a (a) positive phase and a (b) negative phase of the Arctic Oscillation induced atmospheric patterns (From Wallace 2011).

A refined look at the atmospheric forcing has revealed that the second leading mode of the sea level pressure (SLP) anomalies in the Arctic winter (Oct – Mar) might be gaining importance recently with regard to sea ice motion, when compared to the AO (Wu et al. 2006). This pattern is known as the Arctic Dipole Anomaly (DA), or simply Arctic Dipole (AD) in other publications, which is determined by a more local SLP fluctuation where pressure centers over the Laptev Sea (near Siberia) and the Greenland Sea cycle between positive and negative phases in a dipole structured pattern that induces meridional flow (Watannabe et al. 2006; Overland and Wang 2010). While the DA only accounts for 14–19% of the Arctic's variance in SLP (as opposed to 59–63% from AO), it remains important to the advection of sea ice within and out of the Arctic basin since it drives the position of these local pressure centers. A positive phase of the DA is associated with a negative SLP anomaly on the North American side of the Arctic (Overland and Wang 2010). While the anomalous centers of this pattern vary in space, when the positive SLP anomaly is over the western Arctic and the negative SLP anomaly

is over the Greenland Sea, atmospheric forcing increases ice flow along the Transpolar Drift Stream (TDS) due to the meridional nature of the forcing (Wu et al. 2006; Richter-Menge and Overland 2009). This forcing also sets up an acceleration of the melting process in the western Arctic as the oceanic heat flux through Bering Strait is increased, causing delayed formation of new ice in fall and earlier onset of melting in the Chukchi and East Siberian Seas in spring (Wang et al. 2009).

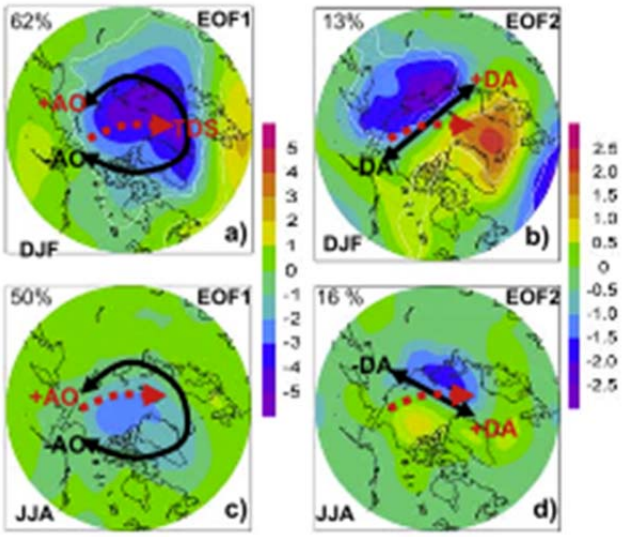

Figure 3. Regression maps of the first two leading modes to the (a and b) winter and (c and d) summer mean Northern Hemisphere SLP field using the NCEP Reanalysis dataset from 1948 to 2008. Contour intervals are 0.5 hPa (see color bars). The black arrows in (a) and (c) indicate the cyclonic (anticyclonic) wind anomaly during the +AO (-AO). In (b) and (d), the black arrows indicate wind anomalies between the western and eastern Arctic during +DA and –DA phases that accelerate or decelerate the TDS (in red-dashed arrows), respectively
(From Wang et al. 2009).

The DA's relative importance to sea ice export and melt was expanded upon by Wang et al. in 2009, as they ran global climate models (GCMs) with forcing from the National Center for Environmental Prediction and the National Center for Atmospheric Research (NCEP/NCAR) reanalysis datasets of years (1948–2004) that included all potential combinations of both AO and DA. They found that regardless of the sign of the AO, sea ice export was greatly increased during years with a positive phase of the DA.

This is likely due to the directional dependence of the TDS, which parallels the Greenwich meridian during years of positive DA, leading to more sea ice export out of the Arctic basin due to the strong low pressure anomaly in the Greenland Sea. During years of negative DA, more ice tends to be held within the basin as the Beaufort gyre is strengthened and flow along the TDS is weakened, which accumulates more ice and fresh water in that region (Wu et al. 2006). A negative DA pattern can however push more ice back into the Arctic leaving more open water in the North Atlantic, which can increases the amount of heat storage in the ocean and eventually impacts the atmospheric circulation through release of this excess heat in fall, preconditioning ice for more retreat in following seasons (Overland and Wang 2010).

2. Sea Ice Thickness

Increased sea ice flow out of the Arctic correlated to these atmospheric forcing patterns in recent years not only increases the ice-albedo effect through an increase in the area of open ocean, but it greatly impacts the distribution of older and thicker ice. Observations of average annual sea ice area flux from satellite imagery from 1978–2002 show a mean rate of approximately 866,000 km^2/year southward through Fram Strait (Kwok et al. 2004a). This average rate was heavily influenced by recent increase in the fluxes where the net exported areal extent was ~400,000 km^2 greater in the 1990s than in the 1980s (Kwok et al. 2004a). The increased export of almost half the annual areal average has influenced the thickness and age distribution, as some of the formerly resilient ice has been flushed out of the Arctic during this period. Data derived from upward looking sonar (ULS) thickness distributions across Fram Strait over an eight year period from 1991 – 1998 provides an estimated average annual ice volume flux of ~2200 km^3 of sea ice through Fram Strait (Kwok et al. 2004a). This volume flux corresponded to a period of overall thickness decrease of 0.45m in the Arctic region through the early 2000s, with a greater decrease of 0.55m in multi-year (MY) ice when compared to previous annual averages (Kwok et al. 2004a). This increased export and decrease in sea ice thickness occurred over a period of consistently high positive AO in both fall (Oct–Dec, 1988–1994) and winter (Jan–Mar, 1989–1997), which helped to trigger the observed sea ice response (Thompson and Wallace 1999; Overland and Wang 2010).

Ice thickness is difficult to observe at basin scale as transects of submarine observations from under the ice cap are limited snapshots in time, moored buoys are only possible at particular points in space, and ice cores are limited in both space and time. The Scientific Ice Expeditions (SCICEX) program, started in the 1990s by the U.S. Navy, sought to address the need for observational data by involving scientists into the planning and actual measurement of ice thickness during dedicated science cruises. While still limited in basin wide coverage, this data collection program provided the best ice thickness data set to date. It has allowed for comparison with previous data released by the Navy from cruises that were declassified from the Cold War era operations from the 1950s to the late 1970s (SCICEX Science Advisory Committee 2010). Analysis of this data revealed that the ice draft along similar transects from the central Arctic basin had decreased by over a meter in the 1990s from the over three meter averages taken from submarine cruises in previous decades (Rothrock et al. 1999). This significant reduction in thickness corresponded to a total sea ice volume reduction of around 40% in a matter of a few decades, which was largely attributed to large heat fluxes from the ocean and atmosphere (Rothrock et al. 2003). An alternative explanation of this volume reduction (Holloway and Sou 2002) has been that the measured thickness changes were due to the redistribution of ice outside the submarine tracks toward the Canadian Archipelago and Siberian shelves. This shows that while the data collected during the 1990s are a vast improvement over the sporadic data available from previous naval operations, they are still limited spatially by narrow range transects of observations and temporally due to the exercise sampling only in late summer months.

To combat these spatial and temporal limitations in ice thickness data, techniques have been developed recently to estimate sea ice age and thickness through a measurement of freeboard from satellite imagery taken from the Ice, Cloud, and land Elevation Satellite (ICESat) campaign, which can cover nearly the entire basin (up to 84^{o}N) and can be measured throughout the year (Kwok et al. 2004b; 2007). Freeboard is the height of ice and snow that is above mean sea level (MSL), from which the ice thickness can be estimated. This approach assumes hydrostatic equilibrium and that snow depth and ice density are known (Kwok and Cunningham 2008). Snow characteristics

are difficult to differentiate from satellite imagery alone, so initial estimates have to be taken from climatology and meteorological products to estimate snow density and distribution throughout a given season. While limitations in estimating the seasonal snow cycle remain, ICESat analysis using these assumptions has given rise to regional estimates with an uncertainty in thickness calculations of ~0.7m. Recent ICESat observations and subsequent estimates of ice thickness have been validated by comparison to submarine and buoy data. The variance between ICESat draft and submarine draft was calculated to be 0.42m (Kwok and Rothrock 2009), while comparisons with buoy data estimates are within 0.5m of buoy observations (Kwok and Cunningham 2008). When used in conjunction with these datasets, satellite derived ice thickness offer an overall picture of basin-wide characteristics of the Arctic sea ice thickness distribution and trends (Figure 4) (Kwok et al. 2009; Kwok and Rothrock 2009). Additional satellite imagery techniques will be further described in following chapters.

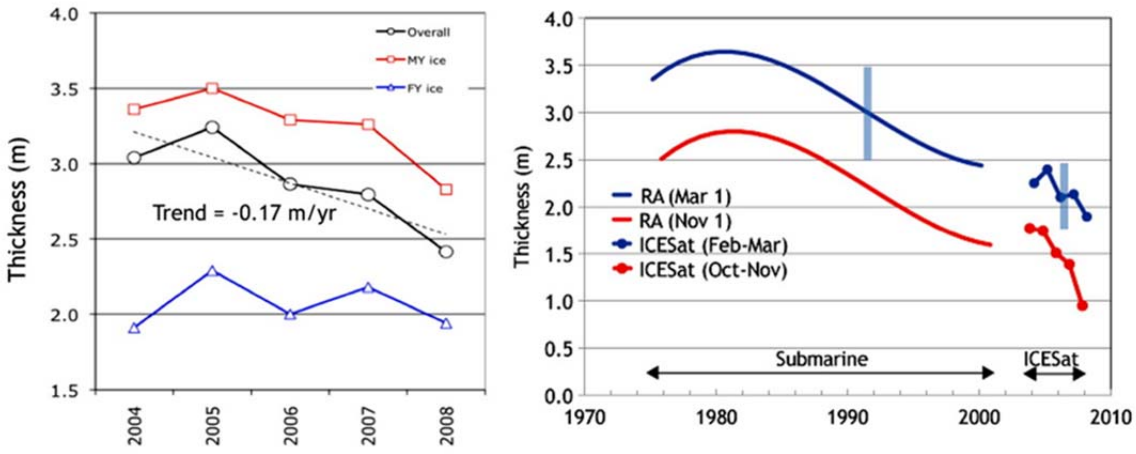

Figure 4. (a) Winter Arctic Ocean sea ice thickness from ICESat (2004-2008). (b) Interannual changes in ice thickness from the submarine (RA) and ICESat campaigns (After Kwok and Rothrock 2009; Kwok and Sulsky 2010).

3. Sea Ice Age

Given the difficulty in measuring sea ice thickness, ice age is used as a proxy for thickness estimations. As blocks of ice remain in seawater over several seasons, pockets of brine created during formation get flushed out reducing the salt content and increasing the strength of the remaining sea ice (Tucker et al. 1992). Due to a different salt content, differences in the brightness temperature (a measure of the emissivity of the surface material) of first year (FY) and multi-year (MY) ice (ice that lasts through at least one melt season) can be detected and tracked by satellite images from Scanning Multichannel Microwave Radiometer (SMMR), Special Sensor Microwave/Imager (SSM/I), and the series of Advanced Very High Resolution Radiometer (AVHRR) sensors (Maslanik et al. 2007). Ice age can be derived from a combination of satellite imagery and validated with ocean buoy data where Lagrangian grid cells are tracked throughout the Arctic Ocean and considered to maintain ice through a melt season as long as they contain at least 15% sea ice concentration (Fowler et al. 2004). These cells when tracked over a number of years determine ice age within a given region. This parameter is important to understanding sea ice dynamics as ice strength generally increases with thickness and age due to brine rejection from within the ice (Kovacs 1996). This process not only impacts the salinity of the ocean and the fresh water storage within the Arctic, but also greatly impacts the rigidity and mobility of the pack.

Observations have shown that since the 1980s, MY ice has been diminished from covering ~80% of the Arctic in that decade to only ~30% of the area since the 1990s (Rigor and Wallace 2004, Drobot et al. 2008, Kwok and Cunningham 2010). Along with sea ice export and melt, redistribution of thick, MY ice has shifted the ice-covered area in the Arctic toward younger and thinner ice, which is more prone to move around, ridge, and melt during the next summer. This younger and thinner ice is also more likely to experience abrupt changes in ice export under the same atmospheric and oceanic forcing that it could resist in the past (Maslanik et al. 2007). Since the all-time record minimum in sea ice extent in 2007, areas such as the central Arctic and the Canadian Archipelago that were relatively stable in the past have now lost vast amounts of old and thick ice, which points to an overall shift in the Arctic sea ice cover (Figure 5) (Maslanik et al.

2011). A significant question remaining is whether sea ice dynamics—specifically, the convergence of thinner MY ice coverage—could be misconstrued as a net loss of ice from melt or export, while it actually represents a reduction in the ice area (Kwok and Cunningham 2010).

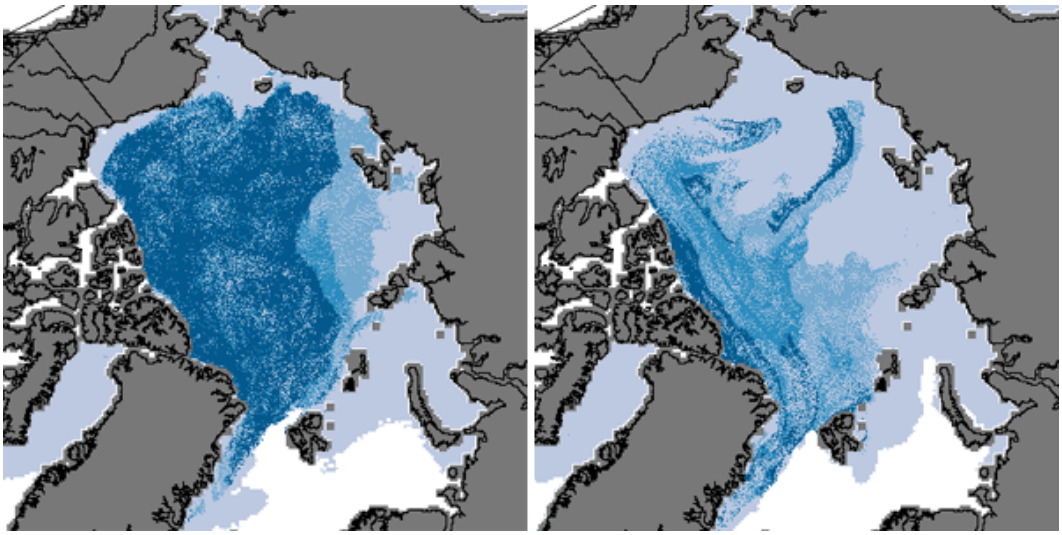

Figure 5. Median age of March sea ice in 1985 (left) and 2011 (right). Overall, the proportion of young ice (light blue) has increased. By March 2011, ice more than four years old (dark blue) accounts for less than 10 percent of the Arctic ice cover (From Maslanik et al. 2007)

B. INTENT OF STUDY

Sea ice extent, age, and thickness have been on the decline in the Arctic over the past several decades, and record low ice concentration and thickness are becoming commonplace at the end of each summer. Data from satellites, buoys, ice-tethered profilers (ITPs), and submarine-based sensors all point to an increasing trend toward seasonal ice coverage in the region. Understanding the mechanisms that drive these trends is the key to determining whether this pattern will continue, or if natural variability is capable of forcing a reversal. There are two types of forces that impact sea ice response to climatic changes in the Arctic: thermodynamic and dynamic forcing. Thermodynamic processes involve changes in surface air temperature (SAT), radiative

fluxes, and oceanic heat transport, while dynamic processes involve changes in sea ice motion and circulation in response to oceanic and atmospheric forcing (Serreze et al. 2007). This study focuses on the kinematics of sea ice in the Arctic to help determine model capabilities in representing the behavior of sea ice.

While few contemporary studies have analyzed these processes, the scientific community has recently begun to look at the dynamical forcing that determines the distribution and mechanical characteristics of sea ice (Rothrock and Zhang 2005; Kwok et al. 2008; Rampal et al. 2009). Understanding the relative contribution of dynamic processes to sea ice state will help improve the current understanding of the role sea ice plays in the Arctic response to climate change. Advances in computing power have offered the possibility of modeling of fine scale processes and forcing to better represent the sea ice thickness distribution in the Arctic and the survivability of sea ice in a given year. Through the analyses of observed and modeled dynamic processes of sea ice drift and deformation presented here, we aim to improve the understanding of the recent changes observed in Arctic sea ice.

Numerical modeling remains a key method of analysis and synthesis of air-ocean-sea ice interactions. While the preponderance of observations remain to be of atmospheric processes and model re-analyses, which have led to many studies on the atmospheric forcing of Arctic sea ice (Serreze et al. 2003, 2007; Stroeve et al. 2005, 2011; Perovich et al. 2007), a better understanding of the sea ice dynamical response to this forcing, and its influence on thickness distribution has been largely overlooked. When looking at the overall heat budget and the increased energy required to melt or deform Arctic sea ice in the manner that has been recently observed, it has become clear that atmospheric forcing alone is not sufficient to account for this loss (Francis et al. 2005; Maslowski et al. 2007). Sea ice deformation and oceanic forcing therefore have to be more closely analyzed to determine their role in the recent decline of sea ice extent and thickness.

C. OVERVIEW

This study analyzes model results from several regional Arctic models developed and maintained at the Naval Postgraduate School (NPS). The model domain includes the sub-Arctic North Pacific and North Atlantic Oceans, the Arctic Ocean, the Canadian Archipelago and the Nordic Seas. The main focus is on the effects of dynamic forcing on sea ice thickness, distribution, and variability within the Arctic region. Seasonal, regional, and interannual variability in sea ice motion fields and deformation rates are investigated. The model results for the Arctic region are synthesized with observational data from RADARSAT imagery to make comparisons to observed sea ice deformation based on previous studies.

This thesis is organized into the following chapters: Chapter II describes U.S. Navy relevance of sea ice research in the Arctic; Chapter III describes the models and data analysis methodology used to conduct this research; Chapter IV presents results and provides discussion; Chapter V consists of a summary and conclusions and; Chapter VI makes recommendations for future research.

THIS PAGE INTENTIONALLY LEFT BLANK

II. NAVY RELEVANCE

International interest in the state of the Arctic has grown in recent years as observations of increasingly open ocean area in summertime have validated what had been reported for decades by the Intergovernmental Panel on Climate Change (IPCC). The IPCC consists of an international scientific body established by the United Nations Environment Programme (UNEP) and the World Meteorological Organization (WMO) in 1988 to report on the current state of knowledge on climate change and its potential environmental and socioeconomic impacts (IPCC 2012). This group is an open consortium of scientists that compiles a report periodically with the intent of building consensus on drivers of observed climate change in a peer-reviewed environment. With the release of its fourth assessment report in 2007 (AR4), the IPCC gained widespread geopolitical attention with its assertion that anthropogenic forcing, specifically the extensive release of greenhouse gases (GHG) from human activities, was causing an amplified impact on melting ice and warming temperatures in the Arctic region (IPCC 2007a).

Although the United States (U.S.) has territorial claims to resources extending from its coast and has operated in the Arctic for exploratory, scientific, and military purposes, it has lacked clearly defined guidance for the management of its interests in the region until recently. Since the Cold War concluded in the early 1990s, the U.S. interest in the Arctic from a military perspective has been on the decline as the former Soviet Union collapsed and the emerging Russian Federation has developed improved relations with the U.S. government. Apart from the U.S. and Russian dynamic, including their geopolitical history and close proximity in the Bering Strait, the Arctic maintains a unique set of geographic challenges based on the number of nations that claim national interest in the region. The Arctic Ocean is confined by remote landmasses of five stakeholder nations including the U.S., Canada, Russia, Norway, and Denmark (Greenland) (Figure 6). These countries along with Finland, Iceland, Sweden, and indigenous representatives developed what is known as the Arctic Council in 1996 as a forum for international cooperation with the intent of protecting national interests and

regulating disputes with a focus on sustainable development and environmental protection (Arctic Council 1996). This body is limited in its authority, however, to oversee legitimate international agreements or impose legally binding restrictions on nations for abusing natural resources or disregarding sovereignty claims due to the U.S. refusal to accept security concerns as part of the Council's charter (Borgerson 2008).

Figure 6. Map of the Arctic Region showing the Arctic Ocean, adjacent seas and political boundaries. Red line shows average 10°C isotherm for July (From U.S. Central Intelligence Agency, 2012).

A. STRATEGIC GUIDANCE

The leading international treaty concerning maritime affairs including the rights and responsibilities of nations for their use of the ocean, as well as guidelines for economic and environmental resources within the world's oceans is the United Nations Convention on the Law of the Sea (UNCLOS). This treaty, which was internationally recognized in 1994, defines the rights of navigation through national and international waters and sets up key provisions for long-disputed territorial claims including continental shelf extent and exclusive economic zones. Over the last century, many nations have debated the definitions that determine their rights to surrounding waters, and the geographical limits of these regions have been extended multiple times. That which was once a three nautical mile extent from the coastal reaches of a nation has been pushed out to a 200 nautical mile exclusive economic zone in which mineral resources and fisheries in this oceanic region can be exploited and protected by that state. While the United States agrees with much of this document, Congress has failed to ratify UNCLOS based on a dispute in Part XI of the Convention, which relates to mineral definitions beyond the twelve mile territorial waters of a state, that has been deemed to be in conflict with American economic and security interests. Based on this discrepancy, the U.S. is not a signatory nation to this unique document and therefore is not currently part of the UN commission which would have jurisdiction over debated rights to resources in regions such as the Arctic (Borgerson 2008).

Despite this discord, recent guidance has been initiated due to gaining acceptance of the IPCC report, growing international recognition for the validity of its contents, and the increased interest in the utilization of the vast resources in the Arctic. In 2009, President George W. Bush signed the National Security Presidential Directive (NSPD) 66 / Homeland Security Presidential Directive (HSPD) 25. This directive was the first in a series of strategic guidance documents that began to define the national security interests and objectives for U.S. diplomacy and potential operational capabilities in the Arctic. Along with its support to ratify UNCLOS, this mandate established requirements for the U.S. to develop and maintain greater capacity to protect sovereign interests extending from our boarders to the extent of the continental shelf, and to increase maritime domain

awareness and global mobility through an enhanced ability to operate within the Arctic (Task Force Climate Change / Oceanographer of the Navy 2011).

In an effort to address the impact of the environmental concerns outlined in the Presidential Directives on naval operations, the Chief of Naval Operations (CNO), Admiral Gary Roughead, created Task Force Climate Change (TFCC) in May 2009. This task force was placed under the direction of the Oceanographer of the Navy, who was charged with an initial goal to develop and implement strategic policy initiatives for the Arctic specifically, and then to follow up with a roadmap for Department of Defense global climate change responses more generally (TFCC / Oceanographer of the Navy 2009). The first actionable document produced was the Navy Arctic Roadmap, which delineated a list of action items to address both the strategic and policy implications of changes in the Arctic, as well as provided a vehicle for the Navy to assess and predict future environmental changes in the region. From a strategic perspective, this document focused on determining the potential impact of increased shipping activity from renewed interest in natural resource exploration, research initiatives, fishing migrations north, and eco-tourism into a more environmentally approachable Arctic. Increased traffic from these activities into this still harsh environment along with the recent opening of interconnected sea routes of the Northwest Passage and the Northern Sea Route across the Arctic in 2008 has rightfully alarmed those who have been operating in the region for some time (Figure 7). Increased activity will undoubtedly bring with it the potential for environmental disasters such as oil spills and increased search and rescue operations as unprepared ships encounter the fast-moving ice in the marginal ice zone (MIZ). This, along with the lack of accurate mapping in the region, due to extensive ice coverage in the past, will likely lead to the need for improved cooperation between Arctic States in order to effectively support the increased operational safety response requirements.

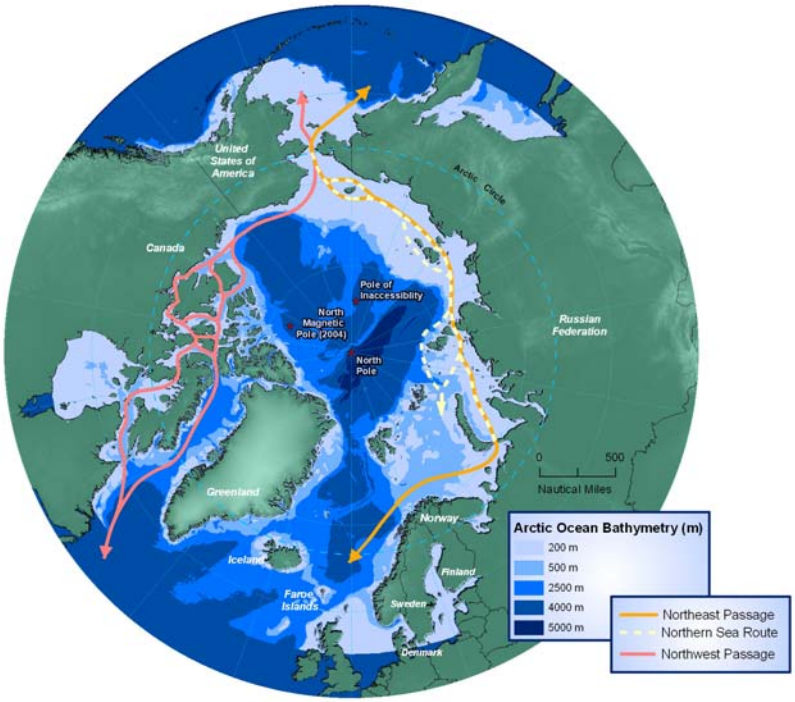

Figure 7. Potential Summer Shipping Lanes (From Arctic Marine Shipping Assessment (AMSA), 2009)

B. ARCTIC NATIONS

Stakeholders in the Arctic all have complex individual and collective relationships with their Arctic neighbors. The Navy Arctic Roadmap listed the development of strong cooperative interagency and international partnerships as one of the primary goals of this renewed focus on the Arctic. The importance of strengthening these relationships is motivated by recent extension claims and disputes over territorial rights of the Arctic region. The Russians have been attempting for over a decade to claim that the underwater Lomonosov Ridge, which extends across the Arctic basin, is an extension of their continental margin and the resources it contains should therefore be considered exclusive property (O'Rourke 2011). The annex of this undersea area would grant Russia over 50% of the Arctic which is estimated by the U.S. Geological Survey (USGS) to hold as much as one-quarter of the world's remaining undiscovered oil and gas deposits (Borgerson 2008). This claim was rejected by the UN in 2001 based on a lack of evidence provided, which the Russians have been working towards ever since. The

Canadian government is particularly opposed to the Russian claim based on their own assertion that part of the Lomonosov Ridge constitutes an extension of their continental shelf. While both countries have proceeded with research intended to produce evidence of their claims, the Russians garnered global attention in 2007 when they used a small submersible vehicle to plant an encased national flag along the ridge at the North Pole (Vasilyeva 2010). Although this act was seen as primarily symbolic, it highlights the potential for brinkmanship that exists when nations debate geographic borders.

Additional disputes have been brought to the forefront as sea ice disappears from the Arctic and new pathways open in this resource-rich environment. The U.S. and Canada dispute their delineated boundary in the Beaufort Sea, Denmark and Canada disagree over the territorial rights to Hans Island between Greenland and Ellesmere Island (Canadian), and Norway and Russia have long disputed an area in the Barents Sea thought to contain vast petroleum deposits under the sea floor (O'Rourke 2011). Some agreement has been achieved between the U.S. and Russia over a contested area of the Bering Sea, and between Norway and Russia in the Barents Sea, but international discourse is continually contested as diminishing natural resources from within the continental margins become increasingly more accessible in the Arctic Ocean (Isachenkov 2010).

The Northern Sea Route (NSR) to the north of the Eurasian continent would open trade between northern Europe and northeast Asia at a potential cost savings in time and money of almost 40% when compared to travel through the Suez Canal (Borgerson 2008). This passage has been dominated by Russian shipping traffic, likely due to their experience in these waters and proprietary rights to mapping documents. The Northwest Passage (NWP), which could potentially run through different routes in the Canadian Archipelago, has potential for cost savings for shipping between northeast North America and northeast Asia as well as routing between northern Europe and northwest North America when compared to canal routes (Suez or Panama) or cape routes (Good Hope or Horn). This path, while more modest in its potential cost savings (~20%) for the shipping community, has been contested by the Canadians as an inland waterway in which their government would maintain sovereignty and control (Borgerson 2008). The

U.S. and the European Union have led an opposing view that the passage constitutes an international strait in which more freedom of passage would prevail (O'Rourke 2011). While diplomatic progress and understandings have prevailed and been sufficient in the past, these passages are becoming more viable options in the summer months, which will require organizations such as the UN to adjudicate some of these disputes in order to keep the relative peace among Arctic Nations.

C. U.S. NAVY ARCTIC CAPABILITIES

The 2010 Quadrennial Defense Review (QDR) identified climate change as one of several key geopolitical trends that may influence future conflict (Office of the Secretary of Defense 2010). It also acknowledged the effect that climate change would have on shaping future operational environments and defining new roles and mission requirements for the Department of Defense (DoD). The impact of these changes has forced the Navy to assess its capabilities and identify shortcomings as a means of adapting to new battlefields and areas of interest in a new climate regime. To implement this new direction, the Navy published the Climate Change Roadmap in 2010 to outline current and desired capabilities in the realm of observing, predicting, and adapting to climate change issues (TFCC 2010). The focus of this effort, as an expansion of the Arctic Roadmap, was to develop a five-year plan of action items to help the Navy determine, through a capabilities based assessment (CBA) process, how prepared it was for the operational challenges ahead and where investments could be most effectively made to prepare for those challenges.

Key findings from this effort were published in both the DoD Report to Congress on Arctic Operations (2011) and the Arctic Environmental Assessment and Outlook Report (2011). These reports identified the operational challenges that exist in this harsh environment. Specifically, communications in the Arctic are significantly limited due to poor satellite connectivity, marginal Global Positioning System coverage, and unreliable long range high-frequency communication capabilities. These limitations are caused by satellite geometry and magnetic and solar phenomena above 70^{o}N that degrade the performance of current communications systems. Surface vessels proceed with difficulty in the Arctic as the equipment they depend on can fail due to icing, while drifting sea ice

and heavy fog conditions impede navigation. Naval air operations are susceptible to similar challenges as ice and weather conditions limit ship maneuverability and increase the difficulty of the launch and recovery of aircraft on icy deck surfaces. In the submarine environment, aside from the avoidance of deep draft sea ice in regions of rafting ice and challenges surfacing in ice covered regions, the acoustic signature can change rapidly as surface water temperature and salinity profiles are altered through the freeze and melt cycle. This process makes acoustic forecast models difficult to predict and warming surface waters can greatly reduce the range of detection capabilities (TFCC 2011).

These environmental factors reduce standard operational capabilities for a Navy that has been built to operate in much warmer climates. Additional significant challenges may arise from a lack of infrastructure and planning for potential operations in this environment. Currently there are no deep draft ports that could support most naval vessels within the Arctic basin. The closest deep water ports are near Baffin Bay at the Air Force base in Thule, Greenland, and in the Aleutian Islands at Dutch Harbor, Alaska (Figure 8). Land-based support facilities are also limited to various service bases in Alaska and Greenland, which leads to dependence on support from our partnership with Canada for use of their bases. In order to achieve the goals of Maritime Domain Awareness (MDA) in the Arctic, the U.S. depends heavily on remote observations from satellites and sporadic data from submarines and aircraft overflight of the region in order to maintain observational coverage for its mission of Intelligence, Surveillance, and Reconnaissance (ISR). Air and Missile Defense (AMD) and Ballistic Missile Defense are well supported missions from an extensive network of early warning radars and communications stations in the region that are monitored from facilities in Alaska and Greenland. This network, along with our relationship with the Canadians as part of the North American Aerospace Defense Command (NORAD) allows the DoD to effectively protect against existing threats in this realm.

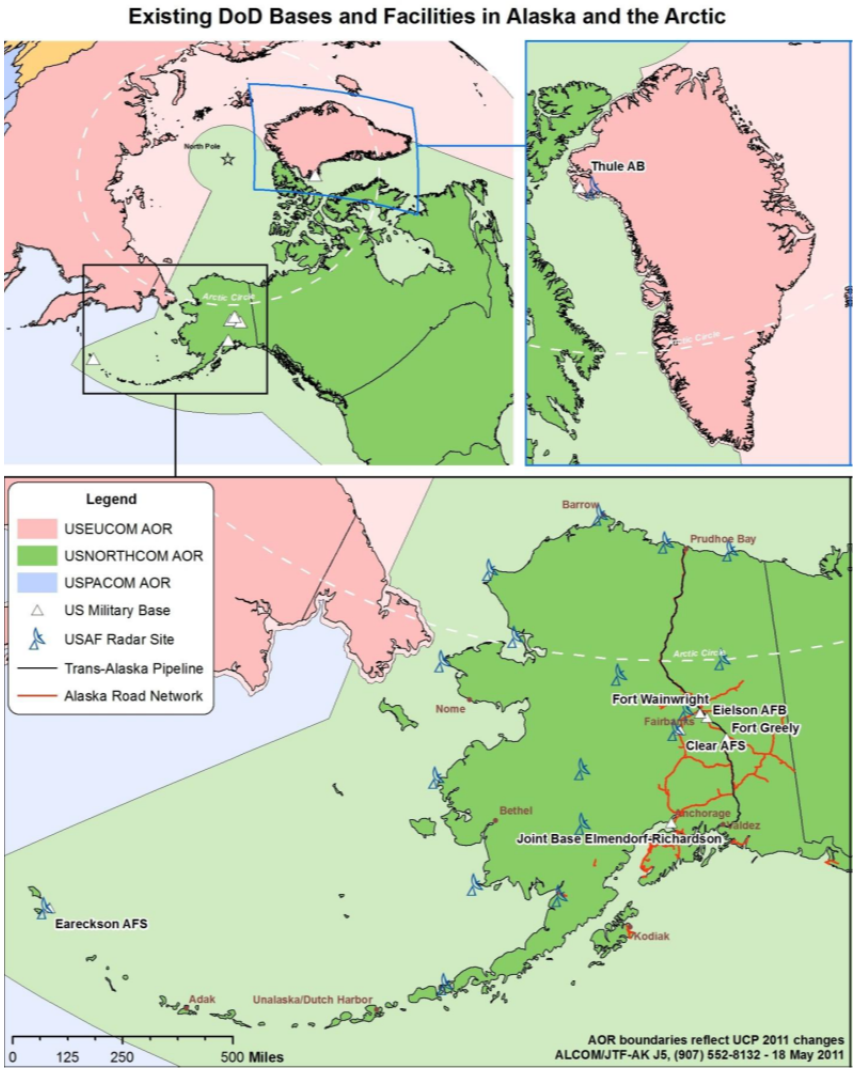

Figure 8. Existing DoD Bases and Facilities in Alaska and the Arctic (From DoD, 2011)

A major point of concern for the Navy's ability to operate in the Arctic as the sea ice continues to recede is the fact that surface ships are not ice-strengthened. In this configuration, Navy ships are not safely deployable into first year ice or even the marginal ice zone without the support of an icebreaker. With no icebreakers in the inventory, USN surface ships are dependent upon the dwindling U.S. Coast Guard (USCG) icebreaking capabilities. The Coast Guard maintains two heavy polar icebreakers, the Polar Star and Polar Sea, and one medium polar icebreaker, the Healy, mostly used for research. The heavy icebreakers have both exceeded their intended

30-year service lives, and the Coast Guard is in the process of decommissioning the Polar Sea (O'Rourke 2011). This reality spreads the USN and USCG very thin in terms of its ability to respond quickly to Search and Rescue and Humanitarian Assistance/Disaster Response (HA/DR) missions that are likely to increase in the Arctic in the coming years. While requests have been made to Congress to augment this fleet by adding up to six heavy and four medium icebreakers to maintain the continuous presence requirements of the Naval Operations Concept, approval has so far been denied which places any augmentation out at least ten years (O'Rourke 2011).

Finally, a key challenge identified from the CBA was in the current ability to observe and forecast both weather and sea ice for operations in the Arctic. The Naval Ice Center in Suitland, Maryland provides sea ice analysis and forecasting products primarily for the submarine community when they operate in the region, but has the ability to support any mission with operational analysis, as well (DoD 2011). Shortcomings exist in the development of these products, partially due to the communication issues to this remote region, but also due to a lack of data coverage and in depth understanding of sea ice dynamics, which are integral to the ability to predict sea ice motion. While the U.S. has made significant investments into the collection of environmental data in the Arctic through the establishment of an Arctic circumpolar observing network from partnerships among various U.S. agencies, academic collaborators, and Arctic residents, sea ice dynamical processes have been more difficult to observe (O'Rourke 2011) than ice extent and motion fields. Satellite imagery, buoy networks, and in situ observations made from research cruises and ice camps are able to provide scientists with observations of current mechanics on the small regional scales; but the underlying dynamics need to be understood in order for numerical modeling to be able to accurately predict basin-wide ice coverage for operational requirements, as well as long-term predictions.

D. OBSERVATIONAL AND TRAINING OPPORTUNITIES

With a rich history as a border nation to the Arctic along the Alaskan coast and a member of the Arctic Council, the U.S. government has a vested interest in environmental changes as well as its operational capabilities in the region. The recent pattern of declining sea ice and general progression towards seasonal ice cover in the

region has renewed concerns about territorial claims and the vast resources available in the area. Understanding the processes that drive the amount of open water and predicting the length of time that Arctic sea passages will be open to navigation will be paramount in determining the amount of resources the U.S. Navy will have to allocate to that region in the foreseeable future.

While there is low potential for armed conflict in the region in the foreseeable future, the existing defense infrastructure was deemed adequate to meet current near- to mid-term U.S. national security requirements (DoD 2011). In order to remain prepared to operate in the Arctic, the Navy needs to remain engaged in current research and operational testing exercises to maintain and build upon current capabilities and to observe changes in the Arctic as they happen. For the last two years, the U.S. Navy has participated in the annual Canadian exercise, Operation NANOOK, in which it has sent guided missile destroyers to train for HA/DR scenarios in the Arctic. The U.S. Marine Corps has also participated in the Norwegian invitational exercise COLD RESPONSE and the Air National Guard and Army Reserve have participated in the Arctic Care mission, which provides medical treatment to remove villages across Alaska. Along with these operations-based exercises, several research opportunities can offer experience to military personnel while improving Arctic sea ice research knowledge within the DoD. Continued involvement in the biennial Ice Exercise (ICEX) program run by Commander, Submarine Force, Pacific offers both an opportunity for submarine training of equipment and tactical procedures, and provides a base for research through an agreement with the Office of Naval Research (ONR). Utilization of USCG and other ships of opportunity research ventures by ONR science initiatives will further improve our knowledge of the changing operational environment in the Arctic.

Apart from its relevance to the broader impacts of global climate change, a better understanding of sea ice dynamics will assist the Navy in determining how to effectively operate in such harsh environments. With the development of Task Force Climate Change and the Arctic Roadmap, the Navy has positioned itself at the forefront of decisions concerning the national security interests of the region. These concerns include, but are not limited to, safety of navigation, resource development, vessel design,

and the ability to exploit the environment for tactical and operational considerations. If the action items from publications such as the Environmental Assessment and Outlook (2011) and the government accountability office (GAO) report to Congress (2012) are adhered to, the Navy will be able to make informed decisions based on a synthesis of the best scientific information available.

Uncertainty remains about the rate and extent of climate change in the Arctic, and the variable rate of change may not unfold in a linear fashion. The amount of increased human activity in the region will attempt to keep pace with the changing environment, which is why continual monitoring of sea ice changes is required to make intelligent and timely investments that will improve naval capabilities in the Arctic. In order to develop the partnerships required for successful integration of international policy in the region, members of Task Force Climate Change will need to understand the dynamics of the region and the timeline of the procurement process that will determine the urgency of action by policymakers.

III. DESCRIPTION OF NUMERICAL MODELS AND OBSERVATIONAL DATA

A. MODEL DESCRIPTIONS

In order to improve understanding of the critical physical processes and feedbacks in the Arctic that determine sea ice variability, numerical model output has been compared to satellite imagery as a means of evaluating which combination of model parameters best represents observational data. This study is a comparative analysis of regional coupled ice ocean models which have been modified with different atmospheric forcing and coupling between parameters. These models were all run by the Naval Postgraduate School Arctic Modeling Effort (NAME) and are described in detail below.

1. Polar Ice Prediction System (PIPS)

The Polar Ice Prediction System (PIPS) is a coupled ice-ocean model with a horizontal grid spacing of $1/12^{o}$ (or ~9km) projected onto a rotated spherical grid to eliminate singularity at the pole (Maslowski et al. 2004). The model domain incorporates the Seas of Japan and Okhotsk in the west, the sub-Arctic North Pacific and North Atlantic Oceans, the Canadian Arctic Archipelago (CAA), and the Nordic Seas in the east (Figure 9). This domain includes all major oceanic inflow and outflow regions of the Arctic Ocean, and all of the seasonally ice-covered seas in the Northern Hemisphere. An artificial channel was introduced into the domain across the North American continent to balance the net northward water transport through the Bering Strait (Maslowski et al., 2004). Bathymetry north of 64^{o}N is derived from the 2.5km resolution International Bathymetry Chart of the Arctic Ocean (IBCAO) field interpolated to the 9km grid (Jakobsson et al. 2000; Maslowski and Walczowski 2002). Bathymetry south of 64^{o}N is derived from ETOPO5 at five-minute resolution. The high horizontal resolution and large domain allow for simulations of realistic exchanges of mass and heat between the Arctic and its surrounding seas (Maslowski et al. 2004). This model is considered eddy permitting as features down to ~37km (four grid points) can be resolved, but smaller

features down to the size of Rossby radius of deformation in the Arctic of ~10km (Maslowski et al. 2008) are not well represented.

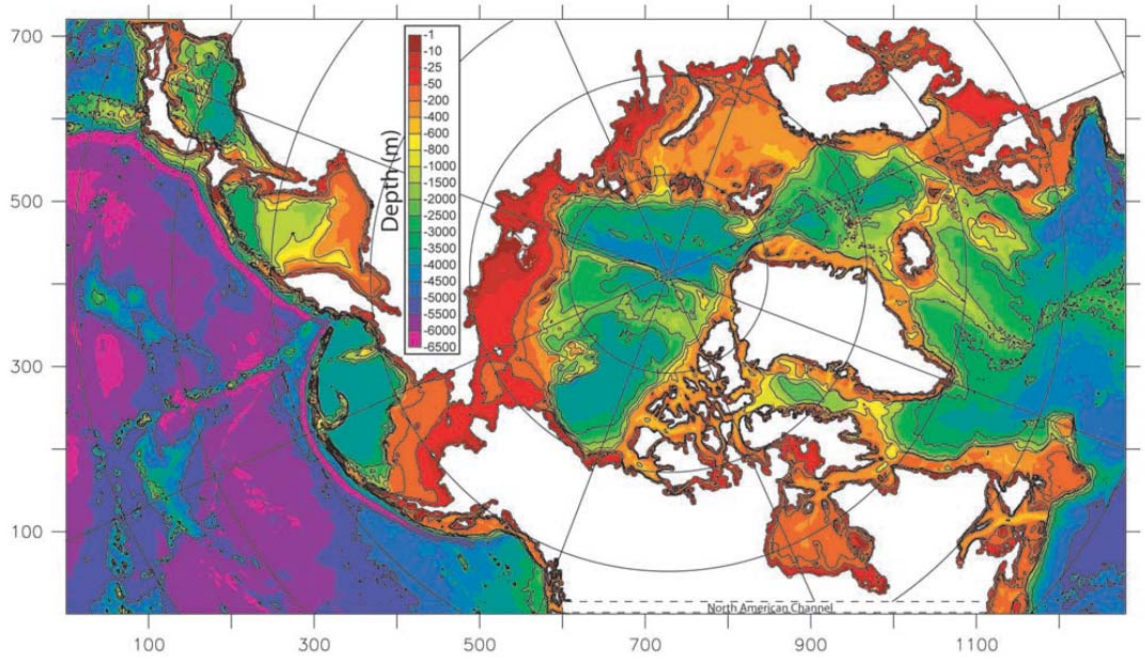

Figure 9. NPS model domain and bathymetry.

The ice model consists of a parallel version of the Hibler-type sea ice model with a viscous-plastic rheology, a zero-layer approximation of heat conduction through ice, and two thickness categories (thick ice and thin ice/open water) (Hibler 1979; Zhang and Hibler 1997; Maslowski and Lipscomb 2003). This ice model is coupled to an ocean model that consists of a regional adaptation of the Los Alamos National Laboratory (LANL) Parallel Ocean Program (POP) model with a free surface formulation (Dukowicz and Smith 1994). The free surface and high resolution allow for use of an unsmoothed and realistic bathymetry which was not possible with rigid lid models (Dukowicz and Smith 1994). There are 45 fixed ocean depth layers in the vertical direction with a concentration of eight levels in the upper 50m and 15 levels in the upper 200m to capture resolution along the vast Arctic continental shelves and slopes (Maslowski et al. 2004 and 2008).

The ocean model was initialized with climatological, three-dimensional temperature and salinity fields from the Polar Science Center Hydrographic Climatology (Steele et al. 2001) and integrated for 48 years in a spin-up mode to produce realistic ocean circulation at the time of integration (Maslowski et al. 2008). The model was then integrated with daily averaged inter-annual atmospheric forcing from the European Centre for Medium-Range Weather Forecasting (ECMWF) for 26 years (1979 to 2004) reanalysis data (Maslowski and Lipscomb 2003). This data set includes downward longwave and shortwave radiation, air temperature and density, specific humidity, precipitation, wind velocity and surface wind stress. River run off is also included in the ocean model to allow for adjustment of the freshwater budget (Maslowski and Lipscomb 2003). The sea ice model was initialized with a uniform 2m thick layer of ice in January over an ocean with climatological surface temperatures less than 0^{o}C to avoid influx of freshwater from melting ice in regions where sea ice is not normally present (Maslowski et al. 2004). Further description of model parameters has been provided elsewhere (Maslowski and Lipscomb 2003; Maslowski et al. 2004).

2. Parallel Ocean Program (POP)—Community Ice CodE (CICE)

The POP-CICE model mirrors the PIPS ocean model, domain, bathymetry, and atmospheric forcing, but differs greatly in its approach to sea ice modeling. The CICE ice model was developed at LANL in an effort to provide a computationally efficient sea ice model to be run with fully coupled global climate models (Hunke and Lipscomb 2001). It can also run in stand-alone mode or coupled to regional models, as has been done in this study. It was designed specifically to be compatible with the POP ocean circulation model, and has several interacting components. These components include a multi-layer thermodynamic model to compute the local growth rate of snow and ice, an ice dynamics model which predicts the velocity field based on ice strength, a transport model that describes advection of ice concentration and volume, and a ridging parameterization that transfers ice among thickness categories based on energetic balances and stain rates (Hunke and Lipscomb 2006).

The primary difference from PIPS ice model is that each grid cell in the CICE model contains multiple ice thickness categories and incorporates elastic-viscous-plastic

(EVP) dynamics, which is important for resolving ice deformation processes (Hunke and Dukowicz 1997). This dynamic model reduces to a viscous plastic configuration for long scale atmospheric forcing, but uses elastic waves on short time scales to improve response times and increase computational efficiency (Maslowski and Lipscomb 2003). The most significant improvement comes from the multiple ice thickness categories allowed in this ice model. The model includes five World Meteorological Organization ice thickness categories, each having four vertical ice layers and one snow layer (Hunke and Lipscomb 2001). Ice strength is one of the key parameters that determine the amount of sea ice deformation that is possible and is dependent upon ice thickness distribution (Maslowski and Lipscomb 2003).

This study will analyze model output using different parameterizations and forcing from within this POP-CICE model, which will be described in the results section. Additional details on this particular sea ice model can be found in the CICE User's Manual (Hunke and Lipscomb 2006).

3. Regional Arctic Climate System Model (RACM)

The Regional Arctic Climate System Model (RACM) is a fully-coupled land, atmosphere, sea ice, and ocean model developed to address deficiencies in and provide guidance to GCMs in representing climate change in the Arctic (Maslowski et al. 2012). RACM was created under the support of the Department of Energy Earth System Modeling program and contains updated versions of POP ocean and CICE sea ice models described previously (Hunke and Lipscomb 2008). Where RACM differs however, is that it incorporates a version of the National Center for Atmospheric Research (NCAR) Weather Research and Forecasting (WRF) atmospheric model (Skamarock et al. 2005) that has been optimized for polar regions (Hines and Bromwich 2008; Bromwich et al. 2009; Higgins et al. 2012). In addition, the Variable Infiltration Capacity (VIC) model (Cherkauer et al. 2003; Andreadis et al. 2009; Bowling and Lettanmaier 2010) represents land surface processes and hydrology. All climate system components within this model are fully coupled so that changes made in one field impact and are responded to by every other field through feedback mechanisms. This means that unlike the previously

described models, where the atmospheric forcing was prescribed, the atmosphere in RACM reacts to changes in the sea ice model and so forth for all interrelated model components.

The RACM model domain encompasses the entire pan-Arctic region (Figure 10), which is extended from previous models discussed. The active ocean and ice domains remain the same, but the atmosphere and land models are extended to include all terrestrial drainage basins that bring freshwater to the Arctic (Maslowski et al. 2012). Similar to previous models, the ocean and sea ice models use a horizontal grid spacing of 9km, while the atmosphere and land models use a horizontal grid spacing of 50km.

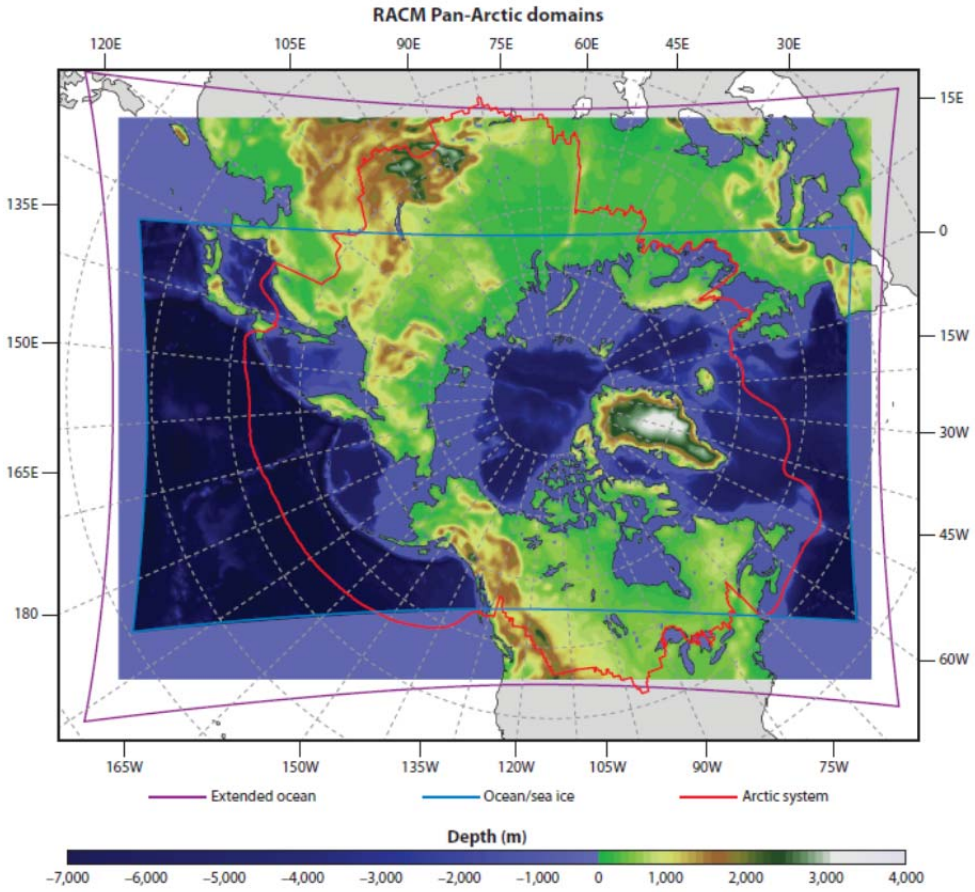

Figure 10. RACM pan-Arctic model domain. WRF and VIC model domains include the entire colored region. POP and CICE domains are bound by the inner blue rectangle. Arctic System domain is bound by the red line (From Maslowski et al. 2012, in press).

The focus of the RACM modeling effort has been to improve the realism in representing critical small-scale processes and pan-Arctic climate dynamics, and to test new physical parameterizations, which will help guide future observational requirements. Evaluation of earlier high-resolution NPS models has shown improvements in the seasonal cycle of sea ice edge, thickness, and volume fluctuations (Maslowski et al. 2007; Clement et al. 2005; McGeehan and Maslowski 2011). Melt rates from these earlier results (Maslowski et al. 2007) compare well with recent observational data (Kwok and Cunningham, 2008; Kwok et al., 2009), which suggest that near ice-free summers in the Artic may occur in the near future (Maslowski et al. 2012). These results provide motivation to utilize the advanced coupling mechanism of a high-resolution RACM model to more accurately reproduce the sea ice dynamics that influence future climate predictions.

This thesis further analyzes the synthesis of the coupled RACM model output as a means of comparison to both prior modeling efforts, and observational data from satellite imagery. While the coupling of constituents found in the RACM model does not offer direct comparison to models with prescribed realistic atmospheric forcing (PIPS and POP-CICE), the qualitative comparison to observational data is appropriate for further model validation. Additional details of the RACM model are provided elsewhere (Higgins et al. 2012; Maslowski et al. 2012).

B. RADARSAT GEOPHYSICAL PROCESSOR SYSTEM (RGPS) DATA SET

RADARSAT Geophysical Processor System (RGPS) is a computer system that analyzes images of sea ice in the Arctic Ocean obtained from RADARSAT-1 as part of NASA's MEaSUREs (Making Earth Science data records for Use in Research Environments) program. This MEaSUREs project has sought to compile data across several different Earth Science fields to produce a unified and coherent data set to address specific scientific questions (Jet Propulsion Laboratory (JPL) 2012). RGPS data is obtained by tracking sea ice motion from satellite images on a high-resolution grid, which is developed into data sets of small-scale kinematic and deformation fields. These fields have been obtained as a primary means of obtaining basin-wide observations, improving

model sea ice dynamics (Coon et al. 2007), and to help determine the impact of Arctic sea ice distribution and deformation on overall climate stability (Lindsay and Stern 2003).

RADARSAT-1 was developed by the Canadian Space Agency (CSA) and launched by the National Aeronautics and Space Administration (NASA) in November 1995 in exchange for access to the data produced by the satellite (CSA 2012). The satellite carries onboard a synthetic aperture radar (SAR) that is focused on the Arctic region for specific tasking from the RGPS project to detect sea ice motion and deformation processes (JPL 2012). The SAR sensor transmits microwave energy at 5.3 GHz in the C band wavelength (5.6cm). The radar returns are recorded and processed into imagery at the satellite facilities in Alaska and California (CSA 2011). Using this active imaging technique allows mapping to be produced for analysis both day and night as well as through various atmospheric conditions common to the region such as cloud cover and snow storms (CSA 2012).

Coverage of the Arctic occurs as the satellite orbits the Earth ~14 times a day with a period of 100.7 minutes. A retrograde inclination (98.6 degrees) determines the path around the Earth in opposite directional rotation as the satellite precesses one degree per day to keep up with the Earth's rotation around the Sun. This allows for an exact repeat path flown every 24 days and complete coverage of the Arctic approximately every 6 days (CSA 2010). Since RADARSAT-1 is a right-looking satellite, it ascends from the equator facing east, and descends from the North Pole facing west which enables images to be taken from opposite sides of the features on the surface. This, along with the ability to alter the direction and width of the beam path, provides observation from many different perspectives as the satellite tracks different features (CSA 2012).

As with all non-polar orbiting satellites, RADARSAT-1 leaves a hole in coverage over the central Arctic since the orbit and range of the SAR never quite reaches the pole (Figure 11). This gap is relatively small in comparison to other satellite constellations, however, as the areal extent missed by RGPS is only about a two-degree radius (~200km) in wide beam mode (Lindsay and Stern 2003). Lack of coverage in this area does not greatly impact deformation analysis of sea ice as predominant ice motion features occur

throughout the Arctic basin and are often concentrated in regions with thinner ice coverage than is found at the pole. With an overall decrease in ice thickness and advection of deformations into this region, extrapolation of nearby features is required to cover this gap in the data for comparison with complete Arctic coverage found in model data (Lindsay and Stern 2003). For the purposes of this research however, the region around the pole is avoided for direct comparison between RGPS and model results.

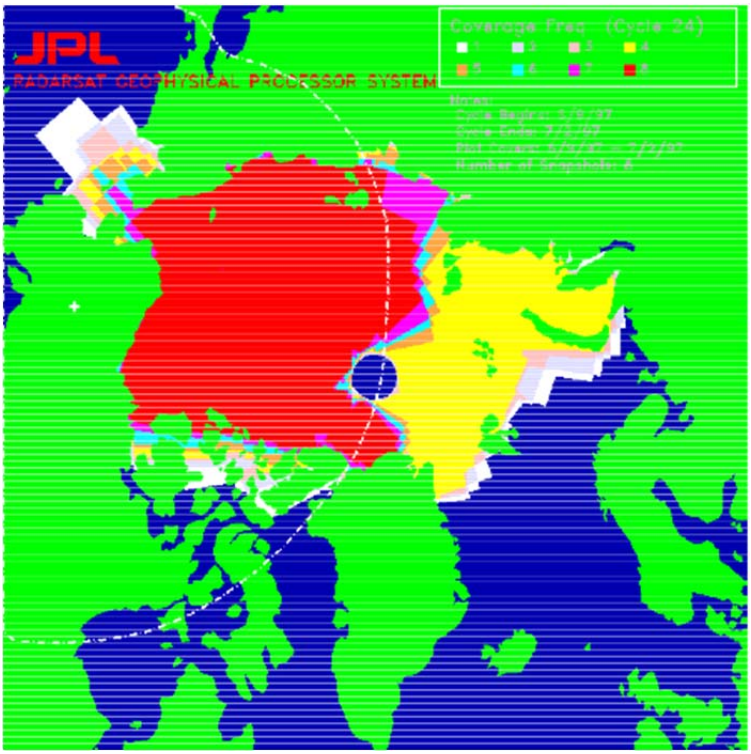

Figure 11. Nominal repeat coverage of the Arctic Ocean over a 24-day cycle (From Kwok and Cunningham 2000)

In wide beam mode, the SAR provides a swath of observations 460 kilometers wide with a pixel resolution of 100 meters (Lindsay and Stern 2003). This allows for reasonable acuity to distinguish different sea ice deformation parameters within the covered area. At high latitudes in the Arctic there is substantial overlap of swath paths, which can be beneficial to tracking of distinct features, but has to be filtered out during analysis so the same feature is not accounted for multiple times which would bias the

data significantly (Lindsay and Stern 2003). Under RGPS guidance, complete coverage of the Arctic is scheduled for every three days and this is generally attained in the western Arctic using the Alaskan station mask, which covers the Beaufort, Chukchi and East Siberian Seas. The Tromso mask covers the eastern Arctic, including the Laptev, Kara, and Barents seas (including Fram Strait) and is generally imaged every six days due to different tasking in that region (Lindsay and Stern 2003). A sampling period of less than three days would be more optimal to capture small-scale kinematic features that occur within that interval (Kwok 2006), but three-day coverage in the western Arctic has provided for observational analysis of ice motion that was not possible before the launch of RADARSAT-1.

The data set collected from RGPS represents one of the most comprehensive sets of observations in the harsh environment that is the Arctic. The data is read and analyzed at JPL in Pasadena, California, as well as at the Alaska SAR Facility (ASF) in Fairbanks, Alaska (Kwok and Cunningham 2000). This redundancy has allowed for both validation of the data and provided assurance that data is received from the satellite in the case that either site is down for any reason. Understanding the accuracy of the data is imperative to the ability to justify the analysis and any conclusions drawn from its research.

1. RGPS Data Validation

While RGPS data has been developed into several products that address sea ice kinematics, validation and analysis for this study will be focused on the more fundamental products of Lagrangian ice motion (LIM) and sea ice deformation fields. The RGPS data set is developed with a Lagrangian approach in which sea ice velocity fields are calculated from trajectories of tracked ice features from an initial uniformly spaced grid of ~10 km (Kwok et al. 2008). The initial grid then moves and deforms throughout the selected time frame to produce displacement and trajectory fields of the ice pack. An ice motion tracking algorithm was developed at ASF to achieve the ability within the RGPS program to pair images from successive satellite passes and match features within these images (Kwok et al. 1990). The tracking device produces an array of points from the center of a grid point of interest at an initial time, and acquires the trajectory for each point as it moves with the ice field (Kwok et al. 1998). This allows for

tracking of ice floes to produce velocity fields from which deformation products such as divergence, vorticity, and shear can be derived.

RGPS data has been validated through a number of methods. Initially, comparisons were made by analyzing the velocity fields produced by the two processing sites at JPL and ASF. Through use of the same tracking algorithms, automation of the velocity fields by both sites has produced minimal error in which the average displacement difference was 90 meters, which is smaller than the pixel size of the images (Lindsay and Stern 2003). More significant error is introduced however when there is ambiguity in the equivalent backscatter within the images produced (Kwok and Cunningham 2002). An automatic feature within the system flags areas in which there is low contrast between successive images or excessive deformation and rotation over the variable time step. In this scenario, operator intervention is required to determine the discrepancy and make a judgment on the outcome. From this personal interpretation, errors are introduced on the order of ~2.5 km from initial position of a feature on the first image to the determined position on the second image (Lindsay and Stern 2003). Manual interpretation is only required however in less than 0.5% of the cases analyzed for validation. Therefore, from this perspective the error is assumed to be no more than the pixel size of the images, or 100 m, which is consistent with the observed 95^{th} percentile of the displacement differences (Lindsay and Stern 2003).

RGPS data error has also been validated through comparison with the more limited data set from buoy trajectories from the International Arctic Buoy Program (IABP). This program maintains a network of buoys in the Arctic to provide real time operational and research data to interested users. The position error for these buoys has been estimated as 0.3 km by Thorndike and Colony (1980). Correlation of the displacement vectors between buoy and RGPS data was performed by Lindsay and Stern (2003) and determined to be 0.996 for all cases and 0.998 in cases without manual intervention. RGPS locational uncertainty, when compared to in situ buoy position error, can therefore be assumed to be on the same order as buoy estimates, or approximately 323 meters (Lindsay and Stern 2003).

The remaining errors to be assessed arise from conflict in geolocation of points and those errors that propagate through deformation calculations. For deformation analysis, geolocation errors do not play a role in the statistics since displacements are calculated from relative motion vectors from a common set of images, so these errors can be ignored (Lindsay and Stern 2003). Deformation calculations are derived from three invariants determined from the spatial gradient of the velocity field. These invariants of divergence, shear, and vorticity do not change relative to the coordinate system chosen, which allows them to be utilized over any grid. The errors in calculating these deformations are dependent upon tracking errors and the amount of time between images. Assuming a time differential of three days, the error for all three invariants is estimated to be 0.5% per day by Lindsay and Stern (2003). This error in deformation calculation can be reduced by grouping cells and taking an areal average, but this comes at the expense of spatial resolution.

This unprecedented observational coverage has given scientists a unique look into the temporal changes in the ice pack, which will offer a better understanding of the momentum, mass, and energy balance of the Arctic system. To date this data has been used extensively in scientific studies of the region for a variety of analysis including sea ice areal coverage, production, thickness, and deformation.

2. RGPS Sea Ice Deformation Calculations

Sea ice velocity is the fundamental observational field used by RGPS to calculate deformation characteristics of the Arctic sea ice. Sea ice motion is calculated from time-sequential satellite imagery taken from RGPS data sets (Kwok 2010). By observing how the identifiable features in the ice pack move from one observation to the next, average ice velocity gradients are derived from cross-correlation between snapshots of the same feature. Using a Lagrangian approach, an array of trajectories is produced from movement of individual ice features in space and time (Kwok et al. 1995), from which deformation fields can be derived.

Deformation within sea ice is derived from strain rates caused by spatial variability in the ice motion fields (Lindsay and Stern 2003). There are three invariants that can be calculated from the velocity gradients formed by moving ice fields. The first

is divergence, which is a measure of the rate of area change of the ice. The second is vorticity, which is a measure of the rotation rate. The third is shear, which is a scalar measure of the relative deformation of adjacent surfaces (Kwok 2006). These invariants are calculated by the following equations (Lindsay and Stern 2003; Kwok et al. 2008):

$$Divergence = \frac{\partial u}{\partial x} + \frac{\partial v}{\partial y} \tag{1}$$

$$Vorticity = \frac{\partial v}{\partial x} - \frac{\partial u}{\partial y} \tag{2}$$

$$Shear = \left[\left(\frac{\partial u}{\partial x} - \frac{\partial v}{\partial y}\right)^2 + \left(\frac{\partial u}{\partial y} + \frac{\partial v}{\partial x}\right)^2\right]^{1/2} \tag{3}$$

The strain rate components are computed by RGPS from approximations of the line integral around the boundary of each of the cells. For example,

$$\frac{du}{dx} = \frac{1}{A}\oint u \cdot dy \cong \frac{1}{2A}\sum_{i=1}^{n}(u_{i+1} + u_i)(y_{i+1} - y_i) \tag{4}$$

where *n* is the number of vertices for the cell and A is the area of the call. The area is computed by,

$$A = \frac{1}{2}\sum_{i=1}^{n}(x_i y_{i+1} - y_i x_{i+1}) \tag{5}$$

where x_i and y_i are the position coordinates of the vertices. In a similar manner, the rest of the gradients are calculated as follows:

$$\frac{du}{dy} = -\frac{1}{A}\oint u \cdot dx, \quad \frac{dv}{dx} = \frac{1}{A}\oint v \cdot dy, \quad \frac{dv}{dy} = -\frac{1}{A}\oint v \cdot dx \tag{6), (7), (8}$$

In this study, the invariants of divergence and shear will be the focus of the comparative analysis between RGPS and model output. This study follows the framework of Kwok et al. (2008) in its approach to determine what improvements have

been made due to recent model development. Seasonal drift and regional deformation of sea ice from RGPS fields will be compared to several different runs of NPS model output both qualitatively and quantitatively. Seasonal and regional deformation calculations will be made for comparison with RGPS values as well. Finally, shear and divergence snapshots will be taken to compare model capability in representing the linear kinematic features (LKFs) seen in RGPS output. Throughout, additional approaches will be analyzed to determine if alternate calculations of model output better represents RGPS analysis and assumptions.

THIS PAGE INTENTIONALLY LEFT BLANK

IV. RESULTS

In this chapter, results of sea ice drift and deformation from the previously described models are compared with RGPS derived ice motion and deformation fields. A more detailed analysis and discussion of these results and their implications for model improvements and future studies can be found in following chapters.

A. SEASONAL DRIFT AND DEFORMATION

In order to assess model performance for comparison to the RGPS data set, spatial gradients and ice motion are analyzed in this section initially on seasonal and regional scales before moving to comparisons of smaller scale deformation processes. Adapted from the approach taken in the Kwok et al. (2008) paper, seasonal RGPS coverage of Arctic sea ice is broken into five regions based on average thickness distribution and common forcing influences within each region (Kwok et al. 2008). The regions are defined following Kwok et al. (2008) as S1 and S2 containing ice from the Beaufort and Chukchi Seas respectively, which are covered with predominantly seasonal and thinner sea ice. S3 contains a mixture of ice types with seasonal ice toward the edges of the East Siberian and Laptev seas. S4 and S5 contain generally older and thicker perennial ice from the central Arctic and Canadian Basin, respectively. S4 is the only region not subject to direct coastal influences, and the southern edges of S1, S2, and S3 are generally exposed to open ocean in the fall (Kwok et al. 2008).

1. PIPS and CICE Comparison to RGPS Data

Figures 12 through 15 show selected sea ice drift and regional deformation analysis over four winter seasons (1996 to 2000) of RGPS observations and various model runs based on availability. In each figure, the first two panels show the initial coverage and boundaries of RGPS observations in the fall and the advected and deformed regions at the end of April from RGPS ice drift, with average displacement represented by vectors in the center of each region (in color). Following panels show various model runs and their derived ice motion fields for the same regional boundaries at the end of April for comparison to RGPS results. Model ice drift regional boundaries and their

associated average displacement vectors are shown in black for comparison to RGPS results. Model results are derived from daily average sea ice velocity fields from Eulerian model output. Sampling of RGPS ice motion estimates are not uniform in time and space, so model output is transposed into Lagrangian trajectories to match RGPS output (Kwok et al. 2008). Additional details of this process can be found in the RGPS Data User's Handbook (Kwok and Cunningham 2000).

The PIPS model output (noted as NPS in the figure) was analyzed as in the Kwok et al. (2008) paper to ensure continuity in techniques that were used in this thesis for deriving motion fields. Several runs of the POP-CICE model were analyzed, two of which are provided here based on availability and similar time frame coverage. Both runs utilized ECMWF reanalysis (ERA-15: 1979–1993) extended with operational products (after 1993) as atmospheric forcing. (An extensive description of the ERA-15 can be found at: http://www.ecmwf.int/research/era/ERA-15/). This dataset has been used widely in the modeling community as a consistent dataset for various hindcast studies. The POP-CICE R2 (noted as NPS_CICE_R2) model run modified the sea ice strength parameterization based on the relationship of ice thickness distribution and the behavior of sea ice (Rothrock 1975; Hibler 1980; Hopkins and Hibler 1991; Zhang and Rothrock 2003; Maslowski and Lipscomb 2003). The POP-CICE S3 (noted as NPS_CICE_S3) model run utilized the same ice strength parameterization, but also altered coupling parameterizations for calculating stresses from the atmosphere and ocean to the sea ice (Hunke and Lipscomb 2006).

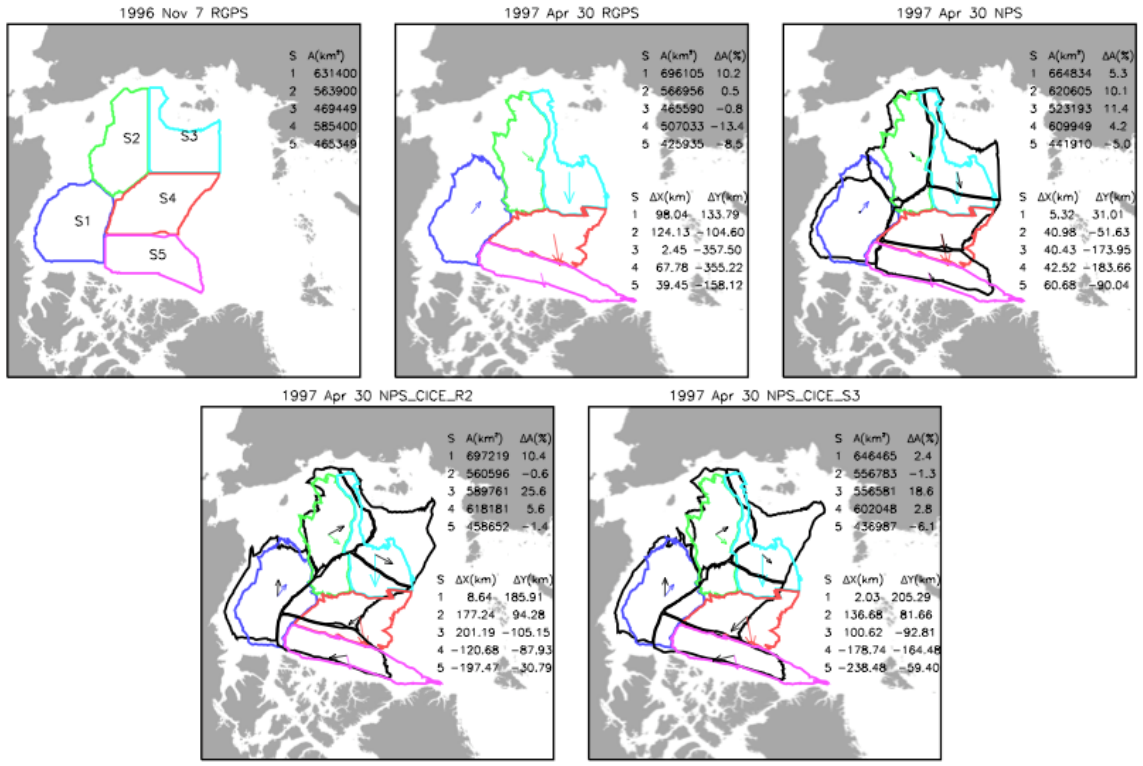

Figure 12. Differences in regional advection and deformation between model and RGPS estimates, November 1996 to April 1997. Model-derived regional boundaries are in black, RGPS boundaries are in color. Vectors (model in black, RGPS in color) near the center of each region show the average displacement of the boundary samples computed from model and RGPS data.

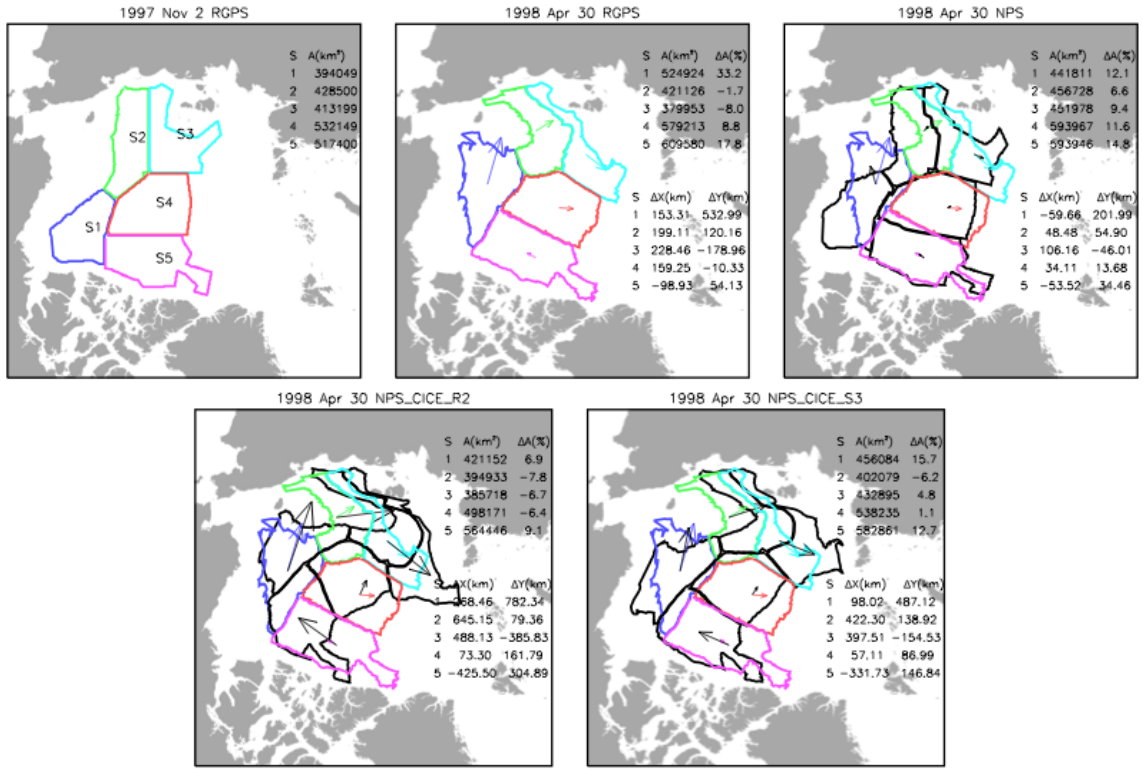

Figure 13. Differences in regional advection and deformation between model and RGPS estimates, November 1997 to April 1998. Model-derived regional boundaries are in black, RGPS boundaries are in color. Vectors (model in black, RGPS in color) near the center of each region show the average displacement of the boundary samples computed from model and RGPS data.

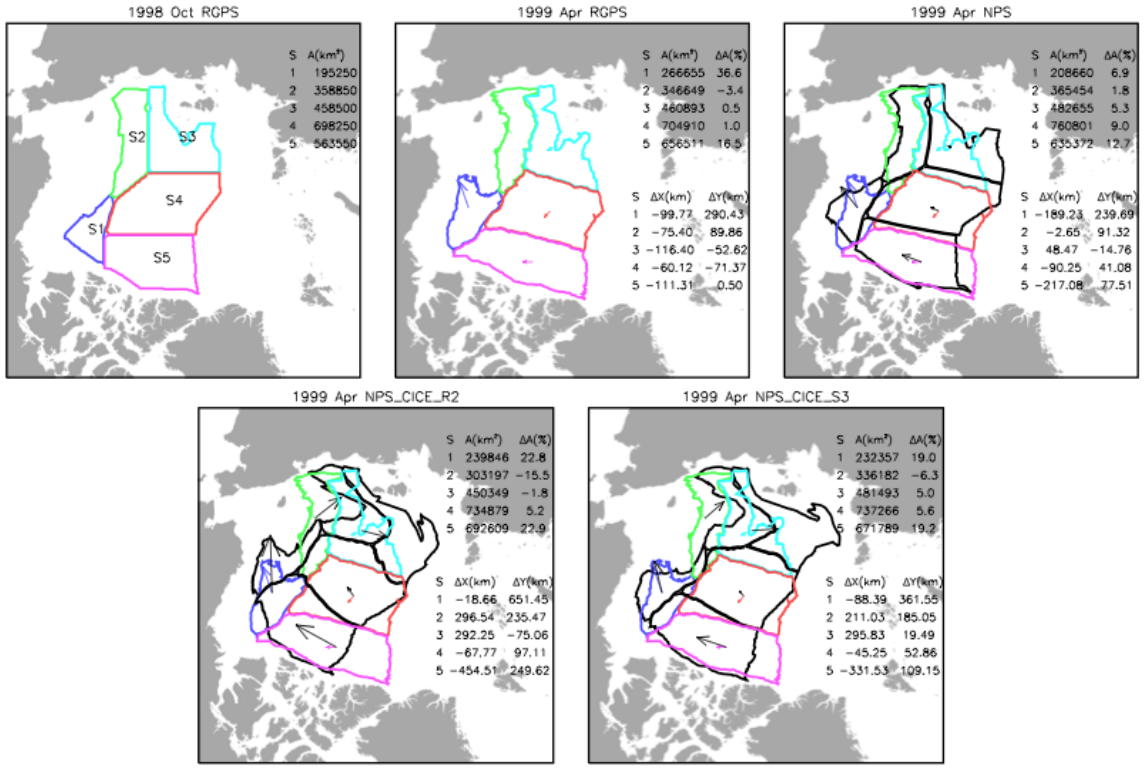

Figure 14. Differences in regional advection and deformation between model and RGPS estimates, October 1998 to April 1999. Model-derived regional boundaries are in black, RGPS boundaries are in color. Vectors (model in black, RGPS in color) near the center of each region show the average displacement of the boundary samples computed from model and RGPS data.

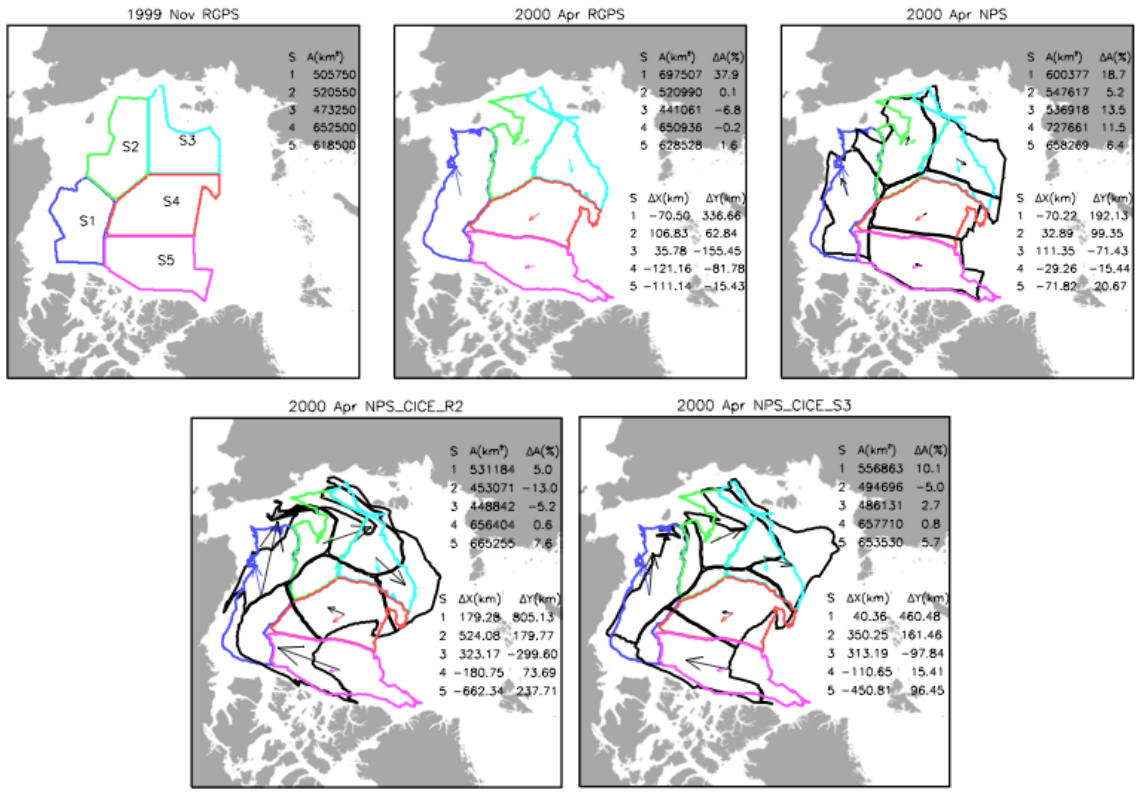

Figure 15. Differences in regional advection and deformation between model and RGPS estimates, November 1999 to April 2000. Model-derived regional boundaries are in black, RGPS boundaries are in color. Vectors (model in black, RGPS in color) near the center of each region show the average displacement of the boundary samples computed from model and RGPS data.

The displacement and deformation of these regional sea ice boundaries in the Arctic represent the large-scale drift patterns and response of sea ice to the prevailing forcing mechanisms over a winter season. These results have been quantified and summarized in the following table to help determine the correlation between RGPS and model results, as well as to determine if different parameterizations within individual model runs have made improvements to previous modeling efforts. Table 1 displays calculations of the total displacement of individual regions from the different model runs as a fraction of RGPS displacement, the directional difference between model and RGPS displacement vectors, and the percentage of regional area change of model output compared to RGPS estimates (Table 1).

	RGPS		NPS - PIPS				NPS - CICE_R2				NPS - CICE_S3			
Region	Drgps (km)	ΔA/A (%)	Dmodel/ Drgps	Δθ (deg)	ΔA/A (%)	ΔA Diff (%)	Dmodel/ Drgps	Δθ (deg)	ΔA/A (%)	ΔA Diff (%)	Dmodel/ Drgps	Δθ (deg)	ΔA/A (%)	ΔA Diff (%)
							Nov 1996 - Apr 1997							
S1	166	10.2	0.19	26.5	5.3	-4.9	1.12	33.6	10.4	0.2	1.24	35.7	2.4	-7.8
S2	162	0.5	0.41	-11.4	10.1	9.6	1.24	68.1	-0.6	-1.1	0.98	71.0	-1.3	-1.8
S3	358	-0.8	0.50	12.7	11.4	12.2	0.63	62.0	25.6	26.4	0.38	46.9	18.6	19.4
S4	362	-13.4	0.52	2.2	4.2	17.6	0.41	-64.7	5.6	19.0	0.67	-58.2	2.8	16.2
S5	163	-8.5	0.67	20.0	-5.0	3.5	1.23	-95.1	-1.4	7.1	1.51	-90.0	-6.1	2.4
							Nov 1997 - Apr 1998							
S1	555	33.2	0.38	32.5	12.1	-21.1	1.49	-2.9	6.9	-26.3	0.90	4.7	15.7	-17.5
S2	233	-1.7	0.31	17.4	6.6	8.3	2.80	-24.1	-7.8	-6.1	1.91	-12.9	-6.2	-4.5
S3	290	-8.0	0.40	14.6	9.4	17.4	2.14	-0.3	-6.7	1.3	1.47	16.8	4.8	12.8
S4	160	8.8	0.23	25.6	11.6	2.8	1.11	69.3	-6.4	-15.2	0.65	60.4	1.1	-7.7
S5	113	17.8	0.56	-4.1	14.8	-3.0	4.64	-6.9	9.1	-8.7	3.22	4.8	12.7	-5.1
							Nov 1998 - Apr 1999							
S1	307	36.6	0.99	19.3	6.9	-29.7	2.12	-17.3	22.8	-13.8	1.21	-5.2	19.0	-17.6
S2	117	-3.4	0.78	-38.3	1.8	5.2	3.23	-91.5	-15.5	-12.1	2.39	-88.8	-6.3	-2.9
S3	128	0.5	0.40	138.7	5.3	4.8	2.36	141.3	-1.8	-2.3	2.32	159.4	5.0	4.5
S4	93	1.0	1.06	-74.4	9.0	8.0	1.27	-105.0	5.2	4.2	0.75	-99.3	5.6	4.6
S5	111	16.5	2.07	-19.4	12.7	-3.8	4.66	-28.5	22.9	6.4	3.14	-18.0	19.2	2.7
							Nov 1999 - Apr 2000							
S1	344	37.9	0.59	8.2	18.7	-19.2	2.40	-24.4	5.0	-32.9	1.34	-16.8	10.1	-27.8
S2	124	0.1	0.84	41.2	5.2	5.1	4.47	-11.5	-13.0	-13.1	3.11	-5.7	-5.0	-5.1
S3	160	-6.8	0.83	44.4	13.5	20.3	2.76	34.2	-5.2	1.6	2.06	59.7	2.7	9.5
S4	146	-0.2	0.23	-6.2	11.5	11.7	1.34	-56.2	0.6	0.8	0.76	-41.9	0.8	1.0
S5	112	1.6	0.67	-24.0	6.4	4.8	6.27	-27.6	7.6	6.0	4.11	-20.0	5.7	4.1
							Average							
S1	343	29.5	0.54	21.6	10.8	-18.7	1.78	-2.75	11.28	-18.20	1.17	4.6	11.8	-17.7
S2	159	-1.1	0.59	2.2	5.9	7.1	2.93	-14.76	-9.23	-8.10	2.10	-9.1	-4.7	-3.6
S3	234	-3.8	0.53	52.6	9.9	13.7	1.98	59.31	2.98	6.75	1.56	70.7	7.8	11.6
S4	190	-1.0	0.51	-13.2	9.1	10.0	1.03	-39.14	1.25	2.20	0.71	-34.8	2.6	3.5
S5	125	6.9	0.99	-6.9	7.2	0.4	4.20	-39.56	9.55	2.70	2.99	-30.8	7.9	1.0

Table 1. Average seasonal RGPS displacements (Drgps) of the boundary points of the five regions, model displacements (Dmodel) as a fraction of Drgps, directional differences (Δθ) between model and RGPS displacement vectors (negative to the right of RGPS vector), seasonal percentage area change of the five regions, and model area change difference from RGPS estimates.

2. RACM Comparison to RGPS Data

Using the same analysis techniques as in the previous section, results from the RACM model were compared with RGPS regional drift and deformation estimates as a means of determining improvements made in the fully coupled model. Since the atmosphere is fully predicted in this model, this analysis is simply a statistical comparison due to the difference in atmospheric forcing and sea ice response found in the RACM model. At the time of this publication, RACM model output is only available through the mid-1990s, so a generic RGPS year was chosen for comparison since observational data was not available for the same years. The winter season of 2000–2001 was chosen due to the anticyclonic nature of the resulting observations, which matched closely with the behavior of sea ice from the model output during the 1991 and 1992 winters that were assessed (Figure 16).

Four cases from the RACM model output were analyzed in comparison with RGPS ice motion estimations. RACMa was used as a control case. This version of the model included a momentum flux correction in the atmospheric model (WRF). This flux correction required that the u* value calculated and used by WRF be averaged with the u* value obtained from the coupler in RACM. In a perfect coupling case, all u* values should derive from the coupler, since these values consistent with those used by other component models in RACM (POP, CICE and VIC). The u* flux correction in WRF was found to be neccessary due to instabilities resulting from previous land-atmosphere coupling in RACM. With new land–atmosphere coupling procedures, the RACMb case sought to correct the u* flux correction so that WRF only used surface stress consistent across the entire coupled framework. Both RACMa and RACMb model runs used a 20-minute dynamic time step in the sea ice model. In the RACMg case, the dynamic time step from was reduced from 20 minutes to five minutes, and the RACMh case further shortened this dynamic time step down to one minute. These reductions in sea ice timestepping were based on analysis of the paper by Hunke (2001), which examined EVP behavior in sea ice dynamic models. The following equation was used to determine the impact of altering the dynamic time step:

$$\frac{P}{\max(\Delta;\Delta_{min})} < \frac{CT\Delta x\Delta y}{\Delta t_e^2} \tag{9}$$

where P is the internal ice pressure (N/m), Δ is a function of the strain rates (s^{-1}), C is a tuning parameter constant, T is the damping time scale (s), Δx and Δy represent the grid cell lengths (m), and Δt_e^2 is the EVP time step (s). From this relationship, it can be seen that a reduction of the time step increases the relative contribution of the plastic component of deformation in sea ice dynamics by allowing smaller strain rates to be accounted for by given compressive stresses while maintaining stability in the model (Hunke 2001). Results from this analysis are displayed in Figure 16.

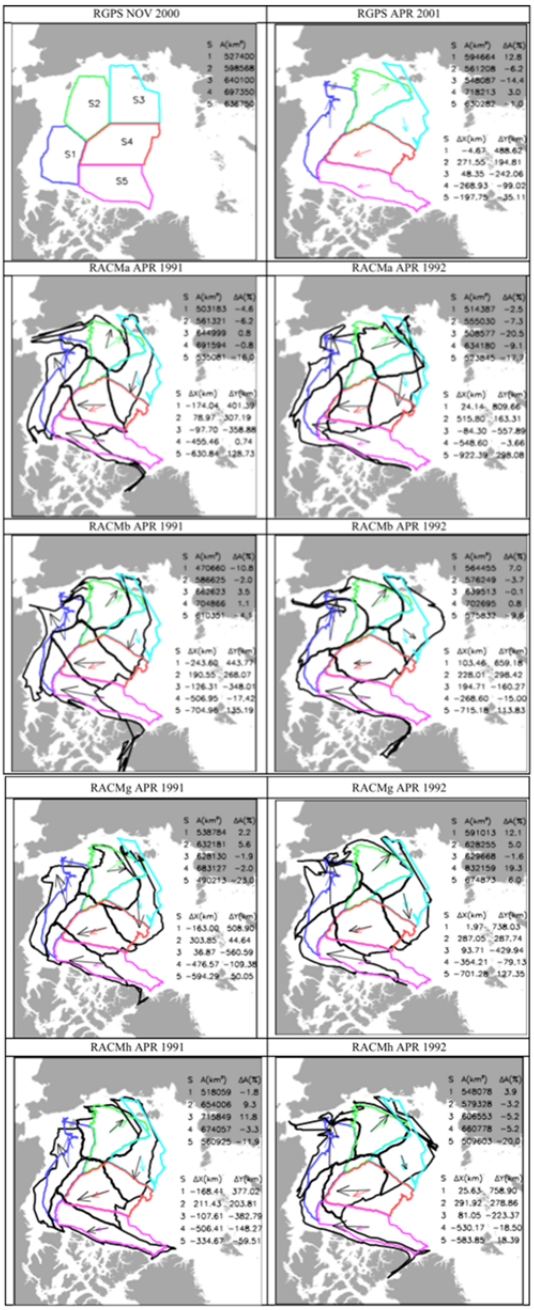

Figure 16. Differences in regional advection and deformation between model and RGPS estimates. RGPS results (top row) from 2000–2001 season are compared to two seasons ((1990–1991 and 1991–1992) of each model run; RACMa (second row), RACMb (third row), RACMg (fourth row), and RACMh (fifth row). Model-derived regional boundaries are in black, RGPS boundaries are in color. Vectors (model in black, RGPS in color) near the center of each region show the average displacement of the boundary samples computed from model and RGPS data.

As in the previous analysis for the POP-CICE model, the RACM model case results have been quantified by direct comparison of total displacement differences, directional displacement differences, and regional area change comparisons with RGPS estimates (Table 2).

	RGPS		NPS - CICE_RACMa				NPS - CICE_RACMb				NPS - CICE_RACMg				NPS - CICE_RACMh			
Region	Drgps (km)	ΔA/A (%)	Dmodel / Drgps	Δθ (deg)	ΔA/A (%)	ΔA Diff (%)	Dmodel / Drgps	Δθ (deg)	ΔA/A (%)	ΔA Diff (%)	Dmodel / Drgps	Δθ (deg)	ΔA/A (%)	ΔA Diff (%)	Dmodel / Drgps	Δθ (deg)	ΔA/A (%)	ΔA Diff (%)
	(2000 – 2001)									*Nov 1990 - Apr 1991*								
S1	489	12.8	0.90	22.9	-4.6	-17.4	1.04	28.2	-10.8	-23.6	1.09	17.2	2.2	-10.6	0.85	23.5	-1.8	-14.6
S2	334	-6.2	0.95	39.9	-6.2	0.0	0.98	18.9	-2.0	4.2	0.92	-27.3	5.6	11.8	0.88	8.3	9.3	15.5
S3	247	-14.4	1.51	-26.5	0.8	15.2	1.50	-31.2	3.5	17.9	2.28	-7.5	-1.9	12.5	1.61	-27.0	11.8	26.2
S4	287	3.0	1.59	-20.3	-0.8	-3.8	1.77	-18.2	1.1	-1.9	1.71	-7.3	-2.0	-5.0	1.84	-3.9	-3.3	-6.3
S5	201	-1.0	3.21	-21.6	-16.0	-15.0	3.57	-20.9	-4.1	-3.1	2.97	-14.9	-23.0	-22.0	1.69	0.0	-11.9	-10.9
	(2000 – 2001)									*Nov 1991 - Apr 1992*								
S1	489	12.8	1.66	-2.3	-2.5	-15.3	1.37	-9.5	7.0	-5.8	1.51	-0.7	12.1	-0.7	1.55	-2.5	3.9	-8.9
S2	334	-6.2	1.62	-18.1	-7.3	-1.1	1.12	17.0	-3.7	2.5	1.22	9.4	5.0	11.2	1.21	8.0	-3.2	3.0
S3	247	-14.4	2.29	-19.9	-20.5	-6.1	1.02	39.2	-0.1	14.3	1.78	1.0	-1.6	12.8	0.96	8.6	-5.2	9.2
S4	287	3.0	1.91	-19.8	-9.1	-12.1	0.94	-17.0	0.8	-2.2	1.27	-7.6	19.3	16.3	1.85	-18.2	-5.2	-8.2
S5	201	-1.0	4.83	-28.0	-17.7	-16.7	3.61	-19.1	-9.6	-8.6	3.55	-20.4	6.0	7.0	2.91	-11.9	-20.0	-19.0
										Average								
S1			1.28	10.3	-3.6	-16.4	1.20	9.4	-1.9	-14.7	1.30	8.3	7.2	-5.7	1.20	10.5	1.1	-11.8
S2			1.28	10.9	-6.8	-0.6	1.05	18.0	-2.9	3.4	1.07	-8.9	5.3	11.5	1.04	8.2	3.1	9.3
S3			1.90	-23.2	-9.9	4.6	1.26	4.0	1.7	16.1	2.03	-3.3	-1.8	12.7	1.29	-9.2	3.3	17.7
S4			1.75	-20.1	-5.0	-8.0	1.35	-17.6	1.0	-2.1	1.49	-7.5	8.7	5.7	1.85	-11.1	-4.3	-7.3
S5			4.02	-24.8	-16.9	-15.9	3.59	-20.0	-6.9	-5.9	3.26	-17.6	-8.5	-7.5	2.30	-5.9	-16.0	-15.0

Table 2. Average seasonal RGPS displacements (Drgps) of the boundary points of the five regions, model displacements (Dmodel) as a fraction of Drgps, directional differences (Δθ) between model and RGPS displacement vectors (negative to the right of RGPS vector), seasonal percentage area change of the five regions, and model area change difference from RGPSestimates.

B. SMALL-SCALE DEFORMATIONS

Representation of small-scale kinematics of deformation processes may assist in the ability of modeling efforts to better represent larger-scale sea ice motion and its contribution to sea ice thickness distribution and changes in the Arctic. In this section, comparisons are made between deformation fields derived from RGPS and model output. Fracture patterns in the ice cover represent the mechanical response of sea ice to atmospheric and oceanic forcing (Kwok et al. 2008). The ability of model output to produce similar structures to observed sea ice deformation fields will help to determine the relative impact of kinematic forcing to ice production and thickness distribution in the Arctic.

Direct comparison of the spatial invariants derived from RGPS and model results is difficult based on the differences in how these features are derived from each dataset. RGPS invariants are calculated from ice motion fields estimated after features in the sea ice are tracked over a mosaic of repeated images taken from various satellite passes. On average, the western Arctic is covered over a three-day period, which means that velocity fields derived from repeated swaths cover a six-day period. Deformation fields are then calculated from these six-day velocity fields. Model sea ice velocity fields, by contrast, are available at each point on the Eulerian grid and at each time step, i.e., every 48 min, with the standard output archived on the daily basis. For the purposes of this study, average velocity fields were taken from daily snapshots of model output.

1. Shear Deformation Analysis

RGPS deformation fields show a high density of LKFs within the ice cover which vary in location and orientation pattern (Kwok et al. 2008). In order to assess model capability of representing these LKFs, a visual comparison of RGPS and model deformation fields has been presented in this section. The initial approach applied to achieve this comparison mirrors the approach taken in the Kwok et al. (2008) paper, whereby daily velocity fields from the model output are used to calculate the deformation fields over the same six-day period as in the RGPS coverage. This is accomplished by taking daily velocity snapshots from model output, calculating the velocity gradients over

a Lagrangian grid, and then calculating the average deformation produced by the model over a defined time period (6 days in this analysis). PIPS results are compared in this manner, as in the paper, with the addition of new model results from the POP-CICE S3 model run described previously. An example from 1997 from the Kwok et al. (2008) paper is used for direct comparison (Figure 17).

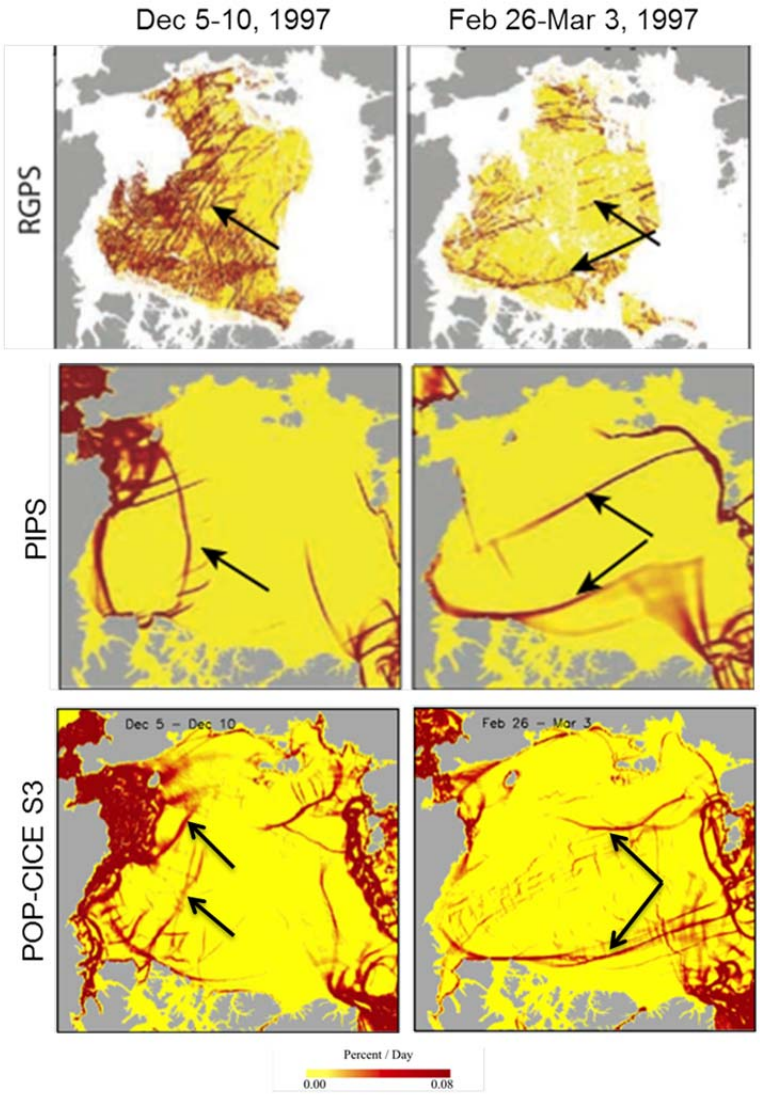

Figure 17. Examples showing correspondence between patterns of 6-day shear deformation from model fields and RGPS estimates. Linear kinematic features (indicated by arrows) in the model seem to line up with patterns from RGPS results (Adapted from Kwok et al. 2008).

An increase in the density of deformation features over the PIPS results can be easily seen in the POP-CICE S3 figure, likely due to the multiple ice thickness categories represented in each grid cell of this model. However, since the model velocity fields are available on a daily basis, deformations can be diagnosed on a daily basis as well to analyze ice kinematics at shorter time frames than RGPS data allow. Figures 18 and 19 offer examples of this analysis from the same time period (1997), in which the top figure shows the six-day averaged model deformation field, and the bottom rows show daily snapshots of deformation as represented by the model. From this analysis, it can be seen that many features present in the daily model snapshots are not present in the six-day averaged plots as calculated following the approach from Kwok et al. (2008). Based on these results, additional methods of intercomparisons of model ice deformations with those derived from RGPS are pursued in the next section.

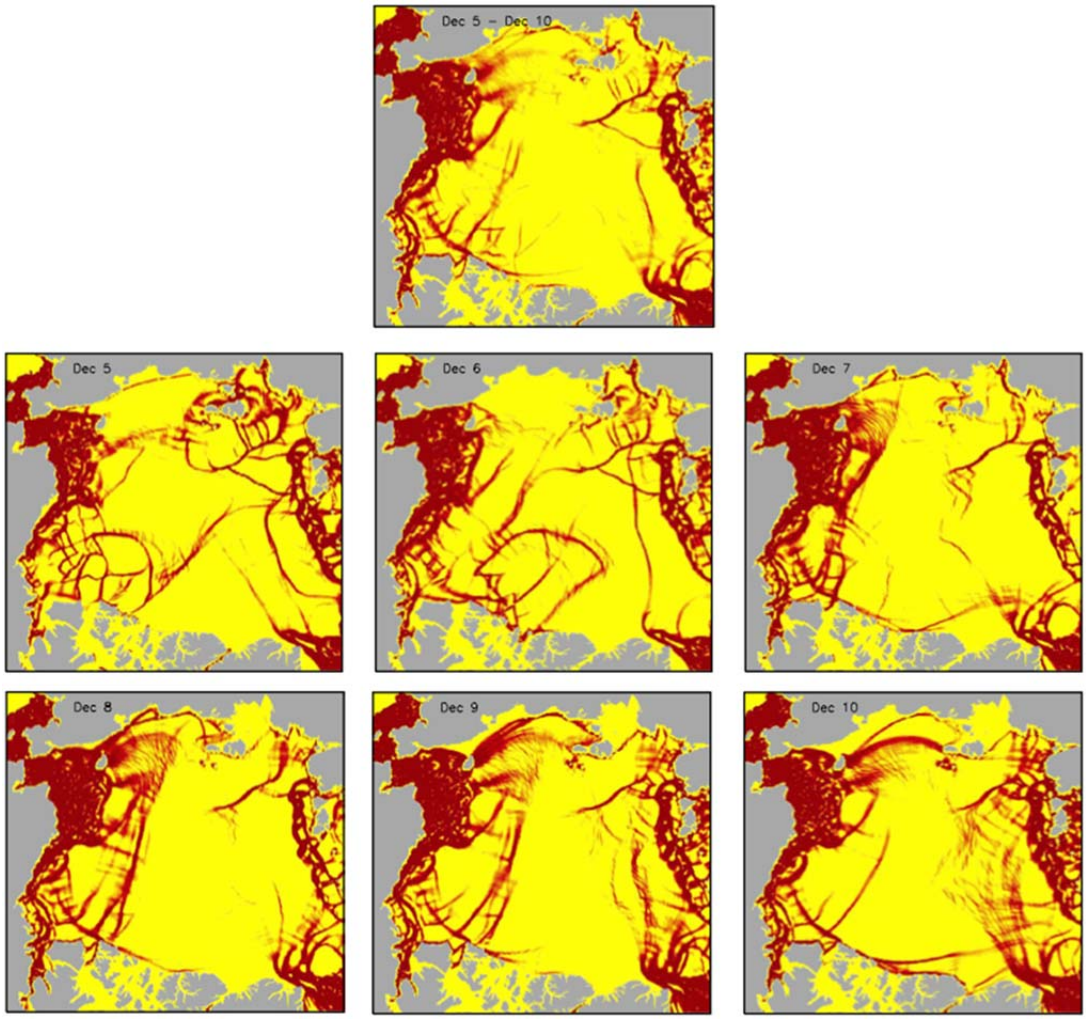

Figure 18. December 1997 shear example with 6-day average model field shown (top row) with comparison of daily shear snapshots from the same 6-day period (bottom two rows). Additional features present in daily snapshots compared to 6-day average.

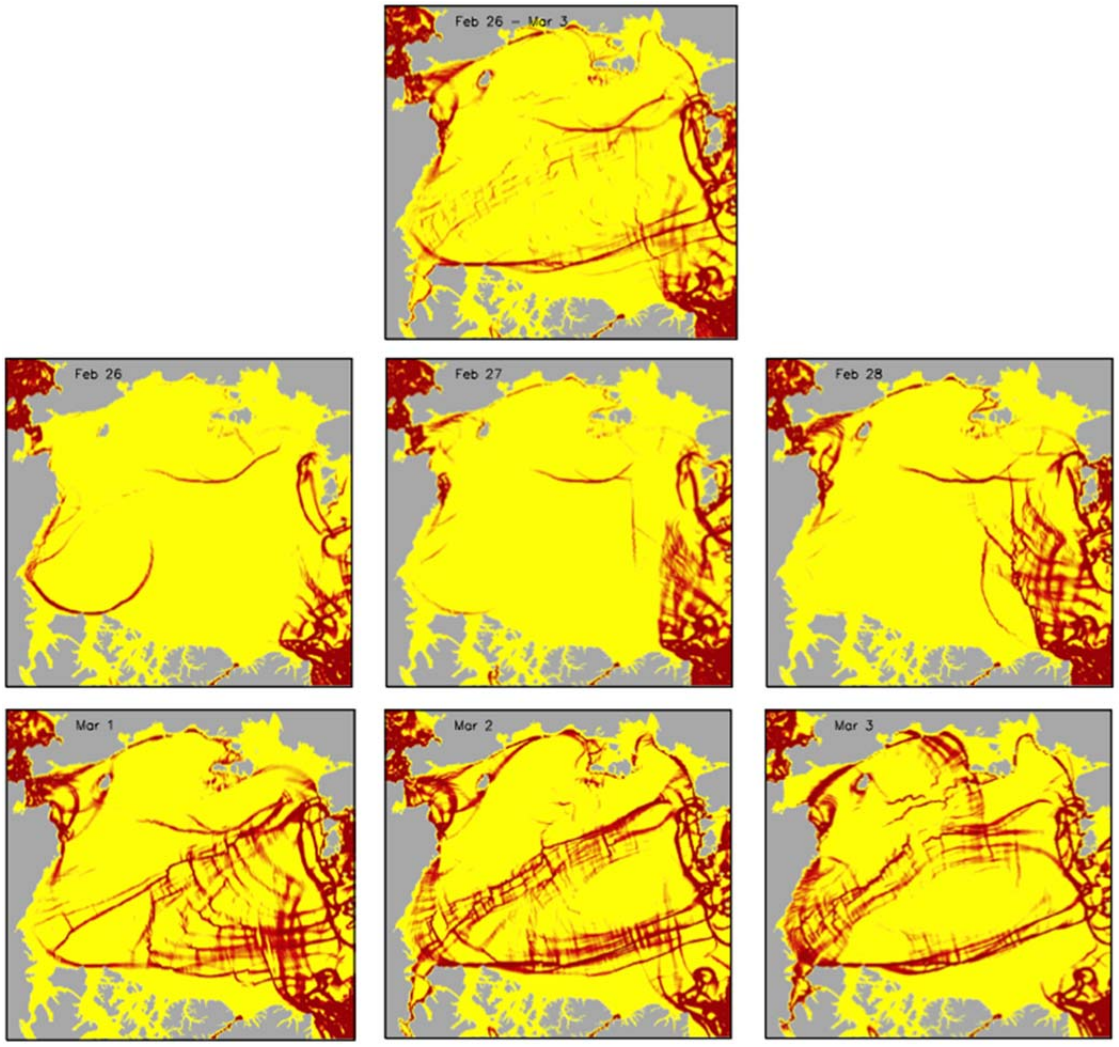

Figure 19. February 1997 shear example with 6-day average model field shown (top row) with comparison of daily shear snapshots from the same 6-day period (bottom two rows). Additional features present in daily snapshots compared to 6-day average.

2. Alternative Model Shear Estimations

In this section, an alternative method of calculating shear deformations from velocity fields within the POP-CICE S3 model output is described. Four years (1996–1999) are analyzed to match both the December and February results offered by the Kwok et al. (2008) paper. This method was developed as a means of showing an additional methodology to represent the small-scale deformations found in the model in a way that possibly helps to minimize the differences in model-data estimates of sea ice deformations due to different types of data used (i.e., Lagrangian-type observations versus Eulerian-type model output) and time required for basin coverage.

In order to transpose daily average velocity fields and their associated gradients and deformation fields calculated by the model onto six-day estimates by RGPS, daily sea ice velocity fields are averaged over the same period (6 days) covered in the RGPS dataset in the former method. By averaging the model velocity over six days, the magnitude of spatial variability of the sea ice velocity field is reduced, which is reflected in the deformation calculations resulting in a lower density of deformation features across the domain. This process was used to overcome the difficulties of direct comparison between RGPS and model output discussed earlier, and is one way of diagnosing the model capabilities to reproduce kinematic features, but it possibly filters out some of the details actually present in model output.

To account for the loss of features resolved in the model by this method, average velocity fields are taken at shorter time steps, and the deformations are summed instead of averaged out which allows shorter-lived features to be represented. By summing the resulting deformations, some features can be counted multiple times leading to exaggerated deformation density. Still this approach allows for more realistic representation of model-resolved deformations in the central Arctic.

Figures 20 through 27 show results obtained by taking average velocities from model output at reduced time interval compared to the six-day averages taken in the original RGPS comparisons. Five-day averages represent taking the average model velocities from days 1–5 and days 2–6 during the same six-day window, and using those velocities to calculate the deformations. In a similar manner, four-day averages take days

1-4, 2–5, 3-6; three-day averages take days 1–3, 2–4, 3–5, 4–6; and two-day averages take days 1–2, 2–3, 3–4, 4–5, 5–6. In order to determine an appropriate summation range, these time step averages were taken and deformations were calculated in the same manner by dividing by the number of time steps (top row in Figures 20 through 27), and also by simply taking a sum of the deformations (bottom row in Figures 20 through 27) calculated from the applicable time step. The density of deformations increases, as expected, due to the reduction of velocity temporal smoothing. Outcome of the summation of these results is described next.

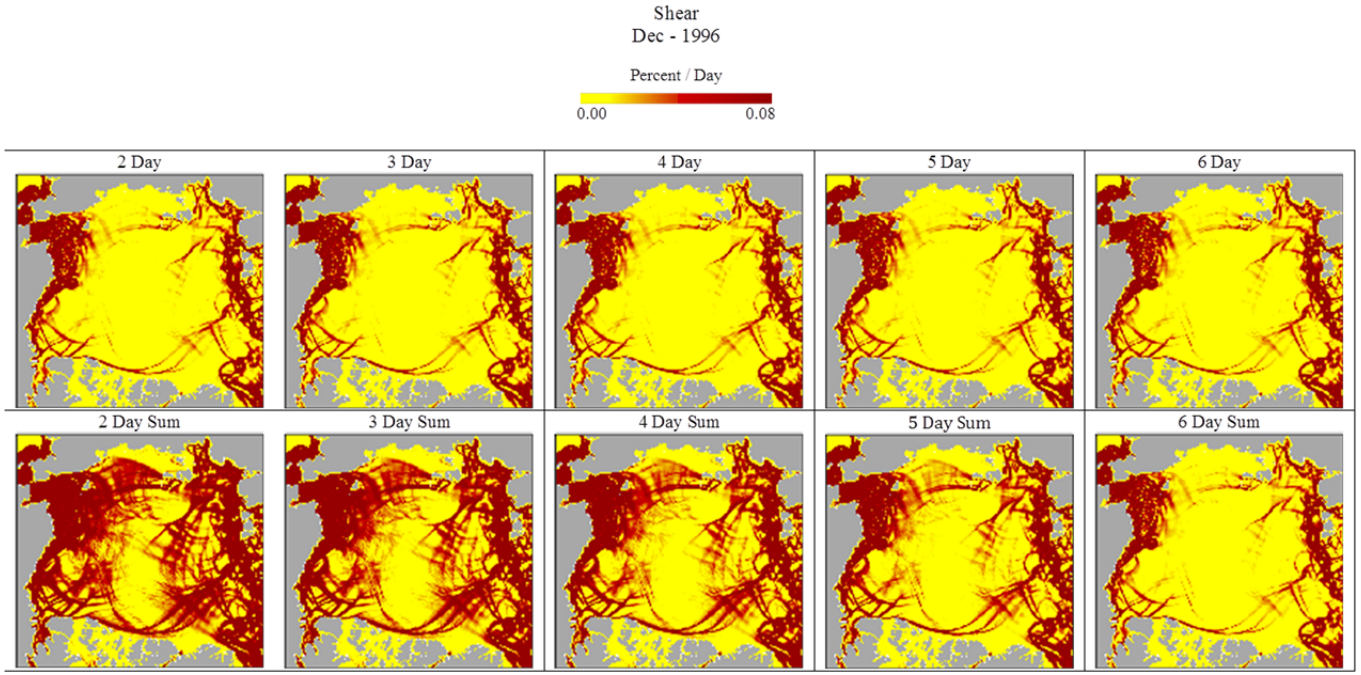

Figure 20. December 1996 example of alternative shear calculations from POP-CICE S3 model output. Top rows show shear deformations from multi-day averaged velocity fields, averaged through division of the number of time steps in the 6-day window. Bottom rows show a summation of the shear deformations from multi-day averaged velocity pairs at different time steps.

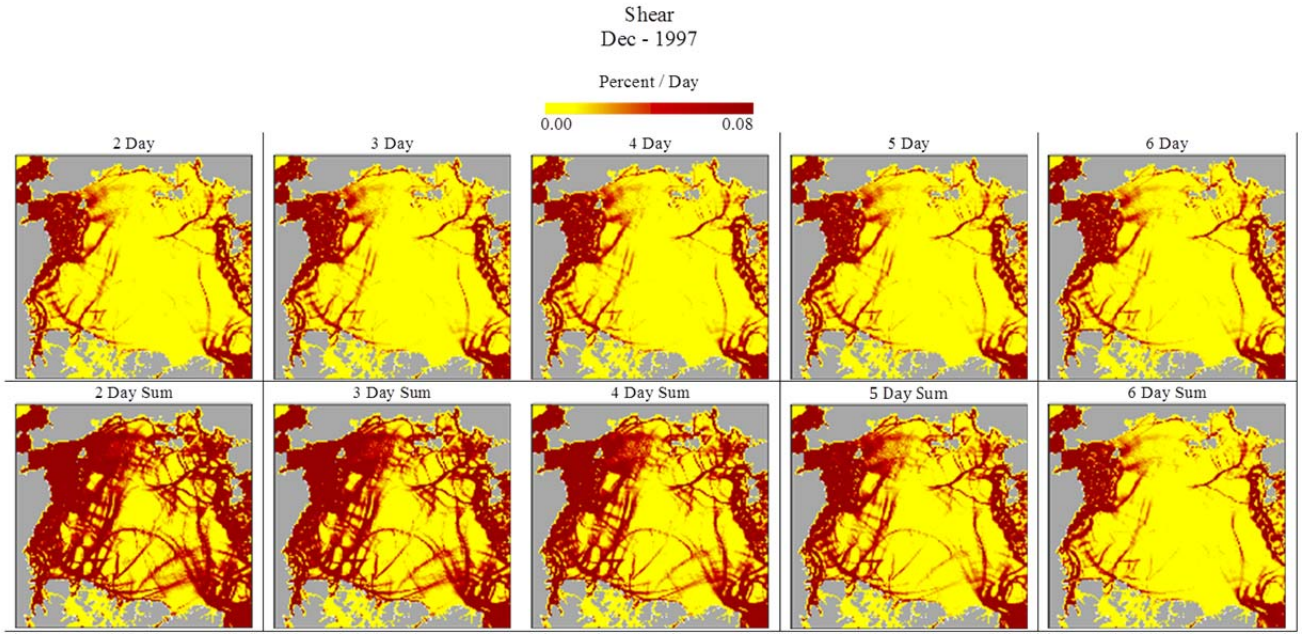

Figure 21. December 1997 example of alternative shear calculations from POP-CICE S3 model output. Top rows show shear deformations from multi-day averaged velocity fields, averaged through division of the number of time steps in the 6-day window. Bottom rows show a summation of the shear deformations from multi-day averaged velocity pairs at different time steps.

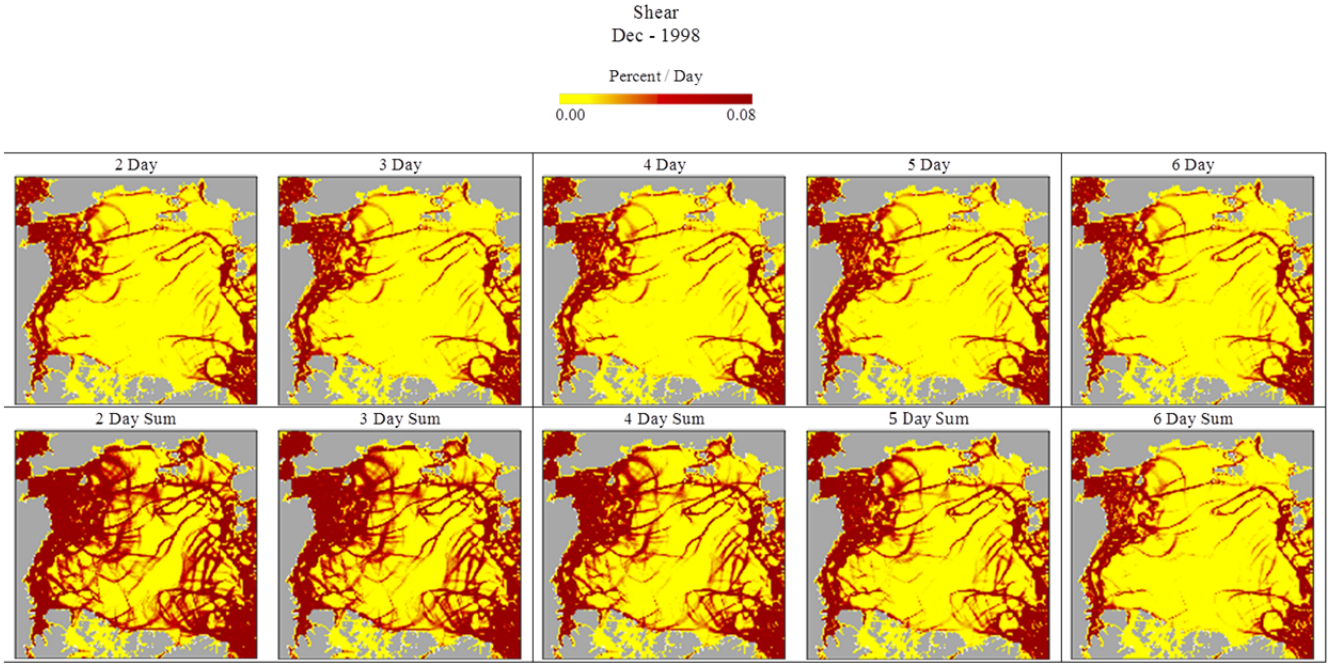

Figure 22. December 1998 example of alternative shear calculations from POP-CICE S3 model output. Top rows show shear deformations from multi-day averaged velocity fields, averaged through division of the number of time steps in the 6-day window. Bottom rows show a summation of the shear deformations from multi-day averaged velocity pairs at different time steps.

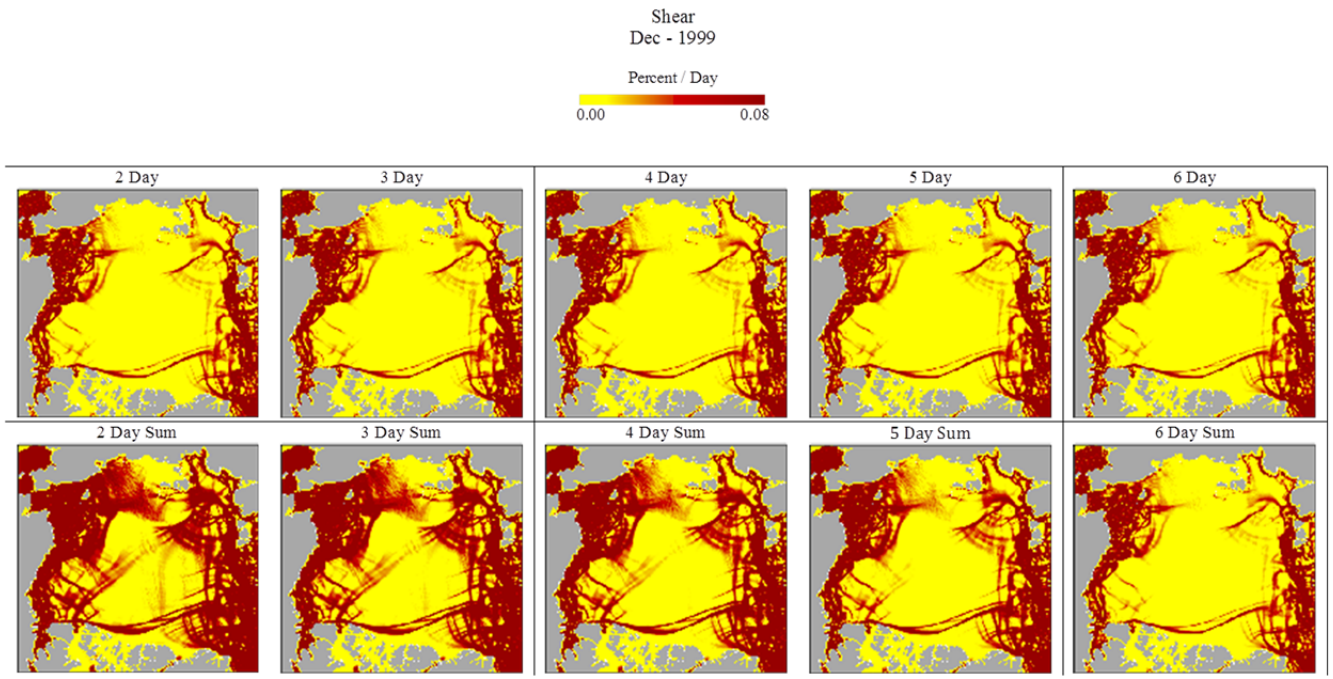

Figure 23. December 1999 example of alternative shear calculations from POP-CICE S3 model output. Top rows show shear deformations from multi-day averaged velocity fields, averaged through division of the number of time steps in the 6-day window. Bottom rows show a summation of the shear deformations from multi-day averaged velocity pairs at different time steps.

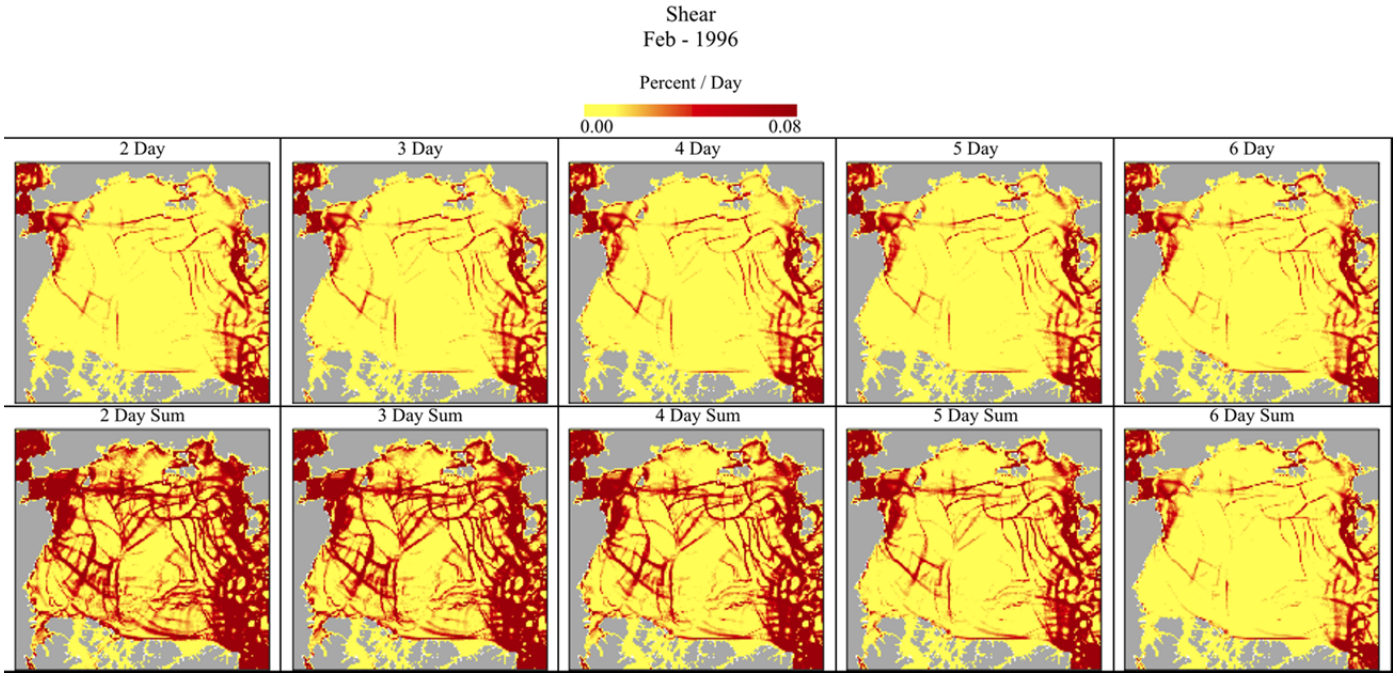

Figure 24. February 1996 example of alternative shear calculations from POP-CICE S3 model output. Top rows show shear deformations from multi-day averaged velocity fields, averaged through division of the number of time steps in the 6-day window. Bottom rows show a summation of the shear deformations from multi-day averaged velocity pairs at different time steps.

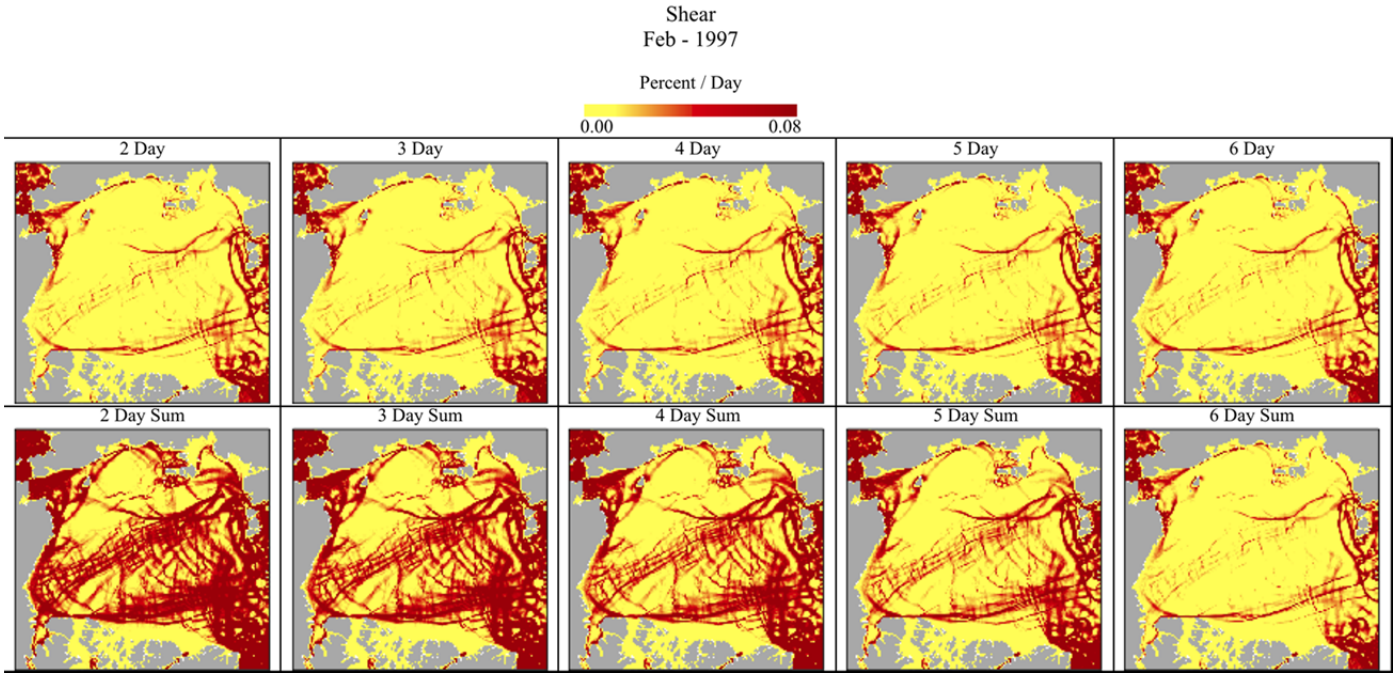

Figure 25. February 1997 example of alternative shear calculations from POP-CICE S3 model output. Top rows show shear deformations from multi-day averaged velocity fields, averaged through division of the number of time steps in the 6-day window. Bottom rows show a summation of the shear deformations from multi-day averaged velocity pairs at different time steps.

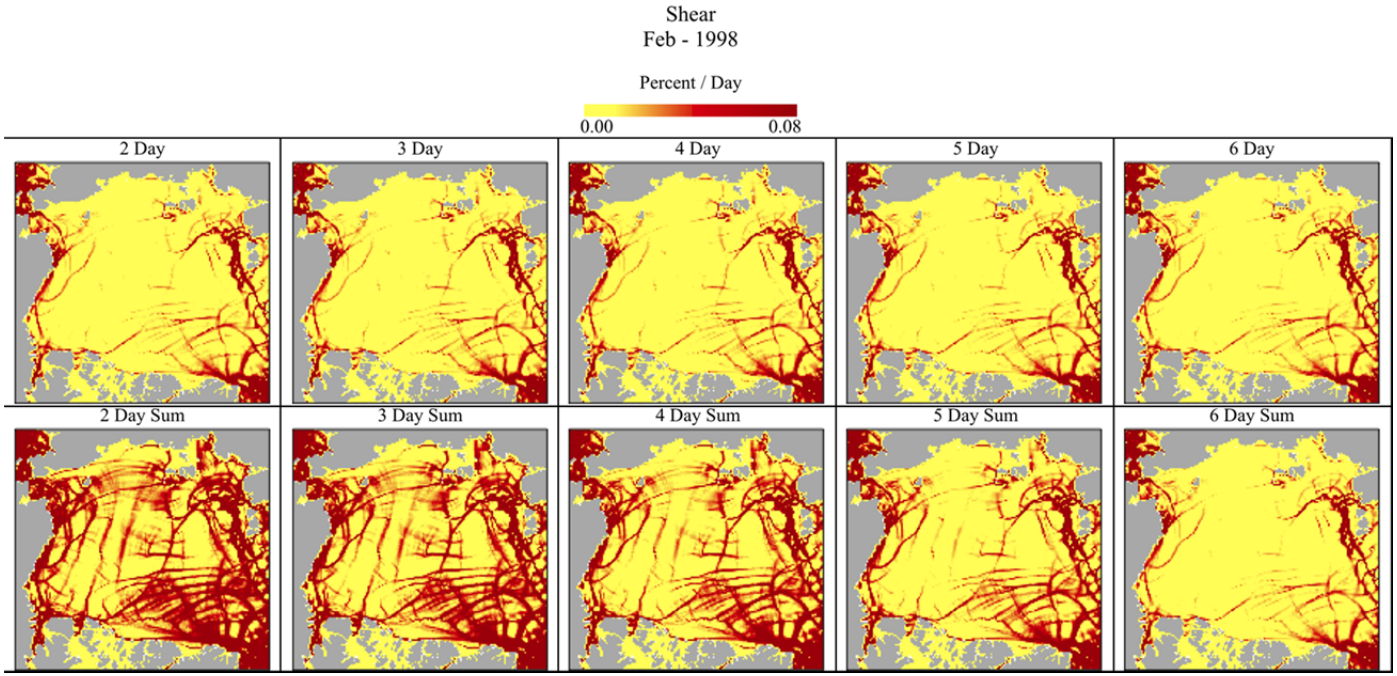

Figure 26. February 1998 example of alternative shear calculations from POP-CICE S3 model output. Top rows show shear deformations from multi-day averaged velocity fields, averaged through division of the number of time steps in the 6-day window. Bottom rows show a summation of the shear deformations from multi-day averaged velocity pairs at different time steps.

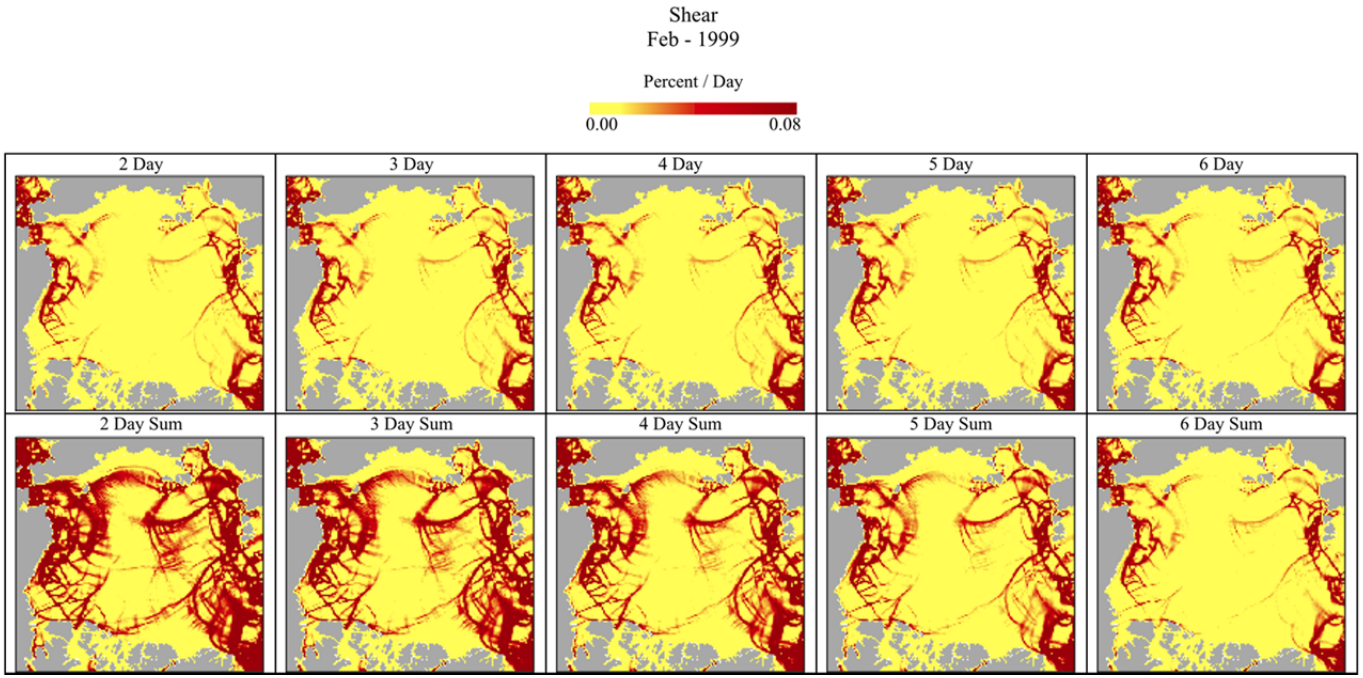

Figure 27. February 1999 example of alternative shear calculations from POP-CICE S3 model output. Top rows show shear deformations from multi-day averaged velocity fields, averaged through division of the number of time steps in the 6-day window. Bottom rows show a summation of the shear deformations from multi-day averaged velocity pairs at different time steps.

C. REGIONAL DEFORMATION COMPARISON

This section provides regional, small-scale deformation results from PIPS (NPS in figures) and POP-CICE S3 model runs compared to deformation calculated from RGPS ice motion fields over three winter seasons (Figures 28 through 30). Time series analysis is presented from six-day shear calculations from model- and RGPS-derived velocity fields separated into the five regions described in section A. Calculations for this section were performed using the original six-day averaging approach described by Kwok et al. (2008). These time series show spatial and temporal correlations between model and RGPS deformation calculations over entire winter seasons. Deformation magnitude and temporal phase agreement of model output and RGPS estimates are analyzed in the next chapter. Statistical analyses of these plots are provided in Table 3.

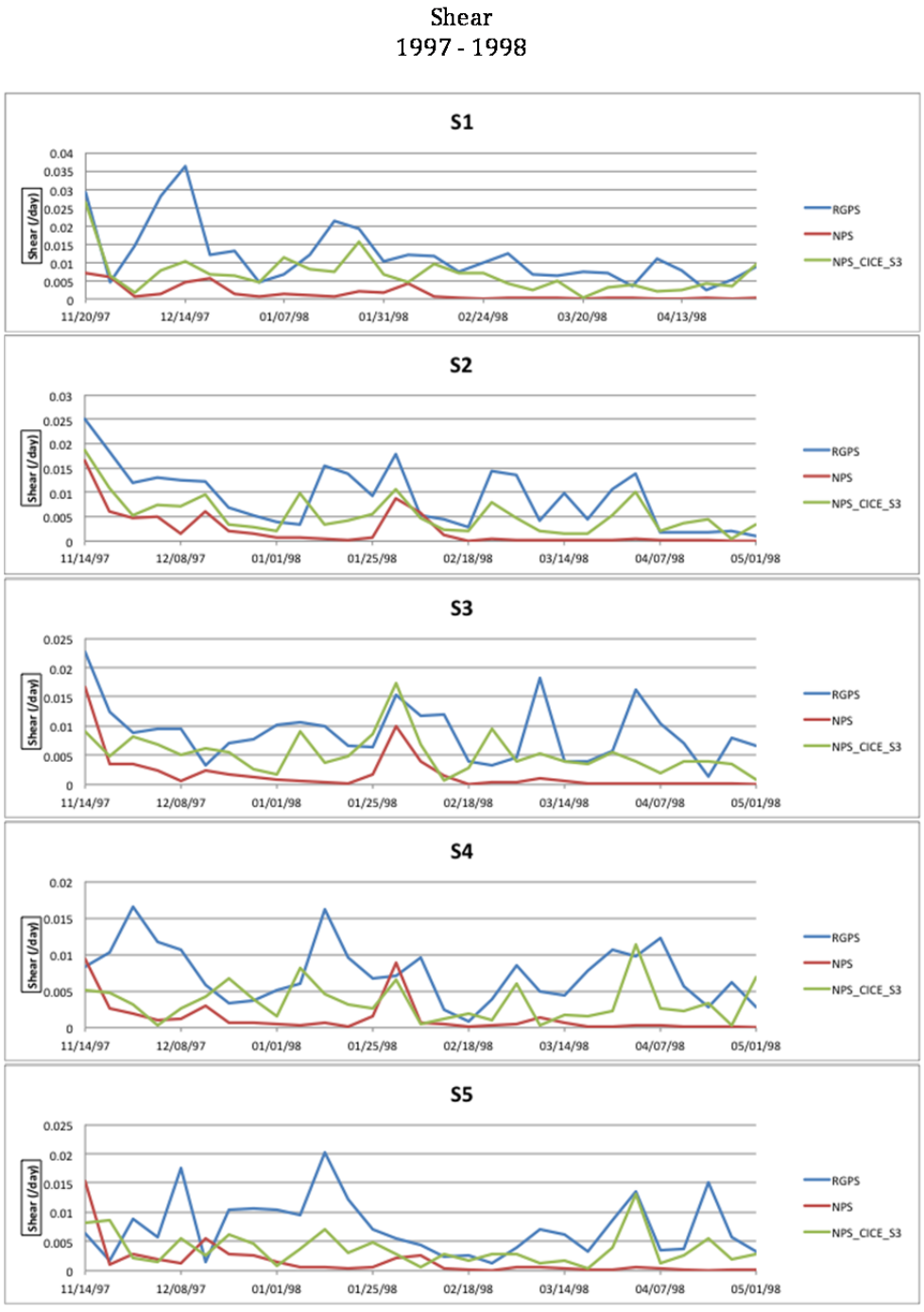

Figure 28. Time series (1997–1998) of the mean 6-day regional shear derived from model and RGPS ice drift for regions S1 through S5 (defined previously) between November 1997 and April 1998.

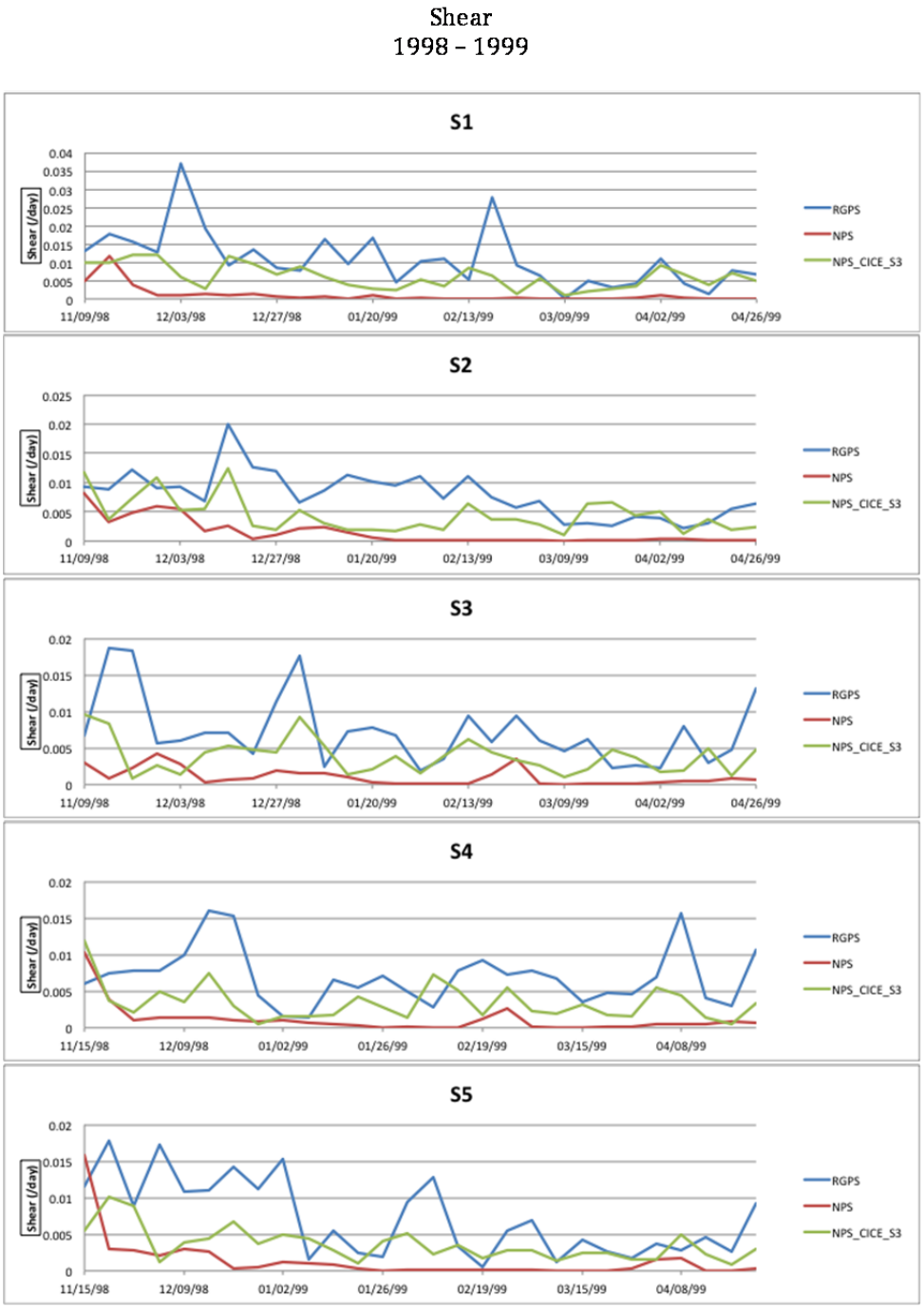

Figure 29. Time series (1998–1999) of the mean 6-day regional shear derived from model and RGPS ice drift for regions S1 through S5 (defined previously) between November 1998 and April 1999.

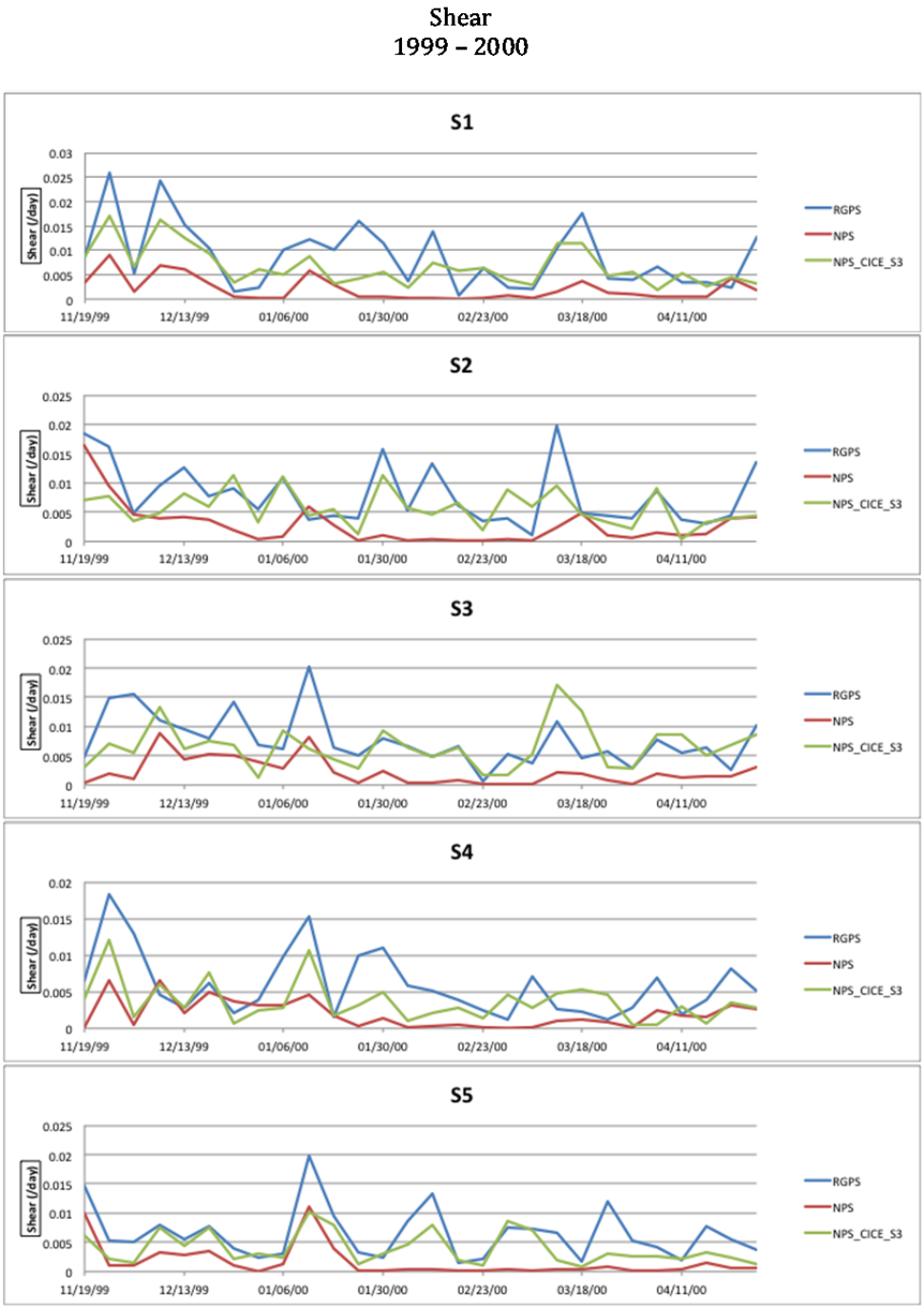

Figure 30. Time series (1999–2000) of the mean 6-day regional shear derived from model and RGPS ice drift for regions S1 through S5 (defined previously) between November 1999 and April 2000.

	RGPS	NPS	S3	RGPS	NPS	S3	RGPS	NPS	S3
	1997-1998			*1998-1999*			*1999-2000*		
	S1			**S1**			**S1**		
Mean	1.18	0.14	0.67	1.08	0.11	0.61	0.85	0.22	0.69
Std Dev	0.82	0.20	0.51	0.78	0.23	0.33	0.66	0.25	0.41
Max	3.64	0.69	2.62	3.71	1.18	1.20	2.58	0.90	1.72
Min	0.23	0.00	0.03	0.01	0.00	0.09	0.07	0.00	0.19
CORREL		0.48	0.58		0.29	0.27		0.61	0.67
	S2			**S2**			**S2**		
Mean	0.90	0.22	0.54	0.79	0.15	0.45	0.80	0.28	0.57
Std Dev	0.62	0.36	0.39	0.39	0.21	0.30	0.52	0.35	0.30
Max	2.51	1.65	1.86	2.00	0.82	1.23	1.98	1.64	1.14
Min	0.10	0.00	0.04	0.22	0.00	0.10	0.11	0.01	0.03
CORREL		0.66	0.75		0.37	0.35		0.50	0.58
	S3			**S3**			**S3**		
Mean	0.89	0.19	0.53	0.72	0.10	0.39	0.76	0.23	0.65
Std Dev	0.48	0.35	0.33	0.47	0.12	0.24	0.43	0.23	0.36
Max	2.26	1.68	1.72	1.88	0.42	0.95	2.02	0.89	1.70
Min	0.14	0.00	0.07	0.19	0.00	0.08	0.07	0.02	0.12
CORREL		0.65	0.28		0.26	0.34		0.63	0.31
	S4			**S4**			**S4**		
Mean	0.74	0.13	0.35	0.70	0.11	0.34	0.59	0.20	0.38
Std Dev	0.39	0.23	0.27	0.38	0.20	0.25	0.43	0.19	0.29
Max	1.66	0.94	1.14	1.60	1.02	1.20	1.83	0.66	1.21
Min	0.09	0.00	0.03	0.14	0.00	0.05	0.11	0.00	0.05
CORREL		0.12	0.06		0.05	0.28		0.39	0.53
	S5			**S5**			**S5**		
Mean	0.73	0.16	0.37	0.72	0.14	0.36	0.64	0.16	0.40
Std Dev	0.49	0.29	0.28	0.52	0.30	0.22	0.43	0.27	0.27
Max	2.01	1.54	1.30	1.78	1.59	1.01	1.98	1.10	1.02
Min	0.13	0.00	0.03	0.05	0.00	0.09	0.15	0.00	0.08
CORREL		-0.06	0.46		0.33	0.53		0.75	0.76

Table 3. Statistical comparison of seasonal shear values from Figures 28 through 30. Mean, Standard Deviation (Std Dev), Maximum (Max), Minimum (Min), and Correlation (CORREL) values of shear are displayed by region (all values $*10^{-2}$).

THIS PAGE INTENTIONALLY LEFT BLANK

V. DISCUSSION AND SYNTHESIS OF RESULTS

Results and analyses of NPS model output and RGPS datasets were presented in the previous chapter, with the primary purpose of determining model skill in representing the variability in sea ice kinematics and deformation processes that impact ice thickness distribution in the Arctic. These results are intended to offer an improved insight into potentially critical physical processes and feedbacks that determine the survivability of sea ice in the Arctic. The following discussion and conclusions attempt to define what improvements have been made through sea ice model parameterizations and forcings, and how the performed analyses advance the simulation and prediction of ice thickness distribution in the Arctic. The challenges of direct comparison between model results and RGPS data arise from the differences in how the basin-wide velocity fields, gradients, and deformations are derived. The main difference is due to the respective frame of reference (i.e., Eulerian for model output vs. Lagrangian for RGPS data), which to some degree can be overcome through computational translation between those frameworks to improve spatial and temporal details available from both datasets compared to previous techniques of intercomparison. The strength of the RGPS dataset is that it allows for comparative analysis of modeled small-scale deformations at near basin-scale and at synoptic, seasonal, and inter-annual time scales. This allows for the investigation of short- and long-term responses of modeled sea ice to applied forcing and provides a diagnostic tool to improve the understanding of sea ice model sensitivity to different parameterizations and coupling.

A. LARGE-SCALE DISPLACEMENT AND DEFORMATIONS

Results from the regional analysis of net seasonal displacement and deformation fields of PIPS and POP-CICE model output (Figures 12 through 15) shows the large-scale response of sea ice to prescribed forcing. From the PIPS model results, it can be seen that seasonal displacement was slower than RGPS observations and the areal deformation of each region was subsequently minimal by comparison. This was likely due to the simplified ice strength parameterization and thermodynamics represented in the PIPS model. The POP-CICE model runs, with multi-layer ice strength

parameterizations (R2) and atmosphere-ice / ice-ocean coupling parameterizations (S3), show a large increase in ice motion, which was overestimated particularly along the Canadian Arctic Archipelago (CAA) and Alaskan coast. Table 1 shows that the displacement difference alone was on average 1.8 to 4.2 times greater in the R2 run than RGPS estimates for regions with coastal influence (S1, S2, S3, and S5). This ratio was reduced to an average of 1.2 to 3.0 times greater in the S3 run by weakening the sea ice coupling with the atmosphere and the ocean, however, total sea ice motion was overall still too large. Directional differences of displacement vectors were not improved from PIPS results, and based on the overestimated displacement, the regional deformations were too large as well. These results point to high model sensitivity to ice strength parameters and the influence of modified air-ice and ice-ocean coupling. In the CICE model, ice strength of a grid cell is a function of the fraction of the thinnest ice category, which appears to lead to overestimation of ice drift and deformation without optimal tuning of sub-grid parameterizations controlling ice behavior at a given spatial and temporal resolution.

Regional displacement and deformation fields from various runs of the RACM model (Figure 16), while limited to statistical comparison due to the predictive nature of atmospheric forcing (i.e., RACM atmospheric condition being different from the real atmospheric forcing embedded in RGPS data), show improvements over the previous models. The control cases of RACMa and RACMb, with 20-minute dynamic time steps in the sea ice model, show similar overestimation of regional displacements, but seem to show some improvement in the directional differences from RGPS output, however this could be a coincident with the selected year of model output. The RACMg case, which reduced the dynamic time step to five minutes bringing the sea ice solution closer to plasticity, still represents too much ice motion particularly along the CAA (region S5), where the average displacement ratio ranges from 1.07 to 3.26, but continues the improvement in directional changes where the average maximum angular difference is ~17 degrees (compared to greater than 20 degrees in previous model results). Finally, the RACMh case (one-minute time step) greatly reduces the displacement ratio down to a range of 0.85 to 1.84 (1990–1991 case) when compared to RGPS regional displacements

(Table 2). This improvement is accompanied by further improved directional differences in the displacement vectors in which the average maximum angular difference is reduced to ~11 degrees, and the geometrical representation of the regional deformation looks physically similar to the RGPS estimates.

The high-frequency air-ice feedbacks in addition to spatially high-resolution predicted atmosphere likely play a role in the improved responses seen in these RACM model runs. Winds produced in the WRF model are orders of magnitude greater than the smoothed winds prescribed by the atmospheric forcing used in the POP-CICE and PIPS model runs. The sea ice dynamic time step size allows the model more realistic representation of sea ice thickness build up compared to longer time steps when the elastic and viscous response in sea ice motion is overestimated prior to plastic failure. While exact replication of RGPS analysis is not expected, statistical diagnostics of sea ice model behavior against this dataset will continue to help modelers better understand the sensitivity and impact of various parameterizations.

B. SMALL-SCALE DEFORMATIONS

Linear kinematic features (LKFs) observed in the RGPS analysis represent the prevalence of fracture and failure deformation that occurs in sea ice as blocks of different thickness move relative to one another based on the varying forcing mechanisms found in the Arctic. Shear deformations are one of the prime examples, which display this reaction in the sea ice as cracks and failure lines represent the dynamic nature of the ice sheet. Difficulties in comparing RGPS deformations to model representation of these features are inherent to the difference in methodology of estimating such shear deformations. As briefly mentioned earlier, RGPS deformations are derived from repeat orbit swaths of satellite imagery to determine displacements which then are used to calculate mean sea ice drift, velocity gradients, and finally deformations, which provide a full composite coverage of the western Arctic roughly every six days. Model output provides domain-wide snapshots of ice motion, which can be converted into deformation fields at every model timestep. To minimize the differences resulting from different types of data (i.e., Lagrangian vs. Eulerian) and methods to estimate basin-wide

deformation fields, alternative techniques have been evaluated to optimize intercomparison of deformation features between the two data sources.

The amount of LKFs presented by RGPS analysis has proven difficult to reproduce by the PIPS model, likely due to the simplified ice thickness parameterization used in the model. Figure 17 shows that the POP-CICE model, run with the same resolution as the PIPS model, was able to represent an increased amount of shear deformations and LKFs through the sub-grid representation of multiple ice thickness categories and other parameterizations used in the CICE model. Further analyses (Figures 18 and 19) however revealed that the averaging of model-derived deformation fields over a six-day period to match the composite coverage of RGPS analysis left out many short-lived shear deformations, especially in the deep basin. By this method, only more persistent model events relative to the six-day averaging remain.

To address this issue, an alternative method was developed in an attempt to permit some of the short-term LKFs present in model output, which are naturally included in RGPS data. This method reduces the time period (i.e., number of days) over which velocity averages are calculated, and sums the results, but does not divide (average) them by the number of days for each deformation increment. A disadvantage of this approach is that at shorter averaging time periods, persisting deformation features can be counted multiple times resulting in deformation fields with regions of exaggerated magnitudes. Figures 20 and 27 however, show that shortening the time step and summing the deformation fields reveal additional features from the model output. A four-day summation appears to represent a good balance between too many repeat counts along the margins, and higher resolution of short-term features in the central Arctic. This four-day summation (bottom middle panel in each figure) represents velocities averaged from the beginning (days 1–4), middle (days 2–5), and end (days 3–6) of the six-day period covered by RGPS analysis. The areas with overly increased shear percentages lie primarily outside the region represented in the RGPS plots, so it is difficult to quantify their realism. While there is no optimal comparison of model output to RGPS coverage, the four-day summations display the full breadth of features that are present in the model, and are in better agreement with RGPS-derived deformation fields.

C. REGIONAL DEFORMATION COMPARISON

While it is not expected that sea ice modeling efforts should be capable of exactly reproducing events from the past, especially at the synoptic scale of the atmospheric forcing which provides most of the impetus for sea ice motion, seasonal analysis of deformation features can be expected to approach the general timing, if not the absolute magnitude of events based on observational re-analysis. In this respect, the POP-CICE S3 model shows a vast improvement of deformation representation over the PIPS model presented in the Kwok et al. (2008) paper. Comparison of the time series of regional shear over the three seasons presented (Figures 28–30), the PIPS model displays only occasional periods of increased shear represented during large events in the RGPS record, but overall is significantly underestimating the amount of shear present in the sea ice. Almost no shear is present in PIPS for weeklong to monthly periods where RGPS shows an entirely different behavior of the sea ice. As discussed previously, this is likely due to overestimation of ice strength, which is determined as a function of the mean grid cell thickness in PIPS compared to being a function of the fraction of the thinnest ice in CICE model. The POP-CICE S3 model results show an improvement, not only in the phase agreement of most of the events, but also by approaching the magnitude of shear deformations represented in RGPS data.

The increase in magnitude of shear events throughout the seasons analyzed is expected from the improved sea ice model representing multiple thickness layers. As can be seen in Table 3, the POP-CICE S3 mean seasonal shear values for all regions defined, range from two to seven times the shear magnitudes represented in the PIPS model. While on average, these values still lag behind the magnitude of shear represented in the RGPS data, this is a significant improvement especially given the low-resolution and daily averaged atmospheric forcing prescribed in those runs. It is also worth noting that shear magnitudes in the model were all calculated using the original method of deformation averaging (used by Kwok et al. 2008 as discussed in Chapter IV Section B), which means that many short-lived shear features present in the model are likely filtered out through this process. Also, with the overestimation of regional velocity vectors presented in Figures 12 through 15, it is interesting to note that small-scale deformations

taken from six-day averages do not often produce shear values beyond the magnitude of those represented by the RGPS observations. Further analysis will be required to determine the significance of anomalous large-scale sea ice velocity fields and if improving the velocity estimations alters the amount of small-scale deformations produced from model output.

Phase agreement among RGPS data and POP-CICE model output is still somewhat reduced due to the previously discussed problems with direct comparison between the two datasets. As mentioned earlier, the POP-CICE S3 model run still uses re-analysis of atmospheric forcing, which is still a model product characterized by smoothed wind fields and low spatial resolution relative to the sea ice model, and more importantly, can only be roughly compared to the actual atmospheric conditions to which sea ice response is recorded in RGPS data. Nonetheless, reasonable phase correlation can be observed in the relative timing of various shear events, particularly in regions along coastal boundaries (regions S1, S2, and S5 in Table 3). Improvements in the phase correlation for particular regions may indicate that certain combinations of sea ice and forcing regimes common to the defined regions are better represented in the model. Additional analysis is required to determine if such trends exist, but such investigation is beyond the current scope of this work. Remaining discrepancies in the magnitude and phase of shear deformations between POP-CICE and RGPS will continue to be analyzed in future RACM model runs once model output overlapping with the period of RGPS data is available. The presented analyses however, provide the first significant step in diagnosing improvements and skill in simulating regional and seasonal deformations by high-resolution multi-category sea ice models.

VI. CONCLUSIONS AND FUTURE RECOMMENDATIONS

A. CONCLUSIONS

The analyses of results presented in this thesis show that model skill in representing sea ice kinematics has improved as a direct result of recent upgrades to the POP-CICE and RACM models within the NPS Arctic Modeling Effort. This assessment of modeling capabilities is by no means comprehensive, but is intended to evaluate and where possible quantify a portion of the model improvements related to the representation of sea ice thickness distribution that has been made in CICE model and how it influences the representation of sea ice kinematics. The sea ice dynamical response to external forcing in the Arctic is one of the most critical indicators of the Earth's response to the changing climate that has been observed and reported in recent decades. With ice extent continuously on the decline, and ice thickness diminishing whether through export, melting, or redistribution, a new regime of sea ice and the potential for seasonal sea ice coverage is likely on the horizon, if not already there. Therefore, the ability of numerical models to represent and predict sea ice response to anticipated changes in forcing is paramount to those who live and operate in the region, as well as to those who need to model and predict responses to global climate change in general.

Regional high-resolution models, such as the ones analyzed in this research, are currently not practical for calculations on a global scale due to the computational constraints of current computing capabilities. However, the ability of regional models to represent small-scale processes and determine their relative influence on larger-scale climate is important for advancements in earth system modeling. The efficiency and predictive capability of global models relies, at least in part, on understanding and representation of processes at smaller scales. Sea ice displacement and subsequent deformation patterns depend on a number of complex factors, which need to be isolated to determine their relative importance and contribution to ice thickness predictions. In this study, we have attempted to move this effort forward through analyses of sea ice dynamics and the ability of coupled models to reproduce observational estimates of

deformation fields. A continuation of this effort with output from subsequent model runs, in concert with a synthesis of model thermodynamic performance, will better position the scientific community to make determinations that may help improve sea ice prediction capabilities in the future.

Results from the NPS coupled models of POP-CICE and RACM reveal several key indications that new model parameterizations are contributing to the ability of models to represent kinematic features in Arctic sea ice. Multiple category sea ice thickness models begin to address the issue of resolving the relatively small-scale dynamic features that develop from sea ice response to forcing mechanisms, which influence overall ice thickness distribution. Increased ice motion from these models, while overestimated in several regions, show that new model parameterizations allow the modeled sea ice to have an appropriate physical response to anticipated forcing, but the estimated magnitude needs to be tuned. Fully coupled regional model runs (RACM) show improvements to displacement fields in this initial analysis by decreasing the dynamic time step, which allows for more plastic behavior of the sea ice. This behavior, along with additional feedbacks from sea ice strength and coupling of predicted atmospheric and oceanic influence may lead to more realistic representation of kinematic features, which can then be compared to the thermodynamic response of sea ice to determine their relative contribution to ice thickness distribution.

Improvements to the small-scale deformations represented by the POP-CICE model is an additional indication that sea ice thickness is an important parameter to correctly model. Sub-grid representation of multiple thickness categories in this model allow deformations to occur based on the weakest category present in a grid cell, which has led to increased resolution of deformations derived by the model. The relatively high frequency of model output (compared to RGPS data) has revealed additional short-term deformations present in model output, which could lead to improved insight into sea ice behavior. Improved magnitude and phase agreement of shear deformations found in the POP-CICE model over seasonal analysis show promise in the ability of such models to improve the representation of sea ice thickness distribution and the response and survival of sea ice in this environment. These enhanced deformation fields diagnosed to greatly

improve upon the comparison to RGPS observations, will help modelers understand the sensitivity of ice parameterizations that are required to physically represent in future model advancements under different spatial and temporal resolution configurations.

The improved representation of sea ice deformations found in this study show that ice thickness and forcing parameterizations are integral to the ability of regional and global models to represent sea ice kinematics. Deformation patterns observed in the Arctic are a direct response to the dynamic forcing the ice cover experiences, and as physical changes to sea ice properties are imposed under changing climate, the ability of models to represent these features will lead to better understanding of the underlying processes. The methodology displayed here will serve as an analysis tool to be used on future modeling efforts as means of diagnosing modifications to physical and temporal parameterizations, and help quantify the importance of incorporating kinematic feature resolving models into global climate modeling efforts.

How significant a role the dynamical response of sea ice plays in determining the sea ice production and redistribution of ice thickness is still being investigated, at the same time as thermodynamic changes in the region likely have a large impact as well. By honing in on model capabilities to represent sea ice dynamics, future studies will be able to better attribute the changes observed in the ice pack, and determine the relative contribution of dynamic and thermodynamic patterns. Atmospheric and oceanic feedback processes that impact sea ice are challenging to quantify and attribute direct cause and effect parameters for sea ice modeling, but this effort must continue, especially at high-resolution, in the face of increased activity and significant climate change observed in the Arctic.

The political environment has changed in the recent past, and a focus on the interdependence of national interests on a global economy would be a logical framework from which future operations in the Arctic should proceed. Increased demand for natural resources through the proliferation of industrialized nations poses a national security and environmental challenge through increased operations in the Arctic, but should also provide an opportunity for increased research due to higher demand for expertise in the region, as well as the potential for improved international cooperation through the goal of

finding solutions toward a common interest of managing our changing environment. Future responses to climate change will be dependent upon our ability to improve predictability of Arctic climate change and properly prepare for the challenges that lie ahead.

B. FUTURE RECOMMENDATIONS

The ability of numerical models and RGPS analysis to accurately represent the dynamic environmental conditions found in the Arctic is paramount to the goal of predicting future responses to climate change. Observational trends indicate that sea ice in the Arctic is entering a new regime leading to the potential for seasonal ice cover in an ocean formerly obscured by multiyear ice. A combination of model simulation and observational validation of these trends will be required to determine how the sea ice is responding to this new polar environment. Observational techniques have been developed recently for in-situ instrumentation and data processing capabilities, which will help to verify current representation and prediction capabilities of the Arctic models analyzed in this study. To build upon current capabilities of modeling techniques to represent the physical characteristics of sea ice in the Arctic, the following recommendations are made for future research considerations.

1. Model Data Limitations

This study was limited based upon availability of various model output results, which were limited to runs through 2002 (PIPS), 2004 (POP-CICE), and the early 1990s (RACM). Future studies could use this analysis as a template for evaluating extended runs in terms of model sea ice drift, deformations, and ice thickness distribution, as well as sensitivity of those fields to sea ice parameterizations and different forcing mechanisms. Honing the skills of choosing appropriate model time steps and coupling parameterizations that allow for improved realism of deformation would not only enable better model validation against satellite observations, but also help to determine the relative importance of representing dynamic and thermodynamic processes.

Improved model resolution could also play an important role in determining which parameters need to be represented in global models. Increased spatial resolution

might capture dynamic processes that are currently underrepresented in the 9 km models used in this study. This is not a trivial or straightforward process however as reducing the grid spacing brings along additional challenges that alter current model assumptions. At a resolution on the order of a few kilometers, sea ice cannot be treated like a fluid, as individual, larger ice floes become resolved so ice moves toward more granular dynamic behavior. Anisotropic modeling techniques, may help indirectly address some of the challenges of representing dynamic sea ice behavior and better handle the linear kinematic features discussed in this study, so such an approach should be further investigated and tested in high resolution sea ice models.

Finally, a combination of high and low resolutions model results should be analyzed in comparison to determine how important physical representation of deformation processes are to the overall behavior and thickness distribution of sea ice in the Arctic. Current efforts towards improving ice dynamic models must work in parallel to achieve a better understanding of the thermodynamic behavior of sea ice in order to determine the relative contribution of each to sea ice distribution. Regional models are capable of resolving dynamic and thermodynamic behaviors at a scale not currently possible in global models. Therefore a thorough analysis of the relative contribution of small-scale processes on the overall behavior of sea ice in global models will help these models incorporate the most pertinent parameters as computational capabilities allow. Regional model validation in this manner will also help to develop usage as an operational tool for defense downscaling applications as predictive capabilities are improved through a better understanding of the underlying processes that drive sea ice behavior in the future

2. Satellite Observations

In this study, RGPS analysis was limited to data for the years 1996 through 2001, although additional data from this satellite observational tool exists through 2007. Once model output is released through this time frame, continuation of this analysis should be conducted to extend the length of this dataset as a means of validation of the conclusions made in this research, and to determine if additional trends are observed. While the

RADARSAT-1 mission extended well beyond its initial five-year charter and has provided data for over 15 years, several new satellite observational tools have been launched (e.g., RADARSAT-2, CryoSat-2, IceBridge) or are in the planning phase of development (e.g., IceSat-2), which will bring about several improvements to the observational capabilities satellites can provide.

The ICESat program, which uses laser altimetry to determine sea ice freeboard as a means of estimating ice thickness and volume distribution, stopped collecting data in 2009 due to the failure of the laser and inability to repair it in flight. With the new ICESat-2 satellite not scheduled for launch until 2016, the IceBridge program was developed as a means of continuing the data collection in the interim by flying aircraft over specific regions to make similar measurements. While limited in range compared to the ICESat coverage, this technique maintains the capability of observing thickness behavior until the launch of the improved ICESat-2 satellite. An additional platform for observation of sea ice is CryoSat-2, which uses radar altimetry similar to RADARSAT-1, at improved resolution to estimate ice thickness and potentially ice motion characteristics of sea ice. This next generation of satellite observations of Arctic sea ice will likely bring about new resolution to sea ice observational techniques, including basin scale estimates of sea ice thickness distribution and volume. These capabilities should be exploited to improve modeling capacity to represent sea ice behavior in a similar manner as the analysis provided here.

3. Additional Model Parameterizations

Several parameterization efforts require additional attention in order to improve sea ice modeling techniques. Consideration should be made to improve the parameterization and prediction of snow cover in the Arctic as it has a large impact on sea ice behavior.

Incorporation of new ridging and melt pond parameterizations that have been developed in the CICE model should be tested in high resolution model configurations and results analyzed to determine the improvements made by characterizing these

important features of sea ice. Thickness validation efforts must continue in order to better understand the three dimensional response of sea ice to environmental forcing.

Atmospheric forcing has been constrained in the modeling efforts by limited resolution, which likely contributes to biases in the sea ice response in certain regions. Whether through smoothed and low resolution forcing prescribed in POP-CICE from ECMWF or from other global re-analyses, the atmospheric forcing present in current models lags in its ability to reproduce the true observed behavior in the Arctic. Realistic atmospheric forcing through improved re-analysis and higher resolution representation, such as predicted atmosphere in RACM, will help improve modeling efforts to resolve smaller scale forcing mechanisms that likely drive sea ice response to the changing climate.

All of these efforts in combination will help not only the modeling community better represent the Arctic environment and its response to climatic forcing, but will help to determine the strengths and weaknesses of different parameterizations in future modeling efforts.

THIS PAGE INTENTIONALLY LEFT BLANK

LIST OF REFERENCES

Alexeev, V. A., 2010: Arctic Amplification: Local or Global?, *A Science Plan for Regional Arctic System Modeling,* Roberts, A. et al., Eds., International Arctic Research Community, 21–22.

Andreadis, K., P. Storck, and D. P. Lettenmaier, 2009: Modeling snow accumulation and ablation processes in forested environments, *Wat. Resourc. Res*., **45**, W05429, doi:10.1029/2008WR007042.

Arctic Council, 1996: Declaration of the Establishment of the Arctic Council, Ottawa, Canada, 5 pp.

Arctic Marine Shipping Assessment (AMSA) 2009 Report, Arctic Council, April 2009 Retrieved from http://www.arcticdata.is/index.php?option=com_phocadownload&view=file&id=106:sipping-routes

Bindoff, N. L., J. Willebrand, V. Artale, A, Cazenave, J. Gregory, S. Gulev, K. Hanawa, C. Le Quéré, S. Levitus, Y. Nojiri, C.K. Shum, L.D. Talley and A. Unnikrishnan, 2007: Observations: Oceanic Climate Change and Sea Level. In: *Climate Change 2007: The Physical Science Basis. Contribution of Working Group I to the Fourth Assessment Report of the Intergovernmental Panel on Climate Change* [Solomon, S., D. Qin, M. Manning, Z. Chen, M. Marquis, K.B. Averyt, M. Tignor and H.L. Miller (eds.)]. Cambridge University Press, Cambridge, United Kingdom and New York, NY, USA.

Borgerson, S. G., 2008: Arctic meltdown: the economic and security implications of global warming. *Foreign Affairs*, **8**, 63–77.

Bowling, L. C., and D. P. Lettenmaier, 2010: Modeling the Effects of Lakes and Wetlands on the Water Balance of Arctic Environments. *J. Hydrometeor*, **11**, 276–295. doi: http://dx.doi.org/10.1175/2009JHM1084.1

Bromwich, D. H., K. M. Hines, and L.-S. Bai, 2009: Development and testing of Polar WRF: 2. Arctic Ocean. *J. Geophys. Res*., **114**, D08122, doi:10.1029/2008JD010300.

Canadian Space Agency (CSA), cited 2010: The RADARSAT Constellation Program. [Available online at http://www.asc-csa.gc.ca/pdf/radarsat_constellation_eng.pdf]

———, cited 2011: RADARSAT Systems: Satellite Characteristics. [Available online at http://www.asc-csa.gc.ca/pdf/Radarsat_IGARSS_eng.pdf]

Canadian Space Agency (CSA), cited 2012: RADARSAT-1. [Available online at http://www.asc-csa.gc.ca/eng/satellites/radarsat1/]

Cherkauer, K. A., L. C. Bowling and D. P. Lettenmaier, 2003: Variable Infiltration Capacity (VIC) cold land process model updates, *Global and Planetary Change* **38**, 151–159.

Chylek, P., C. K. Folland, G. Lesins, M. K. Dubey, and M. Wang, 2009: Arctic air temperature change amplification and the Atlantic Multidecadal Oscillation, *Geophys. Res. Lett.*, **36**, L14801, doi:10.1029/ 2009GL038777.

Clement, J. L., W. Maslowski, L. Cooper, J. Grebmeier, W. Walczowski, 2005: Ocean circulation and exchanges through the northern Bering Sea, 1979–2001 model results. *Deep Sea Research II*, **52**, p. 3509-3540, doi: 10.1016/j.dsr2.2005.09.010.

Comiso, J.C., C.L. Parkinson, R. Gersten, and L. Stock, 2008: Accelerated decline in the Arctic sea ice cover. *Geophysical Research Letters*, **35**, L01703, doi:10.1029/2007GL031972.

Coon, M., R. Kwok, G. Levy, M. Pruis, H. Schreyer, and D. Sulsky, 2007: Arctic Ice Dynamics Joint Experiment (AIDJEX) assumptions revisited and found inadequate, *J. Geophys. Res*., **112**, C11S90, doi:10.1029/ 2005JC003393.

Department of Defense (DoD), 2011: Report to Congress on Arctic Operations and the Northwest Passage, 32 pp.

Drobot, S., J. Stroeve, J. Maslanik, W. Emery, C. Fowler, J. Kay, 2008: Evolution of the 2007–2008 Arctic sea ice cover and prospects for a new record in 2008. *Geophys Res Lett,* **35**, L19501, doi:10.1029/2008GL035316.

Dukowicz, J. K., and R. D. Smith (1994), Implicit free-surface for the Bryan-Cox-Semtner ocean model, *J. Geophys. Res*., **99**, 7991–8014, doi:10.1029/93JC03455.

Francis, J. A., E. Hunter, J. R. Key, and X. Wang, 2005: Clues to variability in Arctic minimum sea ice extent, *Geophys. Res. Lett.*, **32**, L21501, doi:10.1029/ 2005GL024376.

Fowler, C., W. J. Emery, and J. Maslanik, 2004: Satellite-derived evolution of Arctic sea ice age: October 1978 to March 2003, *IEEE Geosci. Remote Sens. Lett*., **1**(2), 71–74, doi:10.1109/LGRS.2004.824741.

Government Accountability Office (GAO), 2012: Report to Congressional Commitees, Arctic Capabilities, 46 pp.

Hibler, W. D. 1979: A dynamic thermodynamic sea ice model. *Phys. Oceanogr.,* **9**, 817–846.

Hibler, W. D., III, 1980: Modeling a variable thickness sea ice cover. *Mon. Wea. Rev.,* **108,** 1943–1973.

Higgins, M. E., J. J. Cassano, A. Craig, W. Gutowski, J. He, J. Jakacki, D. Lettenmaier, W. Maslowski, A. Roberts, and C. Zhu, 2012: The Regional Arctic Climate Model (RACM): Atmospheric implementation and validation, *J. Climate*, in review.

Hines, K. M., and D. H. Bromwich, 2008: Development and Testing of Polar WRF. Part I. Greenland Ice Sheet Meteorology. *Mon. Wea. Rev*., **136**, 1971–1989, doi: 10.1175/2007MWR2112.1.

Holloway, G., and T. Sou, 2002: Has arctic sea ice rapidly thinned?, *J. Clim*., **15**, 1691–1701.

Hopkins, M. A., and W. D. Hibler III, 1991: On the ridging of a thin sheet of lead ice. *Ann. Glaciol*., **15**, 81–86.

Hunke, E. C., 2001: Viscous-plastic sea ice dynamics with the EVP model: Linearization issues. *J. Comput. Phys.,* **170,** 18–38.

———, and J. K. Dukowicz, 1997: An elastic-viscous-plastic model for sea ice dynamics. J. Phys. Oceanogr., **27**, 1849–1867.

———, and W. H. Lipscomb, 2001: CICE: The Los Alamos Sea Ice Model, Documentation and Software, version 3., LA-CC-98-16, Los Alamos National Laboratory, Los Alamos, NM, 52 pp.

———, and ———, 2006: CICE: The Los Alamos Sea Ice Model, Documentation and Software User's Manual, version 3.14, LA-CC-98-16, Los Alamos Natl. Lab., Los Alamos, N. M., 59 pp.

———, and ———, 2008: CICE: The Los Alamos Sea Ice Model, Documentation and Software User's Manual, version 4.0, LA-CC-06-012, Los Alamos Natl. Lab., Los Alamos, N. M., 59 pp.

Intergovernmental Panel on Climate Change (IPCC), 2007a: Climate Change 2007: Synthesis Report. Cambridge University Press, 52 pp.

———, 2007b: Summary for Policymakers. Climate Change 2007: The Physical Science Basis. *Contribution of Working Group I to the Fourth Assessment Report of the Intergovernmental Panal on Climate Change*, Eds. S. Solomon, D. Qin, M. Manning, Z. Chen, M. Marquis, K.B. Averyt, M. Tignor, and H.L. Millar, Cambridge University Press, 18 pp.

———, cited 2012: Organization. [Available online at http://www.ipcc.ch/organization/organization.shtml]

Isachenkov, V., cited 2010: Russia Norway OK Barents Sea border in Arctic. The Associated Press. [Available online at http://www.buffalonews.com/wire-feeds/24-hour-world-news/article190999.ece]

Jakobsson M., N. Z. Cherkis, J. Woodword, R. Macnab, and B. Coakley, 2000: New grid of the Arctic bathymetry aids scientists and mapmakers. *EOS Transactions, American Geophysical Union,* **81**(9):89,93,96.

Jet Propulsion Laboratory (JPL), cited 2012: MEaSUREs: Small-Scale Kinematics of Arctic Ocean Sea Ice, California Institute of Technology. [Available online at http://rkwok.jpl.nasa.gov/radarsat/index.html]

Johannessen, O. M., L. Bengtsson, M. W. Miles, S. I. Kuzmina, V. A. Semenov, G. V. Alekseev, A. P. Nagurnyi, V. F. Zakharov, L. P. Bobylev, L. H. Pettersson, K. Hasselmann, and H. P. Cattle, 2004: Arctic climate change: Observed and modeled temperature and-ice variability, Tellus, Ser. A, 56, 328–341.

Kovacs, A., 1996: Sea ice: Part II. Estimating the full-scale tensile, flex- ural, and compressive strength of first-year ice, Rep. 96–11, Cold Reg. Res. and Eng. Lab., Hanover, N. H., 17 pp.

Kwok, R., J.C. Curlander, R. McConnell, and S.S. Pang, 1990: An ice-motion tracking system at the Alaska SAR facility. *IEEE J. Ocean. Eng.,* **15(1),** 44–54.

———, D. A. Rothrock, H. L. Stern, and G. F. Cunningham, 1995: Determination of ice age using Lagrangian observations of ice motion, *IEEE Trans. Geosci. Remote Sens.*, **33**(2), 392–400.

———, A. Schweiger, D.A. Rothrock, S. Pang, and C. Kottmeier, 1998: Sea ice motion from satellite passive microwave imagery assessed with ERS SAR and buoy motions. *J. Geophys. Res.*, **103(C4),** 8191–8214.

———, and G. F. Cunningham, 2000: RADARSAT Geophysical Processor System: Data User's Handbook (Version 1.0), JPL D-19149.

———, G. F. Cunningham, and S. S. Pang, 2004a: Fram Strait sea ice outflow, *J. Geophys. Res.*, **109**, C01009, doi:10.1029/2003JC001785.

———, H. J. Zwally, and D. Yi, 2004b: ICESat observations of Arctic sea ice: A first look, *Geophys. Res. Lett.*, **31**, L16401, doi:10.1029/ 2004GL020309.

———, 2006: Contrasts in sea ice deformation and production in the Arctic seasonal and perennial ice zones, *J. Geophys. Res.*, **111**, C11S22, doi:10.1029/2005JC003246.

———, 2007: Near zero replenishment of the Arctic multiyear sea ice cover at the end of 2005 summer, *Geophys. Res. Lett.*, **34**, L05501, doi:10.1029/2006GL028737.

———, G. F. Cunningham, H. J. Zwally, and D. Yi, 2007: Ice, Cloud, and land Elevation Satellite (ICESat) over Arctic sea ice: Retrieval of freeboard, *J. Geophys. Res.*, **112**, C12013, doi:10.1029/2006JC003978.

———, and G. F. Cunningham, 2008: ICESat over Arctic sea ice: Estimation of snow depth and ice thickness, *J. Geophys. Res*., **113**, C08010, doi:10.1029/2008JC004753.

———, E.C. Hunke, W. Maslowski, D. Menemenlis, and J. Zhang, 2008: Variability of sea ice simulations assessed with RGPS kinematics. *J. Geophys. Res.*, **113**, C11012, doi:10.1029/2008JC004783.

———, and D. A. Rothrock, 2009: Decline in Arctic sea ice thickness from submarine and ICESat records: 1958–2008, *Geophys. Res. Lett*., **36**, L15501, doi:10.1029/2009GL039035.

———, G. F. Cunningham, M. Wensnahan, I. Rigor, H. J. Zwally, and D. Yi, 2009: Thinning and volume loss of the Arctic Ocean sea ice cover: 2003–2008, *J. Geophys. Res.*, **114**, C07005, doi:10.1029/2009JC005312.

———, and G. F. Cunningham, 2010: Contribution of melt in the Beaufort Sea to the decline in Arctic multiyear sea ice coverage: 1993–2009, *Geophys. Res. Lett*., **37,** L20501, doi: 10.1029/2010GL044678.

———, 2010: Satellite remote sensing of sea-ice thickness and kinematics: a review, *J. Glaciology*, **56(200)**, 1129–1140.

———, and D. Sulsky, 2010: Arctic Ocean Sea Ice Thickness and Kinematics: Satellite Retrievals and Modeling, *Oceanography*, **23**(4).

Langen, P. L. and V. A. Alexeev, 2007: Polar amplification as a preferred response in an aquaplanet GCM. *Climate Dynamics,* **29**(2-3), 305–317, doi:10.1007/ s00382-006-0221-x.

Lindsay, R. W. and H. L. Stern. 2003: The RADARSAT geophysical processor system: quality of sea ice trajectory and deformation estimates. *J. Atmos. Oceanic Technol.,* **20(9),** 1333–1347.

———, and J. Zhang, 2005: The thinning of Arctic sea ice, 1988-2003: have we passed a tipping point?, *J. Climate*, **18**, 4879–4894.

McPhee, M. G., T. P. Stanton, J. H. Morison, and D. G. Martinson, 1998: Freshening of the upper ocean in the Arctic: Is perennial ice disappearing?, *Geophys. Res. Lett*., **25**(10), 1729–1732.

Maslanik, J. A., M. C. Serreze, and R. G. Barry, 1996: Recent decreases in Arctic summer ice cover and linkages to atmospheric circulation anomalies. *Geophys. Res. Lett.*, **23**(13), 1677–1680.

———, C. Fowler, J. Stroeve, S. Drobot, J. Zwally, D. Yi, and W. Emery, 2007: A younger, thinner Arctic ice cover: Increased potential for rapid, extensive sea-ice loss, *Geophys. Res. Lett.*, **34**, L24501, doi:10.1029/2007GL032043.

———, J. Stroeve, C. Fowler, and W. Emery, 2011: Distribution and trends in Arctic sea ice age through spring 2011, *Geophys. Res. Lett.*, **38**, LXXXXX, doi:10.1029/2011GL047735.

Maslowski, W., and W. Walczowski, 2002: Circulation of the Baltic Sea and its connection to the Pan-Arctic region — a large scale and high-resolution modeling approach. *Boreal Env. Res.* **7**, 319-325. ISSN 1239-6095

———, and W. H. Lipscomb, 2003: High resolution simulations of Arctic sea ice, 1979-1993. *Polar Research*, **22(I)**, 67–74.

———, D. Marble, W. Walczowski, U. Schauer, J. L. Clement, and A. J. Semtner, 2004: On climatological mass, heat, and salt transports through the Barents Sea and Fram Strait from a pan-Arctic coupled ice-ocean model simulation, *J. Geophys. Res.,* **109**, C03032, doi:10.1029/2001JC001039.

———, J. Clement-Kinney, and J. Jakacki, 2007: Toward Prediction of Environmental Arctic Change, *Comp. in Sci. & Eng.*, **9**(6), 29–34.

———, J. L. Clement Kinney, D. C. Marble, and J. Jakacki, 2008: Towards eddy-resolving models of the Arctic Ocean. *Ocean Modeling in an Eddying Regime*, Eds. M.W. Hecht and H. Hasumi, American Geophysical Union, 241–264.

———, J. Clement Kinney, M. E. Higgins, and A. Roberts (2012), Future of Arctic Sea Ice, *Annu. Rev. Earth Pl. Sc.*, accepted.

McGeehan, T., and W. Maslowski, 2011: Impact of Shelf–Basin Freshwater Transport on Deep Convection in the Western Labrador Sea, *J. Phys. Ocean.*, **41**, 2187–2210.

Moritz, R. E., C. M. Bitz, and E. J. Steig, 2002: Dynamics of recent climate change in the Arctic, Science, **297**, 1497–1502, doi:10.1126/science.1076522.

National Snow and Ice Data Center (NSIDC), cited 2011: State of the Cryosphere. [Available online at http://nsidc.org/cryosphere/sotc/sea_ice.html]

Office of the Secretary of Defense (OSD), 2010: Quadrennial Defense Review Report, February 2010, 128 pp.

O'Rourke, R., 2011: Changes in the Arctic: Background and Issues for Congress. Congressional Research Service (CRS), 82 pp.

Overland, J. E., M. C. Spillane, D. B. Percival, M. Wang, and H. O. Mofjeld, 2004: Seasonal and regional variation of pan-Arctic surface air temperature over the instrumental record, *J. Clim*., **17**, 3263–3282, doi:10.1175/1520-0442(2004)017<3263:SARVOP>2.0.CO;2.

———, and M. Wang, 2010: Large-scale atmospheric circulation changes are associated with the recent loss of Arctic sea ice, *Tellus*, Ser. A, **62**, 1–9, doi:10.1111/j.1600-0870.2009.00421.x.

Perovich, D. K., T. C. Grenfell, B. Light, and P. V. Hobbs, 2002: Seasonal evolution of the albedo of multiyear Arctic sea ice, *J. Geophys. Res.*, **107**(C10), 8044, doi:10.1029/2000JC000438.

———, B. Light, H. Eicken, K. F. Jones, K. Runciman, and S. V. Nghiem, 2007: Increasing solar heating of the Arctic Ocean and adjacent seas, 1979–2005: Attribution and role in the ice-albedo feedback, *Geophys. Res. Lett.*, **34**, L19505, doi:10.1029/2007GL031480.

Rampal, P., J. Weiss, and D. Marsan, 2009: Positive trend in the mean speed and deformation rate of Arctic sea ice, 1979–2007, *J. Geophys. Res*., **114**, C05013, doi:10.1029/2008JC005066.

Richter-Menge, J., and J. E. Overland, cited 2009: Arctic Report Card: Update for 2009. [Available online at http://www.arctic.noaa.gov/reportcard/index.html]

Rigor, I. G., and J. M. Wallace, 2004: Variations in the age of Arctic sea-ice and summer sea-ice extent, *Geophys. Res. Lett*., **31**, L09401, doi:10.1029/2004GL019492.

Rothrock, D. A., 1975: The energetics of the plastic deformation of pack ice by ridging. *J. Geophys. Res*., **80**, 4514–4519.

———, Y. Yu, and G. A. Maykut, 1999: Thinning of the arctic sea-ice cover, *Geophys. Res. Lett*., **26**(23), 3469–3472.

———, J. Zhang, and Y. Yu, 2003: The arctic ice thickness anomaly of the 1990s: A consistent view from observations and models, *J. Geophys. Res*., **108**(C3), 3083, doi:10.1029/2001JC001208.

———, and———, 2005: Arctic Ocean sea ice volume: What explains its recent depletion?, *J. Geophys. Res*., **110**, C01002, doi:10.1029/2004JC002282.

SCICEX Science Advisory Committee, 2010: SCICEX Phase II Science Plan, Part I: Technical Guidance for Planning Science Accommodation Missions. US Arctic Research Commission, Arlington, VA, 76pp.

Secretary of the Navy, SECNAV Energy Message to the Fleet, ALNAV068/09 (30 October 2009).

Serreze, M. C., J. A. Maslanik, T. A. Scambos, F. Fetterer, J. Stroeve, K. Knowles, C. Fowler, S. Drobot, R. G. Barry, and T. M. Haran, 2003: A record minimum arctic sea ice extent and area in 2002, *Geophys. Res. Lett*., **30**(3), 1110, doi:10.1029/2002GL016406.

———, M. M. Holland, and J. Stroeve, 2007: Perspectives on the Arctic's Shrinking Sea-Ice Cover. *Science,* **315,** 1533–1536.

———, A. P. Barrett, J. C. Stroeve, D. N. Kindig, and M. M. Holland, 2009: The emergence of surface-based Arctic amplification. *The Cryosphere* **3,** 11–19.

Skamarock, W. C., J. B. Klemp, J. Dudhia, D. O. Gill, D. M. Barker, W. Wang, and J. G. Powers, 2005: A Description of the Advanced Research WRF Version 2, National Center for Atmospheric Research, Boulder, Colorado, 101 pp.

Steele M., R. Morley, and W. Ermold, 2001: PHC: a global ocean hydrography with a high quality Arctic Ocean. *Journal of Climate* **14**(9):2079–2087.

———, M. C. Serreze, F. Fetterer, T. Arbetter, W. Meier, J. Maslanik, and K. Knowles, 2005: Tracking the Arctic's shrinking ice cover: Another extreme September minimum in 2004, *Geophys. Res. Lett.*, **32**, L04501, doi:10.1029/2004GL021810.

———, J. Maslanik, M. C. Serreze, I. Rigor, W. Meier, and C. Fowler, 2011: Sea ice response to an extreme negative phase of the Arctic Oscillation during winter 2009/2010, *Geophys. Res. Lett.*, **38**, L02502, doi:10.1029/2010GL045662.

Task Force Climate Change (TFCC) / Oceanographer of the Navy, 2009: U.S. Navy Arctic Roadmap, 35 pp.

———, 2010: U.S. Navy Climate Change Roadmap, 28 pp.

———, 2011: Arctic Environmental Assessment and Outlook Report, 30 pp.

Thompson, D. W. J, and J. M. Wallace, 1998: The Arctic Oscillation signature in the wintertime geopotential height and temperature fields. *Geophys. Res. Lett.,* **25**, 1297–1300.

———, and ———,1999: Annular Modes in the Extratropical Circulations. Part II: Trends. *J. Clim.*, **13**, 1018–1036.

Thorndike, A. S., and R. Colony, 1980: *Arctic Ocean Buoy Program Data Report, 19 January 1979–31 December 1979.* Applied Physics Labo- ratory, University of Washington, 131 pp.

Tucker, W. B., III, D. K. Perovich, A. J. Gow, W. F. Weeks, and M. R. Drinkwater, 1992: Physical properties of sea ice relevant to remote sensing, in *Microwave Remote Sensing of Sea Ice*, *Geophys. Monogr. Ser.*, vol. **68**, edited by F. D. Carsey, pp. 9–28, AGU, Washington, D. C., doi:10.1029/GM068p0009.

Vasilyeva, N., cited 2010: Russia, Canada make competing claims to Arctic resources. The Associated Press. [Available online at http://www.680news.com/news/world/article/102490--russia-canada-make-competing-claims-to-arctic-resources]

Wang, J., J. Zhang, E. Watanabe, M. Ikeda, K. Mizobata, J. E. Walsh, X. Bai, and B. Wu 2009: Is the Dipole Anomaly a major driver to record lows in Arctic summer sea ice extent?, *Geophys. Res. Lett.*, **36**, L05706, doi:10.1029/2008GL036706.

Watanabe, E., J. Wang, A. Sumi, and H. Hasumi 2006: Arctic dipole anomaly and its contribution to sea ice export from the Arctic Ocean in the 20th century, *Geophys. Res. Lett.*, **33**, L23703, doi:10.1029/ 2006GL028112.

Wu, B., J. Wang, and J. E. Walsh, 2006: Dipole Anomaly in the winter Arctic atmosphere and its association with Arctic sea ice motion, *J. Clim.,* **19**, 210–225, doi:10.1175/JCLI3619.1.

Zhang, J., and W. D. Hibler III, 1997: On an efficient numerical method for modeling sea ice dynamics. *J. Geophys. Res.,* **102,** 8691–8702.

———, and D. A. Rothrock, 2003: Modeling global sea ice with a thickness and enthalpy distribution model in generalized curvilinear coordinates, *Mon. Weather Rev.*, **131**, 845–861.

THIS PAGE INTENTIONALLY LEFT BLANK

INITIAL DISTRIBUTION LIST

1. Defense Technical Information Center
   Ft. Belvoir, Virginia

2. Dudley Knox Library
   Naval Postgraduate School
   Monterey, California

3. Dr. Wieslaw Maslowski
   Naval Postgraduate School
   Monterey, California

4. Dr. Ron Kwok
   Jet Propulsion Laboratory
   Pasadena, California

5. Dr. Andrew Roberts
   Naval Postgraduate School
   Monterey, California

6. Dr. Jaclyn Clement Kinney
   Naval Postgraduate School
   Monterey, California

7. Shirley S. N. Pang
   Jet Propulsion Laboratory
   Pasadena, California

7. Dr. Robert Osinski
   Institute of Oceanology Polish Academy of Sciences
   Sopot, Poland

8. RADM David Titley, USN
   Oceanographer and Navigator of the Navy
   Washington, DC

9. CDR Tony Miller
   Task Force Climate Change
   Washington, DC